

**Elucidation of Chemical Phenomena
By
Means of Computational Chemistry**

Inauguraldissertation
zur
Erlangung der Würde eines
Doktors der Philosophie

vorgelegt der
Philosophisch-Naturwissenschaftlichen Fakultät
der Universität Basel

von

Stanislav Ivan

aus Humenne (Slowakei)

Basel, 2005

Genehmigt von der Philosophischen-Naturwissenschaftlichen Fakultät der Universität
Basel auf Antrag der Herren

Prof. Dr. Bernd Giese

Prof. Dr. Markus Meuwly

Basel, den 5.Juli

Prof. Dr. Hans-Jakob Wirz
(Dekan)

The work presented here was initiated and supervised by Prof. Bernd Giese at the Chemistry Department of the University of Basel, during the time period July 2001 to July 2005.

Excerpts of this work have been published in the following journals:

Krattiger Philipp; Kovasy Roman; Revell Jefferson D; Ivan Stanislav; Wennemers Helma
Increased structural complexity leads to higher activity: peptides as efficient and versatile catalysts for asymmetric aldol reactions. *Organic letters* **2005**, 7, 1101-3.

Sonntag, Louis-Sebastian; Ivan, Stanislav; Langer, Michael; Conza, Matteo M.; Wennemers, Helma. Functionalized cyclotriproline - a bowl-shaped tripodal scaffold. *Synlett* **2004**, 7, 1270-1272.

Grossmann, Birgit; Heinze, Juergen; Moll, Thomas; Palivan, Cornelia; Ivan, Stanislav; Gescheidt, Georg. Electron Delocalization in One-Electron Oxidized Aniline Oligomers, Paradigms for Polyaniline. A Study by Paramagnetic Resonance in Fluid Solution. *Journal of Physical Chemistry B* **2004**, 108, 4669-4672.

De Wild, Michael; Berner, Simon; Suzuki, Hitoshi; Yanagi, Hisao; Schlettwein, Derck; Ivan, Stanislav; Baratoff, Alexis; Guentherodt, Hans-Joachim; Jung, Thomas A.
A novel route to molecular self-assembly. Self-intermixed monolayer phases. *ChemPhysChem* **2002**, 3, 881-885.

I wish to thank:

- Prof. Bernd Giese for the opportunity to study in his group in Basel
- Jérôme Amaudrut and Martin Spichty for the introduction to the Linux operating systems and network administration
- Prof. Hanspeter Huber for detailed insights into the principles of computational chemistry
- Prof. Markus Meuwly for correcting my thesis and competent remarks
- Prof. Helma Wennmers for fruitful collaborations
- Prof. Olaf Wiest for supervising me during my stay in his group and providing me with limitless hours of CPU times on BoB cluster at the Notre Dame
- URZ and CSCS for the hardware support

*“Where shall I start, please your majesty?” he asked.
“Begin at the beginning,” the king said gravely,
“and go on till you come to the end: then stop.”*

Lewis Carroll

I declare that I wrote this thesis “Elucidation of Chemical Phenomena by Means of Computational Chemistry” with help indicated and only handed it in to the faculty of science of the University of Basel and no other faculty and no other university.

Basel, 22.06.2005

Table of Contents

Preface	1
1 Unusual Spontaneous Spirocyclisation of Acridin-9-ylmethyl thioureas	3
1.1 <i>Models</i>	3
1.2 <i>Ab Initio Methods</i>	4
1.3 <i>Basics and Mathematical Tools of Quantum Chemistry</i>	6
1.3.1 Hartree-Fock Methods	6
1.3.2 Linear Combination of Atomic Orbitals (LCAO)	8
1.3.3 Basis Sets	9
1.3.4 Limits of the Hartree-Fock Methods. Electron Correlation.....	13
1.4 <i>Methods Used for Exploring the Energy Surface</i>	14
1.4.1 Energy Minimization Methods	14
1.4.2 Determination of Transition States	16
1.4.3 Reaction Path Following.....	17
1.5 <i>Simulation of Condensed Phases. Continuum Solvent Models</i>	17
1.6 <i>Theoretical Investigation of Nucleophilic Addition to Isothiocyanates</i>	20
1.6.1 Introduction.....	20
1.6.2 Isothiocyanates. Structure and Reactivity	23
1.6.3 Nucleophilic Addition of Isothiocyanates	24
1.6.4 Simulations of Reaction Pathways.....	26
1.6.5 Thermochemistry Calculations in Gaussian	28
1.7 <i>Addition of Acridin-9-ylmethylamine to Isothiocyanates</i>	32
1.7.1 Synchronous Mechanism	34
1.7.2 Consecutive Mechanism	35
1.7.2.1 Nucleophilic Addition to the N=C Bond of Isothiocyanates	35
1.7.2.2 Nucleophilic Addition to the C=S Bond of Isothiocyanates.....	38
1.7.3 The Effect of Electron Correlation	41
1.7.4 Solvation Effects	45
1.8 <i>Spirocyclisation of Acridin-9-ylmethyl thioureas</i>	48
1.9 <i>Summary</i>	60

2	Computational Investigation of Thymine Dimers Incorporated into the DNA double strand.....	61
2.1	<i>DNA Structure.....</i>	61
2.2	<i>Structural Analysis of the DNA.....</i>	64
2.3	<i>Excess Electron Transport through DNA.....</i>	67
2.4	<i>Empirical Force Field methods.....</i>	69
2.4.1	Amber Force Field.....	72
2.4.2	Molecular Dynamics.....	72
2.5	<i>Molecular Dynamic Simulation of the Modified DNA Structure.....</i>	77
2.5.1	Computational Methodology.....	79
2.5.2	MD simulation.....	80
2.5.3	Structural Analysis.....	83
2.6	Summary.....	89
3	Summary of the work.....	90
	Appendix.....	91
	Literature.....	126
	List of Symbols and Abbreviations.....	131

Preface

Understanding chemical, biological or physical process lies in the heart of virtually any research of natural science. Because of complexity of present-day research topics, it is a rare problem of interest that does not occupy the attention of both experimental and theoretical chemists. The synergy between the theory and experiment has vastly accelerated progress in many areas. The tools of the computational chemistry, alternatively called theoretical chemistry or molecular modeling, are often required in the course of the investigation of many phenomena from various fields of the science. The range of systems that can be considered in molecular modeling is extremely broad; from isolated molecules through simple atomic and molecular liquids to polymers, biological macromolecules such as proteins and DNA and solids.

During my PhD study I tried to use the tools of the computational chemistry in order to gain a better insight into the reaction mechanisms. I participated in a variety of projects from different fields of chemistry, hence having an excellent opportunity to apply theoretical calculations in many scientific problems and tasks. I present here two of my projects that involved methods from the “opposite corners” of the computational chemistry field.

The first project focuses on the detailed study of the reaction mechanism of isothiocyanates with acridin-9-ylmethylamine and cyclization of resulting thioureas using high level *ab-initio* quantum chemical methods. I tried to support the synthetic chemists with the calculations in order to provide them with the most probable reaction pathway.

The second project concentrates on the structural properties of the modified DNA strand using molecular dynamics methods. The research group of Prof. Bernd Giese has been over last decade investigating the phenomena of charge transport in deoxyribonucleic acid (DNA). In this particular work, the research was focused on the investigation of negative charge transport (a single electron) through DNA double helix. Unexpected experimental results raised questions about the mechanism of this process. These

questions triggered a theoretical investigation of structural features of modified DNA double strand by means of molecular dynamics.

1 Unusual Spontaneous Spirocyclisation of Acridin-9-ylmethyl thioureas

1.1 Models

All chemists use models. *One possibility to define a model is: “Simplified or idealized description of a system or a process devised to facilitate calculations and predictions”¹*. Beginning chemistry students use plastic models to help them understand and visualize the structures of molecules. These structural models continue to play an important role both in teaching and research, but molecular modeling is also concerned with more abstract models, many of which have a distinguished history. Not all models are physical or pictorial objects. For example, the S_N2 mechanism is a simple model for a particular class of reactions that successfully explains a lot of chemistry. In a similar way, computational chemistry describes chemical structures and reactions numerically, based in full or in part on the fundamental laws of physics.

There is still some confusion over the meaning of the terms computational chemistry and molecular modeling. Computational chemistry is a general term for methods employing the findings from quantum mechanics and classical mechanics for the simulation and prediction of the properties of molecular systems. Molecular modeling is in general more focused on the manipulation of the three-dimensional structures and deriving the properties that are dependent upon them. The significant part in molecular modeling plays the computer graphics. The development of computer graphics, together with new possibilities for visualization, facilitates the deeper and more importantly visual insight into the fundamentals of chemical reactions.

There are many methods and techniques used to make predictions of structural and dynamical properties of the molecular systems. In principle, they can be divided into three main classes: molecular mechanics, molecular dynamics and methods based on quantum mechanics.

Methods of *molecular mechanics* ignore the electronic motions and calculate the energy of a system as a function of the nuclear positions only. Molecular mechanics is commonly used in simulations of systems containing large numbers of atoms due to the implication of rather simple functional forms and empirically obtained parameters. However, molecular mechanics cannot provide properties that depend upon the electron density in the molecule.

In *molecular dynamics* time-dependent properties of the molecular system are simulated. The successive configurations of the system are generated by integrating Newton's laws of motion. The result is a trajectory that specifies how the positions and velocities of the particles in the system vary with time.

If one is interested in the properties that directly depend on the electronic distribution, the more general approach has to be used – *quantum mechanics*. Quantum mechanics explicitly represents the electrons in the calculation, and so it is possible to investigate e.g. chemical reactions in which bonds are broken and formed. There are number of quantum chemical theories for treating molecular systems. The one most widely used is molecular orbital theory. An *ab initio* approach will be discussed here.

1.2 *Ab Initio Methods*

Ab initio strictly means “*from first principles*”, which implies that calculations using such an approach requires as input only physical constants such as the speed of light, Planck's constant, the masses of elementary particles, and so on.

The core of quantum mechanics is the *Schrödinger equation*:

$$\hat{H}\Psi = E\Psi$$

In this equation \hat{H} is the Hamiltonian operator, which consists of kinetic and potential energy terms: kinetic energy of the nuclei, kinetic energy of the electrons, nuclear-nuclear repulsion, electron-electron repulsion and electron-nuclear attraction.

Schrödinger equation can be solved exactly only for a few problems, e.g. the particle in the box, the harmonic oscillator, H_2^+ etc. For more complicated systems, the Schrödinger equation becomes extremely complicated and so some approximation needs to be made. The Born-Oppenheimer approximation is the assumption that the electronic motion and the nuclear motion in molecules can be separated. It leads to a molecular wave function in terms of electron positions and nuclear positions:

$$\Psi_{\text{TOT}}(\text{nuclei, electrons}) = \Psi(\text{electrons}) \Psi(\text{nuclei})$$

The electronic wavefunction depends upon the nuclear positions but not upon their velocities, i.e., the nuclear motion is so much slower than electron motion that nuclei can be considered to be fixed. The total energy equals the sum of the nuclear energy (the electrostatic repulsion between the positively charged nuclei) and electronic energy.

$$E_{\text{TOT}} = E(\text{nuclei}) + E(\text{electrons})$$

For each arrangement of the nuclei (configuration) the Schrödinger equation is solved for the electrons in the field of nuclei – hence the electronic wavefunction is obtained (nuclear part was taken away):

$$\hat{H}_e \Psi_e = E_e \Psi_e$$

Where \hat{H}_e is the *electronic Hamiltonian* and can be written in the following form:

$$\hat{H}_e = \sum \hat{H}_i^{\text{eff}}$$

And \hat{H}_i^{eff} is *one-electron Hamiltonian*

Another approximation is so called ‘orbital approximation’: the electrons are assigned to the certain regions of the space – spatial orbitals.

1.3 Basics and Mathematical Tools of Quantum Chemistry

1.3.1 Hartree-Fock Methods

The electronic Hamiltonian is composed of three terms: kinetic energy of electrons T_e , electrostatic interaction between the nucleus and the electrons V_{ne} and the repulsion between the electrons V_{ee} :

$$\hat{H}_e = T_e + V_{ee} + V_{ne}$$

The last term depends on the coordinates of two electrons at the same time, which is a very limiting fact in the practical calculations and can be accepted only for small systems:

$$\hat{H}_e = \hat{H}^1 + \hat{H}^2 = \Sigma(\hat{H}_r^{\text{core}} + \hat{H}_{ee}) = \Sigma(T_r + V_r) + \sum_{i < j} \sum \frac{1}{r_{ij}}$$

The most computationally demanding part is the electron-electron interaction. To tackle this problem the approximation of independent particles is applied. Then only the interaction of the electron with an *average electron cloud* is considered:

$$\hat{H}^2 = \sum_i^n \hat{V}_i^{\text{av.}}$$

The Schrödinger equation, originally dependent on the coordinates of electrons x_1, x_2, \dots, x_i , is thus reduced to the set of equations:

$$\sum_{i=1}^n \left(\hat{H}_i + \hat{V}_i^{\text{av.}} \right) \Psi(x_1 + x_2 + \dots + x_i) = E \Psi(x_1 + x_2 + \dots + x_i)$$

$$\left(\hat{H}_i + \hat{V}_i^{\text{av.}} \right) \Phi(x_1) = \hat{F}_i \Phi(x_1) = \varepsilon_i \phi_i(x_i)$$

where \hat{F}_i is called the *Fock operator* and wavefunctions Φ_i *one-electron spin orbitals*.

The Fock operator is an effective one-electron Hamiltonian for the electron i in the poly-electronic system. Hartree-Fock equations are of third order in the coefficients ε_i , and can be iteratively solved to self consistency (Self Consistent Field SCF). One way to solve these equations is as follows. First, a set of trial solutions are obtained (for example by assuming that the electron density = 0, thus all coefficients are zero). This reduces the problem to a one electron problem (Hückel type), which is easy to solve. Then these coefficients are used to build the Fock operator \hat{F}_i , with which the system of linear equations is solved to get a new solution (a new electric field). This procedure is repeated until the solution is not longer changing. The SCF method thus gradually refines the individual electronic solutions until the point is reached at which the result for all electrons is unchanged, when they are said to be *self-consistent*.

One important feature of the SCF method is that it fulfills the so called *variational theorem*. Let us imagine an exact wavefunction Ψ_0 with corresponding energy E_0 . The theorem states that the energy calculated from an approximation to the true wavefunction will always be greater than the true energy $E \geq E_0$. The consequence of the variational theorem is that the lower energy corresponds to the better approximation to the 'exact' wavefunction. The energy minimization is equivalent to the optimization of the wavefunction.

In many cases it is convenient to imply the restriction that the doubly occupied orbitals use the same spatial functions for electrons of both α and β spin. This approach is called *spin-restricted* Hartree-Fock theory (RHF). An alternative approach is the spin-unrestricted Hartree-Fock (UHF) theory of Pople and Nesbet, which uses two distinct sets of molecular orbitals: one for electrons of spin α and the other for electrons of spin β . UHF method is thus more general and we can say that RHF is its special case.

In practical calculations RHF is used for simulations of closed-shell and UHF of open-shell systems.

1.3.2 Linear Combination of Atomic Orbitals (LCAO)

To get the orbitals that give a Slater determinant with the lowest energy we have to solve the Fock equation. That is a partial differential equation, and these are generally extremely hard to solve. Fortunately, it is possible to turn the Fock equation into a (generalized) matrix eigenvalue equation. Such equations are relatively easy to solve with standard techniques from numerical mathematics. The way to turn the Fock equation into a matrix eigenvalue equation is to write the orbitals as a linear combination of known functions (single electron orbitals):

$$\varphi_i = \sum_{\mu=1}^N c_{i\mu} \phi_{\mu}$$

The one-electron orbitals ϕ_{μ} are called *basis functions* and often correspond to the atomic orbitals. Because the atomic orbitals are put in the linear combination the procedure is called the *Linear Combination of Atomic Orbitals (LCAO)* approximation. By taking more atomic orbitals in the linear combination the approximation can be made better. The smallest number of basis functions for the molecular system will be that which can just accommodate all electrons in the molecule. More sophisticated calculations use more basis functions than a minimal set.

We can write Hartree-Fock equations under the LCAO theory in the following form:

$$\sum_{\nu} c_{\nu} F_{\mu\nu} = \varepsilon_i \sum_{\nu} c_{\nu} S_{\mu\nu}$$

$S_{\mu\nu}$ is the *overlap integral*:

$$S_{\mu\nu} = \left\langle \varphi_{\mu} \left| \varphi_{\nu} \right. \right\rangle = \langle \mu | \nu \rangle$$

and the elements of the Fock matrix:

$$F_{\mu\nu} = \langle \mu | \hat{F} | \nu \rangle = \langle \mu | \hat{H}_1 | \nu \rangle + \sum_{\lambda, \sigma} P_{\lambda\sigma} \left[(\mu\nu | \lambda\sigma) - \frac{1}{2} (\mu\lambda | \nu\sigma) \right]$$

$P_{\lambda\sigma}$ is the electron density matrix:

$$P_{\lambda\sigma} = 2 \sum_i^{\text{occ.}} c_{i\lambda} c_{i\sigma}$$

The evaluation of two-electron integrals is computationally very demanding and poses the greatest limitation in the use of ab initio Hartree-Fock methods. To carry out a calculation on the reasonably high level requires great numbers of basis functions be used. The number of two-electron integrals scales approximately with fourth power of the number of basis functions. The calculation of these integrals is not just very time-consuming but also consumes a considerable storage capacity. This problem can be significantly reduced using so called *direct-SCF* method. The integrals are not stored on the hard drive but are calculated according to the instantaneous needs. The advantage of such an approach is that cpu's of the modern computers are very fast while I/O operations take usually much more time. Direct-SCF thus became often the only practical solution on the less powerful workstations.

1.3.3 Basis Sets

The basis sets most commonly used in the quantum mechanical calculations are composed of atomic functions (close to atomic orbitals). The radial part of such functions is exponentially decaying function and such functions are called Slater type orbitals (STO):

$$\varphi(r) = c.e^{-\alpha r}$$

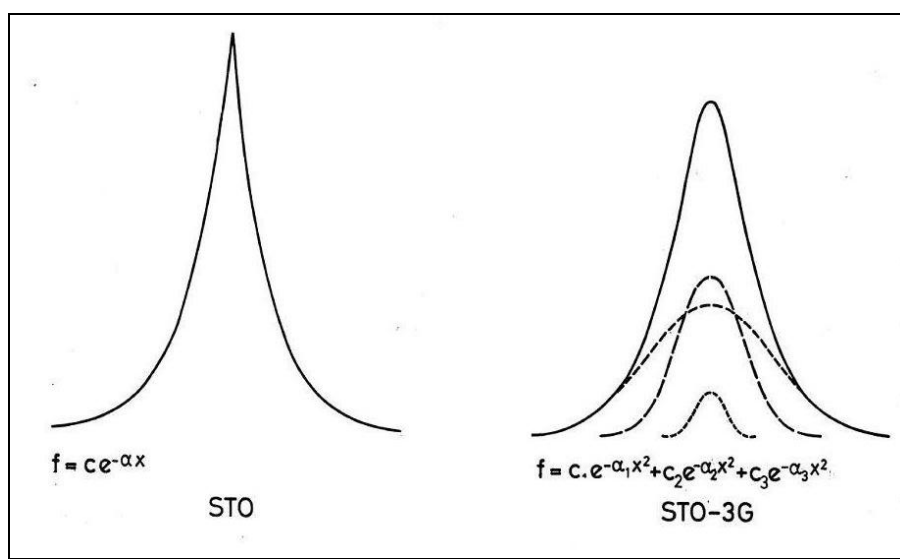
Unfortunately, Slater functions are not particularly suitable for implementation in practical calculations. It is common in ab initio calculations to replace Slater orbitals by Gaussian functions which have the form:

$$\varphi(r) = e^{-\alpha r^2}$$

α determines the radial extent ('spread') of a Gaussian function, r is the distance from the nucleus.

It has been found that replacing a single Slater type orbital with a single Gaussian function leads to large errors. To tackle this problem, each atomic orbital is represented as a linear combination of Gaussian functions. At least three Gaussian functions are required to properly represent each Slater type orbital and so the STO-3G basis set is the minimum that is recommended for ab initio calculations. For example, STO-3G has the following form:

$$f = c_1 \cdot e^{-\alpha_1 x^2} + c_2 \cdot e^{-\alpha_2 x^2} + c_3 \cdot e^{-\alpha_3 x^2}$$



STO-3G modeled by 3 Gaussian functions

A Gaussian expansion contains two parameters: coefficients c_i and exponents α_i . The most flexible way to use Gaussian functions in ab initio calculation permits both of these parameters to vary during the calculation. Such a calculation is said to use uncontracted or primitive Gaussians. However, calculations with primitive Gaussians are computationally very demanding and so basis sets that with contracted Gaussian functions are most commonly used. In contracted function the contraction coefficients and exponents are pre-determined and remain constant during the calculation. Let us assume the following wavefunction (molecular orbital):

$$\psi = c_1\varphi_1 + c_2\varphi_2 + c_3\varphi_3 + \dots c_7\varphi_7$$

In the contracted scheme:

$$\psi = c_1 \underbrace{(\kappa_1\varphi_1 + \kappa_2\varphi_2 + \kappa_3\varphi_3 + \kappa_4\varphi_4)}_{\text{contraction}} + c_2 \underbrace{(\kappa_5\varphi_5 + \kappa_6\varphi_6)}_{\text{contraction}} + c_3\varphi_7$$

c_i are variables, φ_i primitive functions, κ_i coefficients which are kept constant. The advantage of this approach is based on the reduced number of coefficients to be optimized during the SCF cycle. As can be easily seen in this example the number of variables was reduced from seven to three.

In a minimal basis set representation every atomic orbital is described by only one basis function (contraction). Thus for hydrogen, the minimal basis set is just one 1s orbital. For carbon, the minimal basis set consists of a 1s orbital, a 2s orbital and the full set of three 2p orbitals.

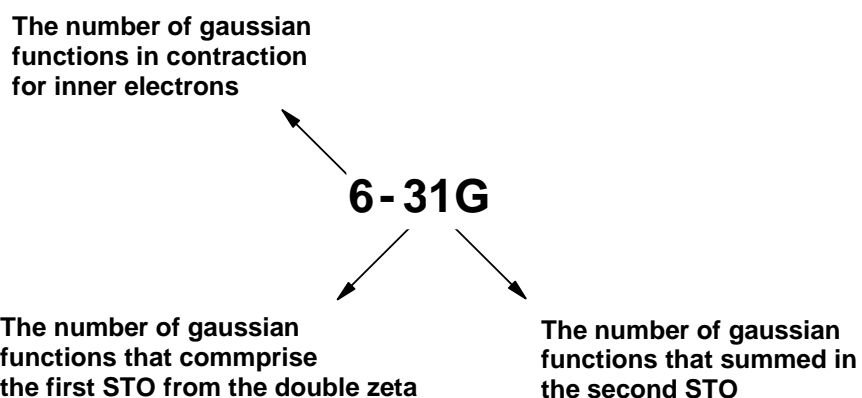
Quantum chemists devised a short-hand notation schemes to denote the basis sets used in ab initio calculations. The most common is the notation devised by Pople and co-workers. The STO-3G, STO-4G, etc (in general STO-nG) are minimal basis sets with n Gaussian function used to represent each orbital (n Gaussian functions contracted = 1 STO \Rightarrow 1 contraction of Gaussian functions). The Pople basis sets are exactly defined and all exponents and contraction coefficients are published in the literature. The minimal basis sets have several drawbacks. With the minimal basis sets, we approximated all

orbitals to be of the same shape, which does not reflect the reality. Double-zeta basis set is important because it allows us to treat each orbital separately when we conduct the Hartree-Fock calculation. This gives us a more accurate representation of each orbital. In order to do this, each atomic orbital is expressed as the sum of two Slater-type orbitals (STOs) (two functions for H or He, ten functions for Li to Ne and so on).

$$\Phi_{2s}(r) = \underbrace{\Phi_{2s}^{STO}(r, \xi_1)}_{\text{Slater Orbital 1}} + \underbrace{d}_{\text{Constant}} \underbrace{\Phi_{2s}^{STO}(r, \xi_2)}_{\text{Slater Orbital 2}}$$

Often it takes too much effort to calculate a double-zeta for every orbital. Instead, a simplification is applied by calculating a double-zeta only for the valence orbital. Since the inner-shell electrons are not so vital for the calculation (or chemical process), they are described with a single Slater Orbital. This method is called a split-valence basis set. A few examples of common split-valence basis sets are 3-21G, 4-31G, and 6-31G.

For example, the notation 6-31G means: the inner shells are represented by 1 contraction constructed from 6 primitives and the valence shell is represented by double zeta with an “inner” contraction constructed from 3 and an “outer” constructed from 1 primitive.



The electron cloud of an atom in the molecule is usually perturbed in comparison with the isolated atom. The most common solution to this problem is to introduce *polarization functions* into the basis set. The polarization function have a higher angular quantum number and so correspond to p orbitals for hydrogen and d orbitals for the first- and second-row elements. The use of polarization functions is indicated by an asterisk (*). For example 6-31G* refers to 6-31G basis set with polarization functions on the heavy (non-hydrogen) atoms. 6-31G** indicates polarization functions on heavy atoms and hydrogen or helium.

To properly describe the species such as anions and molecules containing lone pairs, additional diffuse functions are used. These basis sets are denoted '+'; thus 6-31+G contains an additional single set of diffuse s-and p-type Gaussian functions. 6-31++G indicates diffuse functions included for hydrogen as well as for heavy atoms.

1.3.4 Limits of the Hartree-Fock Methods. Electron Correlation.

The most significant drawback of the Hartree-Fock theory is that it fails to adequately represent electron correlation. The SCF method assumes electrons moving in the average field formed by other electrons, and so the instantaneous position of an electron is not influenced by neighboring electrons. In fact, electrons “tend to avoid each other” giving rise to a lower energy of the system. The difference between an exact and Hartree-Fock energy is *the correlation energy*:

$$E_{\text{correl.}} = E_{\text{exact.}} - E_{\text{HF}} < 0$$

Several methods have been developed that attempt to calculate the correlation energy after the Hartree-Fock calculation. Some examples are the Moller-Plesset perturbation theory (MPn), Configuration interaction (CI), Multiconfiguration SCF (MSSCF) and so on. These methods are particularly important in the systems with unpaired electrons, electron correlation is crucial in the study of dispersive effects, which play a mayor role in intermolecular interactions. On the other hand, Hartree-Fock geometries and relative

energies for equilibrium structures are often in good agreement with experiment as many molecular modeling applications are concerned species at equilibrium and it might be considered that correlation effects are not so important. I will not go into details about correlation methods since this topic is far behind the scope of this thesis and I have not used them in my practical calculations.

1.4 Methods Used for Exploring the Energy Surface.

The potential energy of the molecular system is a multidimensional function of coordinates. For a system with N atoms the energy is a function of $3N-6$ internal or $3N$ Cartesian coordinates. A geometric hypersurface on which the potential energy of a set of reactants is plotted as a function of the coordinates representing the molecular geometries of the system is known as Potential-energy (reaction) surface (PES). Computational chemists are usually interested in stationary point on the PES –minium and saddle points. Minimum points correspond to the stable states of the system. The highest point on the pathway between two minima is known as a saddle point, with the arrangement of atoms being the transition structure. There may be a very large number of minima on the PES, the minimum with the lowest energy is known as the global minimum.

A reaction path simulation usually consists of four subsequent steps:

1. Localization of the minimum points on the PES
2. Search for the transition state candidate
3. Localization of the saddle point and its verification
4. IRC calculation

1.4.1 Energy Minimization Methods

To find minimum points on the PES we use a minimization algorithm which for a given function $F=f(x_1, x_2, \dots, x_i)$ tries to find the values of variables x_i where F has a minimum value. At a minimum point the first derivate of the function with respect to all variables is

zero and the second derivatives are all positive. The minimization methods fall into two categories: those which use derivatives of the energy with respect to the coordinates and those which do not. The derivative methods are most commonly used, because derivations provide information about the shape of the energy surface, the magnitude of the first derivative of the energy (gradient) is related to the steepness of the local curvature and the direction of the gradient indicates where the minimum lies. During the minimisation procedure the energy of the system is lowered by moving each atom in response to the force acting on it (force = minus the gradient). The derivative methods can be classified according to the highest-order derivative used:

- a) first-order methods use the first derivatives (gradients)
- b) second-order use both first and second derivatives

The most frequently first-order minimization algorithms are the method of *steepest descent* and the *conjugate gradient* method. These methods use the gradient information to determine the direction of the next step and so gradually move atoms towards the minimum.

The second-order methods use not only the first derivatives but also the second derivatives to locate the minimum. The simplest second-order method is the *Newton-Raphson* method:

$$x^* = x_0 - f'(x_0).f''^{-1}(x_0)$$

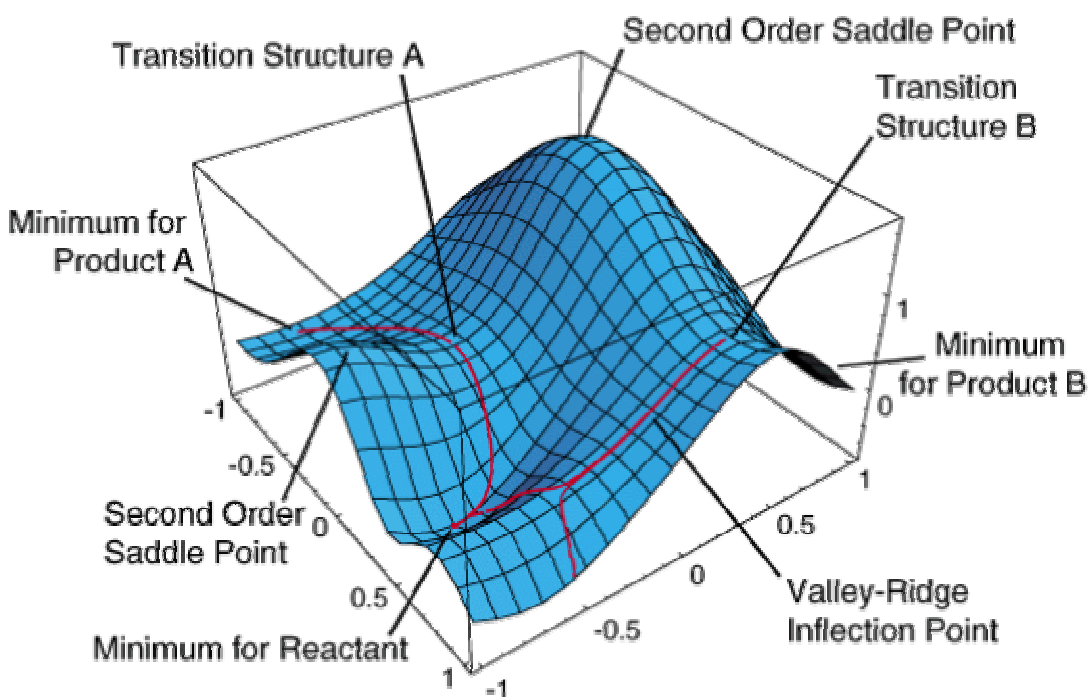
where $f''^{-1}(x_0)$ is the inverse Hessian matrix (matrix of second derivatives), which in the Newton-Raphson Method must be inverted. This can be computationally demanding with many atoms and so the Newton-Raphson method is suited for small molecules (less than 100 atoms). There are many variations on the Newton-Raphson method which aim to eliminate the need to calculate the full matrix of second derivatives. Families of methods called Quasi-Newton require only first derivatives and gradually construct the inverse Hessian matrix as the calculation proceeds.

Most of the modern programs today use the combination of the first and second-order minimization methods in order to speed up the calculation. Far from the minimum the more robust first-order method (e.g. steepest descent, conjugate gradient) is used while close to the minimum more precise second-order method is applied.

1.4.2 Determination of Transition States

To investigate the reaction kinetics it is necessary to explore the nature of the energy surface away from the minimum points. As the system moves from one minimum to another, the energy increases to a maximum at the transition structure and then falls. In the saddle points energy passes through a maximum for movement along the pathway that connects the two minima, but is a maximum for displacement in all other directions perpendicular to the path.

At the saddle point the first derivatives of the potential function with respect to the coordinates are all zero. The located saddle points are usually verified by frequency calculation, result of which is so called Hessian – the matrix of second derivatives of energy with respect to all coordinates. The number of negative eigenvalues in the Hessian matrix determines the order of the saddle point; n th-order saddle point has n negative eigenvalues. The Hessian matrix of the ‘true’ saddle point must contain one and only one negative eigenvalue, which is usually referred as ‘imaginary’ frequency.



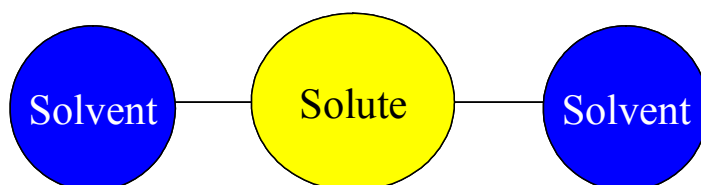
Methods for locating saddle points are usually most effective when the input structure is as close as possible to the transition structure so it is very important to find a reasonable starting structure, where is the highest probability of finding the desired transition state. This process depends mostly on the experiences and chemical intuition of the researcher – that is why the transition state search is often called the ‘*black art*’.

1.4.3 Reaction Path Following

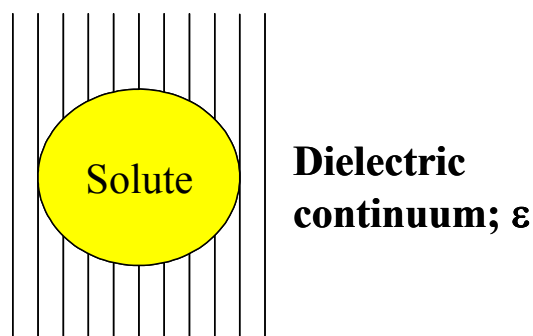
The *intrinsic reaction coordinate* (IRC)^{2, 3} calculation is commonly used to confirm that the saddle point indeed connects the corresponding minima. It simulates the path that would be followed by a particle moving along the steepest descent path with an infinitely small step from the transition structure down to each minimum. The initial directions are obtained from the eigenvector that corresponds to the imaginary frequency at the transition structure.

1.5 Simulation of Condensed Phases. Continuum Solvent Models.

Most chemical reactions take place in a solvent. Solute-solvent interactions have a significant effect on the behaviour of molecular systems; hence, understanding the influence of solvent is crucial for proper modeling of solution environments. In some cases, solvent molecules are directly involved, as for example in ester hydrolysis. Such solvent molecules should be modeled explicitly.



In other systems, the solvent provides a ‘bulk medium’; the dielectric properties of the solvent are of primary importance \Rightarrow continuum solvation models.

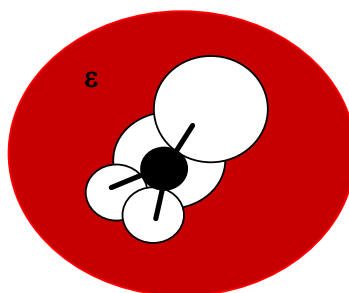


The solvation free energy is the free energy change to transfer a molecule from vacuum to solvent. The solvation free energy contains three components:

$$\Delta G_{solv} = \Delta G_{elec} + \Delta G_{vdw} + \Delta G_{cav}$$

where ΔG_{elec} is the electrostatic component, ΔG_{vdw} van der Waals interaction between the solute and the solvent, ΔG_{cav} is the free energy required to form the solute cavity within the solvent, it comprises the entropic penalty associated with the reorganization of the solvent molecules around the solute.

When a solute is immersed in a solvent, its charge distribution interacts with that of the solvent. In a continuum model, the charge distribution of solvent is replaced by a continuous electric field that represents a statistical average over all solvent degrees of freedom at thermal equilibrium. This field is called ‘reaction field’ in the regions of space occupied by a solute, since it derives from reaction of the solvent to the presence of solute. The reaction field can be incorporated into quantum mechanics, where it is commonly referred as the *self-reaction field* (SCRF) method. The solute is placed into a cavity within the solvent. There are variety of SCRF approaches which differ how they define the cavity and the reaction field. Tomasi’s polarisable continuum method (PCM)⁴ defines the cavity as the union of a series of interlocking atomic spheres.



The cavity surface is divided into a large number of small surface elements, and there is a point charge associated with each surface element. This system of point charges represents the polarization of the solvent. The total electrostatic potential at each surface element equals the sum of the potential due to the solute $\phi_\rho(r)$ and the potential due to the other surface charges $\phi_\sigma(r)$:

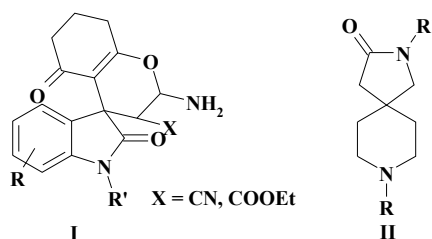
$$\phi(r) = \phi_\rho(r) + \phi_\sigma(r)$$

The PCM algorithm is as follows. First, the cavity surface is determined from van der Waals radii of the atoms. That fraction of each atom's van der Waals sphere which contributes to the cavity is then divided into a number of small surface elements of calculable area. An initial value of the point charge for each surface element is then calculated from the electric field gradient due to the solute alone. The contribution $\phi_\sigma(r)$ due to the other point charges can be then calculated using Coulomb's law. These charges are modified until they are self-consistent. The potential $\phi_\sigma(r)$ from the final part of the charge is then added to the solute Hamiltonian ($\mathcal{H} = \mathcal{H}_0 + \phi_\sigma(r)$) and the SCF calculation initiated. After each SCF calculation new values of the surface charges are calculated from the current wavefunction to give a new value of $\phi_\sigma(r)$ which is used in the next iteration until the solute wavefunction and the surface charges are self-consistent.

1.6 Theoretical Investigation of Nucleophilic Addition to Isothiocyanates

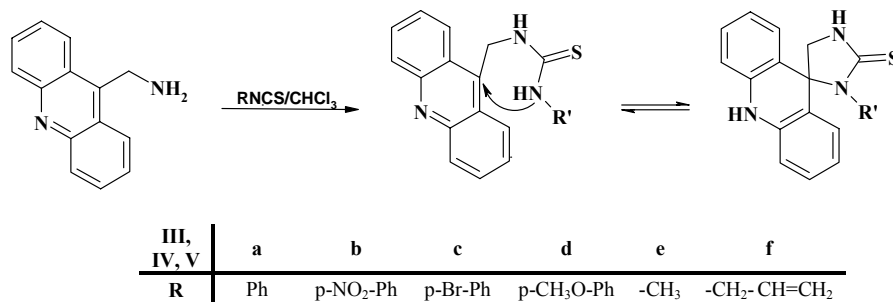
1.6.1 Introduction

Many spirocycles possess important biological activities. For example, the insecticide activity of substituted spiro[4H-1-benzopyrane-4,3'-3H-indole]-3-karbonitriles **I** is well known. Antifungal properties were found among many spiro lactones **II**.



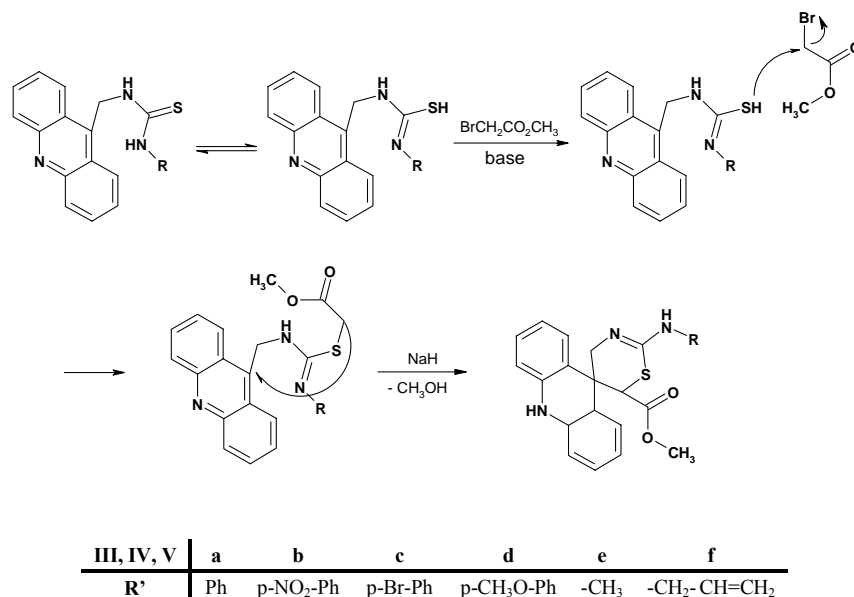
One of the most interesting heterocyclic scaffolds found in variety of biological systems are the derivatives of imidazole. At the present time, a great number of acridine compounds are known as fluorescent, intercalating, antitumor agents, and are tested also against bacteria, malaria and other protozoa infections.^{5, 6} Spirocompounds containing both acridine and imidazole rings are expected to be biologically active agents and their preparation is the subject of an intensive study.⁷⁻¹¹ Along with the synthetic efforts there is still a need for better understanding of the reaction mechanisms and conditions controlling the course of the reaction.

This work deals more in detail with the preparation of the new types of spirocompounds, the mechanism of their formation via nucleophilic addition of acridin-9-yl methyl to isothiocyanates and the cyclization of resulting thioureas (Scheme 1). The reaction mechanism of this particular reaction is investigated using the *ab initio* quantum chemical methods.



Scheme 1

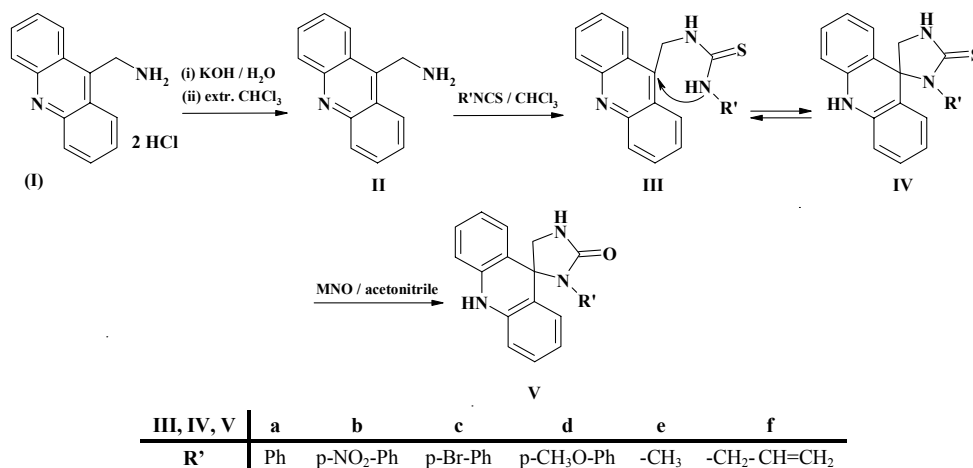
The first impulse for this theoretical investigation was the unexpected observation during the research of my colleagues at the University of Pavol Jozef Safarik in Slovakia. The targets of their synthetic efforts were six-membered spiro acridines, which should, according to the previous studies⁷⁻¹¹, result from the reaction between acridin-9-ylmethylthioureas and methyl bromoacetate (Scheme 2).



Scheme 2

The starting material for this cyclization was the acridin-9-ylmethylamine (ACR-CH₂-NH₂) dihydrochloride **I**, which was obtained from acridin-9-ylmethylbromide by liberating with potassium hydroxide (Scheme 3). The free amine **II** then reacted with the different isothiocyanates to form desired stable thioureas **III**. Surprisingly, the reaction was not

terminated at this point, but the thioureas further spontaneously cyclized in chloroform to spiro[dihydroacridine-9(10H), 5'-imidazolidine]-2'-thiones **IV**.

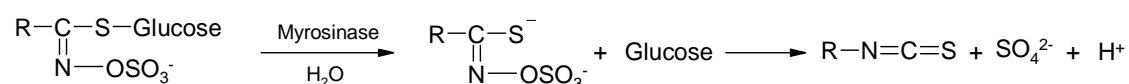


Scheme 3

Repeated attempts to isolate pure thioureas **III** failed due to their reactivity, always only mixtures of **III** and **IV** were obtained. The structures of thioureas and final spirocompounds were confirmed by spectral and derivatisation methods. Spiro[dihydroacridine-9(10H),5'-imidazolidine]-2'-thiones **IV** yielded in the reaction with mesitylnitroxide corresponding spiro[dihydroacridine-9(10H),5'-imidazolidine]-2'-ones **V**, what was an evidence for imidazoline, not thiazolidine structure of **IV**. These unexpected results raised the questions about the reaction mechanism and the methods of quantum chemistry were chosen as a tool to address this question.

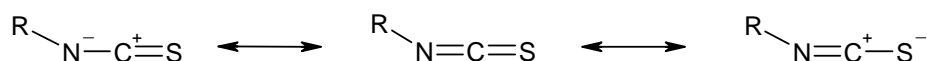
1.6.2 Isothiocyanates. Structure and Reactivity

Isothiocyanates are sulphur containing compounds with the general formula $R-N=C=S$, formed by substituting sulfur for oxygen in the isocyanate $R-N=C=O$ group. Isothiocyanates occur naturally as glucosinolate conjugates in cruciferous vegetables. Isothiocyanates are also responsible for the typical flavour of these vegetables. Glucosinolates are precursors of isothiocyanates. When the raw vegetables are chewed the plant cells are broken and an enzyme (myrosinase) hydrolyses the glucosinolates into isothiocyanates:



Isothiocyanates combat carcinogens by neutralizing them, reducing their poisonous effect and stimulating the secretion of carcinogens of carcinogens. Isothiocyanates act by inhibition of cell proliferation and induction of apoptosis. The isothiocyanates with the strongest anticancer effects are phenylethylisothiocyanate, benzylisothiocyanate and 3-phenylpropylisothiocyanate. Studies have shown that isothiocyanates help to prevent lung cancer and esophageal cancer. Isothiocyanates can also lower the risk of other cancers, including gastrointestinal cancer.

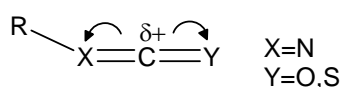
The $N=C=S$ group alone is linear. The value of the angle $R-N-C$ (140° - 180°) depends on the character of the carbon residue R and the hybridization state of the nitrogen atom of the NCS group, respectively. The electronic structure can be expressed by the resonance formulas:



Which of the mesomeric structures will be effective depends on the reagent, medium, catalyst and the residue R . The isothiocyanates with electron donating substituents will

prefer the structure with a negative charge located on the sulphur atom. On the other hand, the negative charge will be located preferably on the nitrogen atom in the case of electron withdrawing groups.

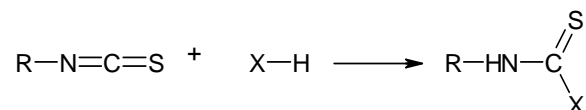
The NCS group is a medium strong electron withdrawing substituent with a negative inductive and a positive mesomeric effect. The central carbon atom of the NCS group has a strong electrophilic character and its electron withdrawing strength is most important for reactions of the NCS group by analogy with the carbon atom in the functional group of isocyanates and other typical heterocumulenes:



The typical reactions of isothiocyanates are nucleophilic additions Ad_N and cycloadditions. The NCS group reacts with convenient agents to form 1,2-, 1,3-, and 1,4-cycloadducts. For the rate of the cycloadditions the steric effects of the substituent is of great importance while its electric effect is significant for nucleophilic additions.

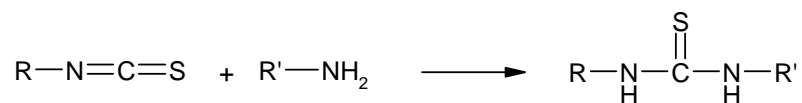
1.6.3 Nucleophilic Addition of Isothiocyanates

The nucleophilic additions of isothiocyanates are governed by the partial positive charge on the carbon atom of the NCS group, which predetermines isothiocyanates to enter nucleophilic additions. These reactions can occur across $\text{N}=\text{C}$ as well as across $\text{C}=\text{S}$ bonds. The general reaction scheme can be written as follows:



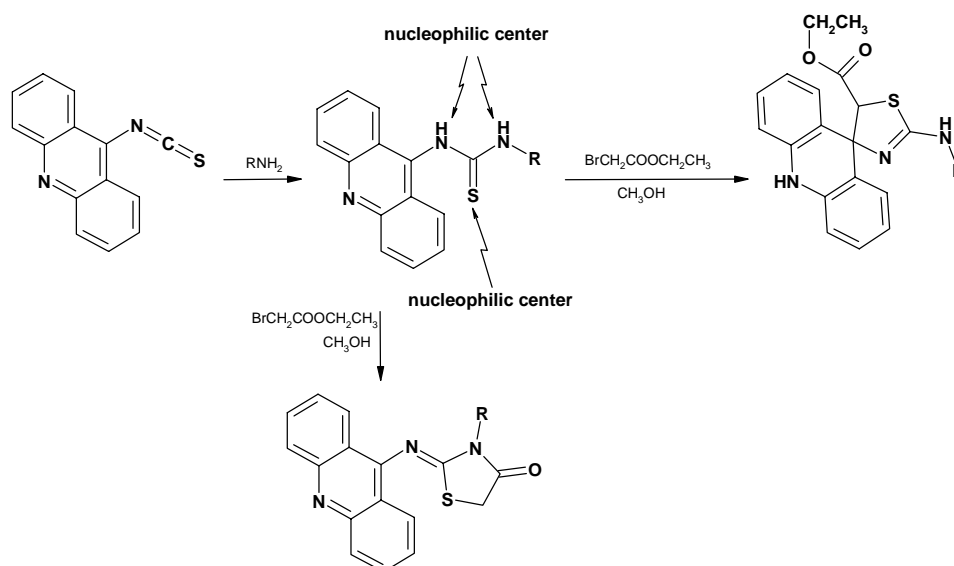
Scheme 4

$\text{Nu}-\text{H}$ is the nucleophile such as hydroxyl ion, ammonia, amines, hydroxylamine, thiols, hydrazines and so on. The best known reactions of isothiocyanates are the additions of nitrogen bases. Reactions of isothiocyanates with ammonia and primary or secondary amines produce the corresponding N-substituted thioureas.



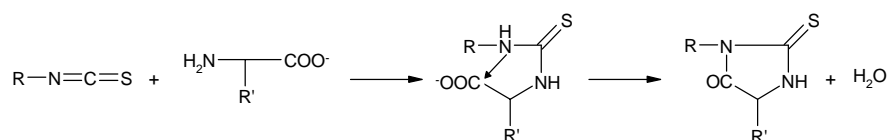
Scheme 5

Thioureas contain three nucleophilic centers which can be effectively used for the preparation of many types of heterocyclic compounds. For example, acridin-9-yl thioureas react with haloorganic compounds to afford different heterocyclic products depending on the character of the reaction partner^{8, 10}:



Scheme 6

The reaction between isothiocyanate and α -amino acid affords the derivatives of thiocarbamoyl amino acid which cyclize in acid medium to yield thiohydantoin derivatives.



Scheme 7

Reactivity of isothiocyanates is often used in the organic synthesis, since they offer wide range of possibilities for the synthesis of new compounds. Edman degradation, the

synthesis of variety of substituted heterocycles as well as the inhibition of enzymes by isothiocyanates are based on the nucleophilic attack on the carbon atom of the NCS group. Despite the numerous studies, the mechanism of these reactions has not been satisfactorily resolved. There are many suggested mechanisms, from the simple bimolecular reactions with the synchronous transition state or higher order reactions involving dimers¹² (trimers) of nucleophiles to consecutive reactions with several nucleophile molecules. The available experimental data are apparently not sufficient for unambiguous conclusions about the mechanism of these nucleophilic additions.

1.6.4 Simulations of Reaction Pathways

The quantum chemistry can be effectively used for reaction paths simulations, since it provides information about the electronic properties of the molecule and thus can be used for modeling of bond-breaking and bond-forming processes. The electron density and especially electrostatic potential present the information about the reaction centers of the molecules, in accordance with it is possible to predict the course of the reaction. To suggest the reaction mechanism of the particular reaction, it is necessary to localize all relevant stationary points on the potential energy surface (PES) – minimum points, which represent the intermediates along the reaction path as well as transition states connecting them.

The following general strategy has been adopted; all calculations were initially performed in the gas phase in order to get informations about the energetics of the reaction. To study the effects of solvation, all obtained stationary points have been then used for subsequent calculations in the solution environment (chloroform).

Calculations were divided to two main stages. In the first stage the reaction mechanism of the nucleophilic addition of acridin-9-ylmethylamine to methyl- and phenylisothiocyanate was investigated. The second stage was dedicated to modeling of cyclization of the thioureas to final spiroacridines. Methyl- and phenyl isothiocyanates were chosen as model systems due to their different spatial and electronic properties; methyl group represents electron donors and phenyl group electron withdrawing substituents.

All stationary points in this study were identified with the Gaussian quantum chemistry package, versions Gaussian 98, Rev. A7¹³ and Gaussian 03, Rev. C01¹⁴. The usual procedure is to localize minima first (by applying the minimization algorithms), and then to try to find corresponding transition states. The crucial part of the transition state search is to find an appropriate candidate. This can be done in many ways, some of which are semi-automated (scan of the PES), automated (STQN method)^{15, 16} or empirical, dependent entirely on the scientist's experiences.

After successful localization of the transition state it is necessary to verify if it is indeed a valid transition state on the potential hypersurface. This is accomplished by a force calculation, the result of which is so called Hessian – the matrix of second derivatives of energy with the respect to all coordinates. The sought transition state of the first order contains one and only one negative frequency (sometimes called imaginary frequency), which corresponds to the maximum in the search direction and a minimum in all other directions. The Hessian calculation is computationally very demanding and is, among other expensive types of calculations, a severe limitation in ab initio calculations of larger molecules. With reference to the system size and computer resources (see experimental part), the moderate Hartree-Fock level of theory with Pople's split basis valence set 6-31G with one polarization and one diffusion function on heavy (non-hydrogen) atoms was used – HF/6-31+G(d)^{17, 18}. Polarization and diffusion functions are necessary for the better description of species with an anisotropic electron distribution and charged intermediates, which were expected to be formed during the reaction.

All stationary points were characterized by the vibrational analysis. These frequency calculations verified that all frequencies for minima are real and that all transition states have only one negative frequency. In addition, intrinsic reaction coordinate (IRC) calculations confirmed that all transition states connect the appropriate minima on the PES. The values of enthalpies and Gibbs free energies were calculated at 298.15 K and 1 atmosphere.

1.6.5 Thermochemistry Calculations in Gaussian

The equations used for computing thermochemical data in *Gaussian* are equivalent to those given in standard texts on thermodynamics¹⁹. The thermodynamic quantities like entropy, enthalpy or heat capacity are calculated from contributions resulting from translational, electronic, rotational and vibrational motions. The starting point in each case is the partition function $q(V,T)$ for the corresponding component of the total partition function. The partition function from any component can be used to determine the entropy contribution S from that component, using the relation:

$$S = Nk_B + Nk_B \ln\left(\frac{q(V,T)}{N}\right) + Nk_B T \left(\frac{\partial \ln q}{\partial T}\right)_V$$

where N is the number of moles, V is volume, T temperature and k_B the Boltzmann constant. Gaussian uses the expression of the following form:

$$S = R \left(\ln(q_t q_e q_r q_v e) + T \left(\frac{\partial \ln q}{\partial T} \right)_V \right)$$

with R being the gas constant, q_i are the corresponding partition functions. The internal thermal energy E can also be obtained from the partition function:

$$E = Nk_B T^2 \left(\frac{\partial \ln q}{\partial T} \right)_V$$

1. Contributions from translation: the translation partition function q_t is calculated using expression:

$$q_t = \left(\frac{2\pi m k_B T}{h^2} \right)^{3/2} \frac{k_B T}{P}$$

where P is the pressure (default 1 atmosphere) and h the Planck constant. The translational partition function is used to calculate the translational entropy.

$$S_t = R \left(\ln(q_t e) + \left(\frac{3}{2T} \right) \right) = R(\ln q_t + 1 + 3/2)$$

Contribution to the internal thermal energy due to translation is:

$$E_t = \frac{3}{2} RT$$

2. Contribution from electronic motion: Gaussian assumes that the first electronic excitation energy is much greater than $k_B T$. Therefore, the *first and higher excited states are assumed to be inaccessible* at any temperature. Further, the energy of the ground state is set to zero. These assumptions simplify the electronic partition function to:

$$S_e = R \ln q_e$$

Since there are no temperature dependent terms in the partition function, the electronic heat capacity and the internal thermal energy due to electronic motion are both zero.

1. Contribution from rotational motion: For a general case of nonlinear polyatomic molecule, the rotation partition function is:

$$q_r = \frac{\pi^{1/2}}{q_r} \left(\frac{T^{3/2}}{(\Theta_{r,x} \Theta_{r,y} \Theta_{r,z})^{1/2}} \right)$$

where $\Theta_r = h^2/8\pi^2 I k_B$. I is the moment of inertia. The rotational contribution to the entropy is:

$$S_r = R \left(\ln q_r + \frac{3}{2} \right)$$

The contribution to the internal thermal energy is:

$$E_r = \frac{3}{2}RT$$

For a linear molecule, the rotational contributions to entropy and internal thermal energy have the forms:

$$S_r = R(\ln q_r + 1)$$

$$E_r = RT$$

For a single atom $q_r = 1$. Since q_r does not depend on temperature, the contribution of rotation to the internal thermal energy, its contribution to the heat capacity and its contribution to the entropy are all identically zero.

4. Contribution from vibrational motion:

The contributions to the partition function, entropy, internal energy and constant volume heat capacity from vibrational motions are composed of a sum (or product) of the contributions from each vibrational mode, K . Only the real modes are considered; modes with imaginary frequencies (with a minus sign in the output) are ignored. Each of the $3N-6$ (or $3N-5$ for linear molecules) modes has a characteristic vibrational temperature, $\Theta_{v,K} = h\nu_K/k_B$.

There are two ways to calculate the partition function, depending on where one chooses the zero of energy to be: either the bottom of the internuclear potential energy well, or the first vibrational level. Gaussian uses the bottom of the well as the zero of energy to determine the thermodynamic quantities. The contribution to the partition function from a given vibrational mode is:

$$q_{v,K} = \frac{e^{-\Theta_{v,K}/2T}}{1 - e^{-\Theta_{v,K}/T}}$$

and the overall vibrational partition function is:

$$q_v = \prod_K \frac{e^{-\Theta_{v,k}/2T}}{1 - e^{-\Theta_{v,k}/T}}$$

The total entropy contribution from the vibrational partition function is calculated using the formula:

$$S_v = R \sum_K \left(\frac{\Theta_{v,K}/T}{e^{\Theta_{v,K}/T} - 1} - \ln(1 - e^{-\Theta_{v,K}/T}) \right)$$

The contribution to the internal thermal energy resulting from molecular vibrations has the following expression:

$$E_v = R \sum_K \Theta_{v,K} \left(\frac{1}{2} + \frac{1}{e^{\Theta_{v,K}/T} - 1} \right)$$

All mentioned contributions are printed out in the Gaussian output from the frequency calculation:

The correction to the internal thermal energy: $E_{\text{tot}} = E_t + E_r + E_v + E_e$

Thermal correction to enthalpy: $H_{\text{corr}} = E_{\text{tot}} + k_B T$

Thermal correction to Gibbs free energy: $G_{\text{corr}} = H_{\text{corr}} - TS_{\text{tot}}$

where $S_{\text{tot}} = S_t + S_r + S_v + S_e$

These values are then used for estimates of the total energy of the molecule, after various corrections are applied:

Sum of electronic and thermal energies: $E = E_0 + E_{\text{tot}}$

Sum of electronic and thermal Enthalpies: $H = E_0 + H_{\text{corr}}$

Sum of electronic and thermal Free Energies: $G = E_0 + G_{\text{cor}}$

where E_0 represents the total electronic energy.

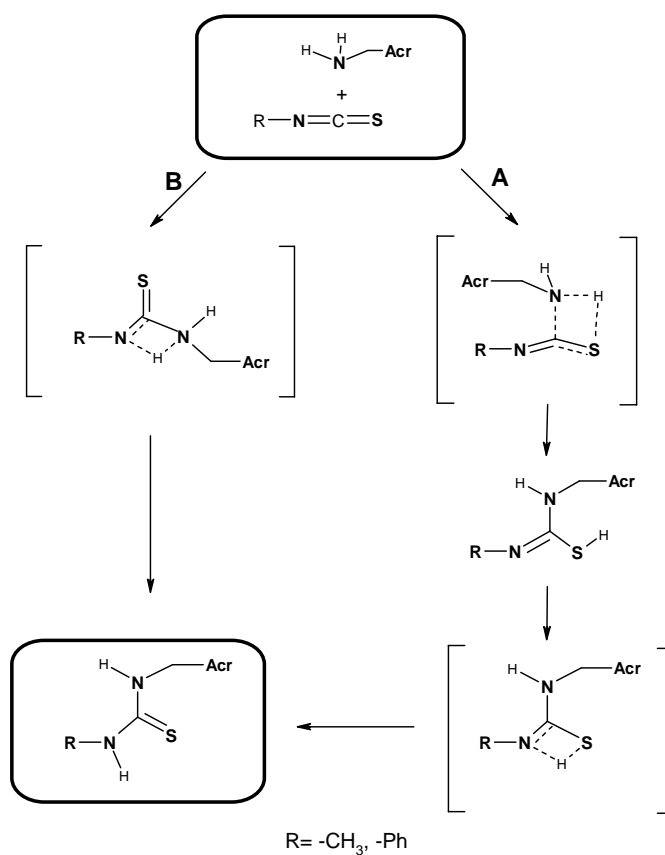
1.7 Addition of Acridin-9-ylmethylamine to Isothiocyanates

The calculation of the reaction pathway comprises the localization and identification of the corresponding stationary points (minima, transition states) along the reaction coordinate. These stationary points are modeled according to the assumed mechanism, which is based on the current state of knowledge, or in many cases simply on the chemical intuition.

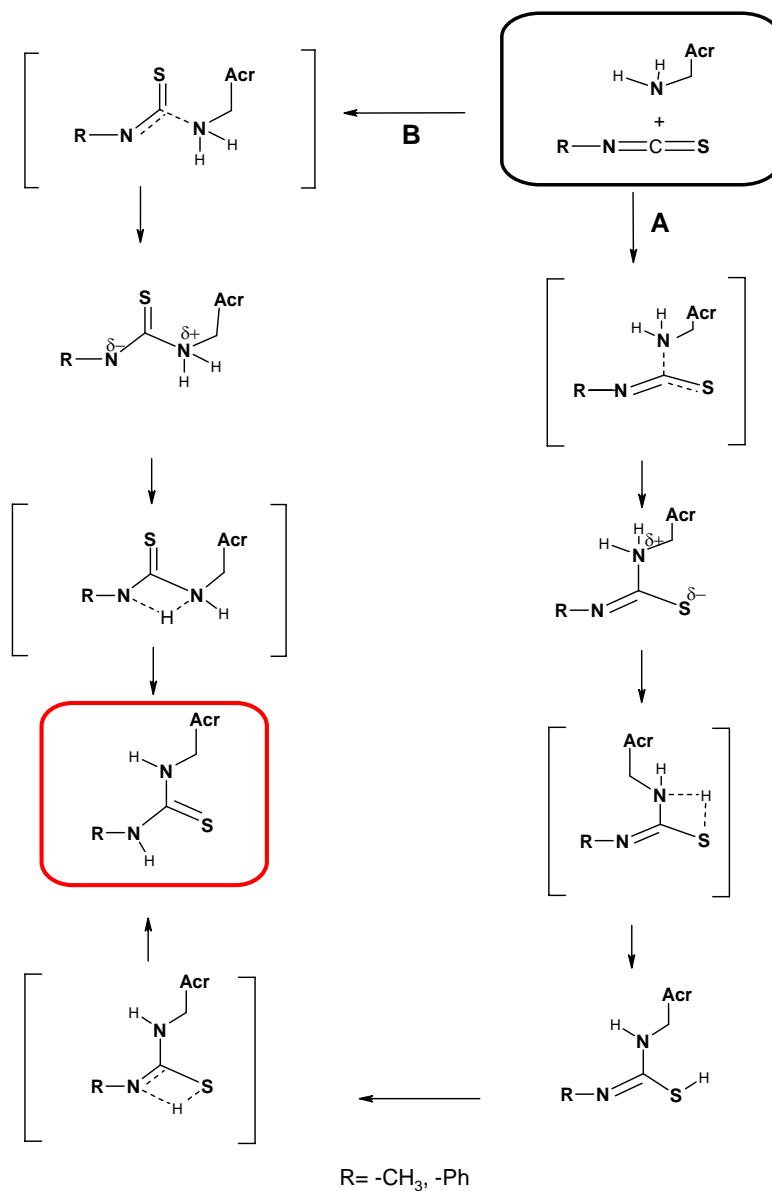
Reaction coordinate is a geometric parameter that changes during the conversion of one (or more) reactant molecular entities into one (or more) product molecular entities and whose value can be taken for a measure of the progress of an elementary reaction (for example, a bond length or bond angle or a combination of bond lengths and/or bond angles; it is sometimes approximated by a non-geometric parameter, such as the bond order of some specified bond). In the formalism of ‘transition-state theory²⁰’, the reaction coordinate is that coordinate in a set of curvilinear coordinates obtained from the conventional ones for the reactants which, for each reaction step, leads smoothly from the configuration of the reactants through that of the transition state to the configuration of the products. The reaction coordinate is typically chosen to follow the path along the gradient (path of shallowest ascent/ deepest descent) of potential energy from reactants to products.

Following the data about Ad_N reactions of isothiocyanates and analogous reactions of isocyanates,^{12,21} the two possible reaction courses were suggested:

- I. synchronous mechanism across N=C or C=S bond (Scheme 8)
- II. consecutive mechanism across N=C or C=S bond (Scheme 9)



Scheme 8 Synchronous mechanism: A. Addition across C=S bond
B. Addition across N=C bond



Scheme 9 Step-wise mechanism: A. Addition across C=S bond

B. Addition across N=C bond

1.7.1 Synchronous Mechanism

In the first part the synchronous reaction mechanism I was modeled, where the thiourea is formed in the first step via the synchronous transition state (Figure 1.1).

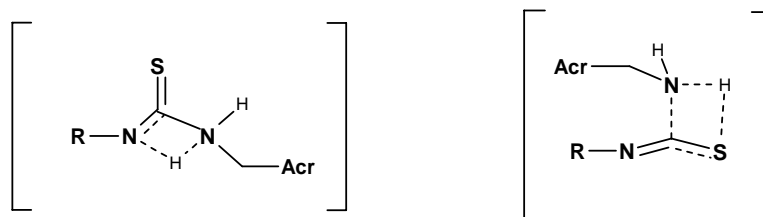


Figure 1.1 Synchronous attack to the N=C and C=S bond of the isothiocyanate

All attempts to find these transition states failed, resulting in the separation of the reactants. This observation led to the conclusion that the formation of the thiourea does not occur via these transition states, probably due to the need of high degree of alignment of such transition geometries.

1.7.2 Consecutive Mechanism

1.7.2.1 Nucleophilic Addition to the N=C Bond of Isothiocyanates

Gas phase calculations of the step-wise pathway were more successful and all assumed stationary points on the PES have been found (Figure 1.2, 1.3). Calculations both with methyl and phenyl revealed the same reaction course: in the first step the nucleophilic amine nitrogen attacks the partially positively charged NCS carbon atom and the ionic intermediate **II** is formed via transition state **TsI**. This zwitterionic species is relatively high on the energy profile (Table 1.1) and can be stabilized by the subsequent proton transfer via **TSII**. The result of this process is the desired thiourea **III**. Calculated reaction enthalpies indicate in both cases the exothermic reaction (Table 1.1). Negative values of Gibbs free energies outline the spontaneous reaction course (Figure 1.4). Formation of the C-N bond is in both cases the rate-determining step (Table 1.2). The phenyl substitution causes an increase in the activation barrier of all processes.

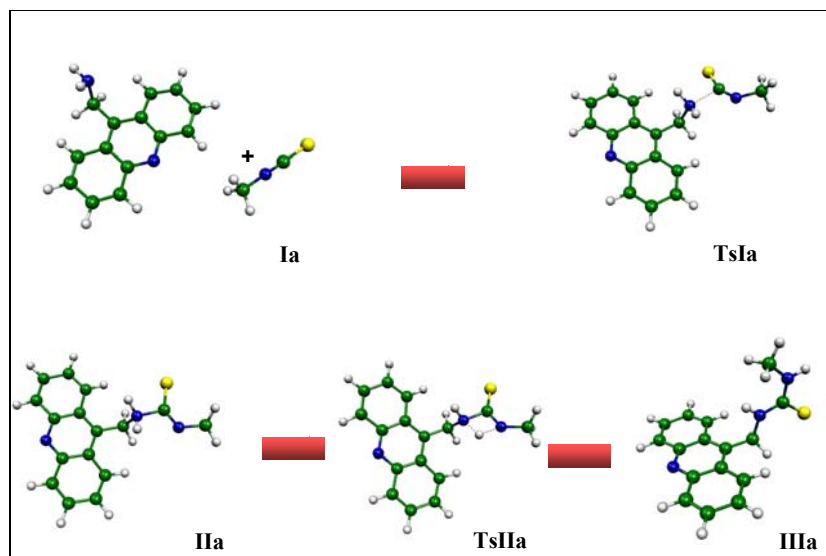


Figure 1.2 HF/6-31+G(d) stationary points on the reaction coordinate: addition to N=C bond of the CH₃-N=C=S

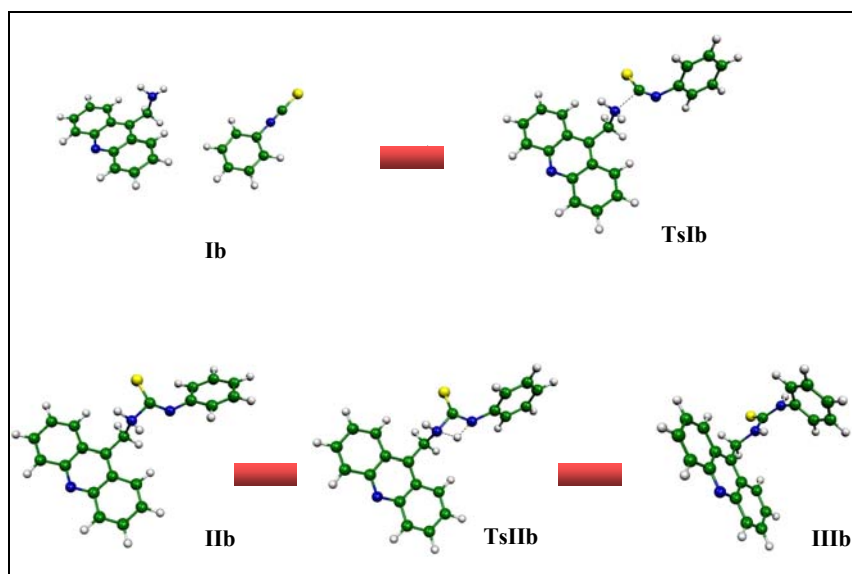


Figure 1.3 HF/6-31+G(d) stationary points on the reaction coordinate: addition to N=C bond of the Ph-N=C=S

R	CH ₃			Ph		
Process	ΔE^\ddagger	ΔH^\ddagger	ΔG^\ddagger	ΔE^\ddagger	ΔH^\ddagger	ΔG^\ddagger
I	0.00	0.00	0.00	0.00	0.00	0.00
TsI	22.56	22.05	33.49	28.52	27.36	43.84
II	14.21	13.37	26.49	15.27	14.72	27.78
TsII	41.16	40.26	53.15	48.26	47.29	61.74
III	-16.45	-17.12	-4.56	-16.46	-16.76	-5.10

Table 1.1 Calculated relative energies (relative to separated reactants) including zero-point-energy correction (ZPE) $\Delta E_{\text{rel.}}^\ddagger$, enthalpies $\Delta H_{\text{rel.}}^\ddagger$, and Gibbs free energies $\Delta G_{\text{rel.}}^\ddagger$, on HF/6-31+G(d) level. All values are in kcal/mol.

R	CH ₃			Ph		
Process	ΔE^\ddagger	ΔH^\ddagger	ΔG^\ddagger	ΔE^\ddagger	ΔH^\ddagger	ΔG^\ddagger
I→TS I	22.56	22.05	33.49	28.52	27.36	43.84
II→TS II	26.94	26.89	26.65	32.98	32.56	33.96

Table 1.2 Computed activation energies ΔE^\ddagger (including ZPE), enthalpies ΔH^\ddagger and Gibbs free energies ΔG^\ddagger on HF/6-31+G(d) level. All values are in kcal/mol.

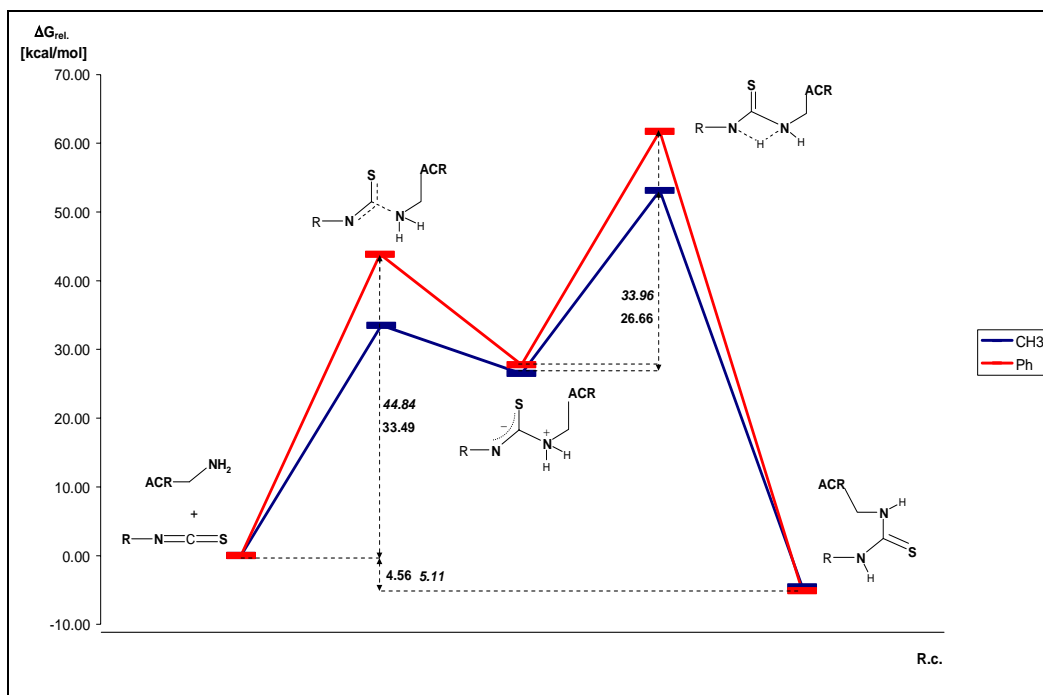


Figure 1.4 Addition to N=C bond. Substituent effect on the energy reaction profile at HF/6-31+G(d) level. Values for the Phenyl substituent are displayed in *italics*.

1.7.2.2 Nucleophilic Addition to the C=S Bond of Isothiocyanates

Another way of reactants to product transformation could be via the nucleophilic addition to the C=S bond of isothiocyanates. Reaction path simulations suggested in both methyl and phenyl case the following reaction mechanism (Figure 1.5, 1.6): in the first step the nucleophilic amine nitrogen reacts with the reactive carbon center of the isothiocyanate group and an ionic intermediate **IV** is formed via transition state **TS III**. This process is followed by the intramolecular proton transfer (**TS IV**) to the terminal sulphur atom of the NCS moiety which yields the isothiourea isomer **V**. Intermediate **V** does not have the proper geometry for the further reaction continuance and needs to undergo fast rotation around the C-S single bond (**TS V**). The reaction proceeds then from the isothiourea isomer **VI** via intramolecular proton transfer (**TS VI**) to the desired thiourea derivate **III**.

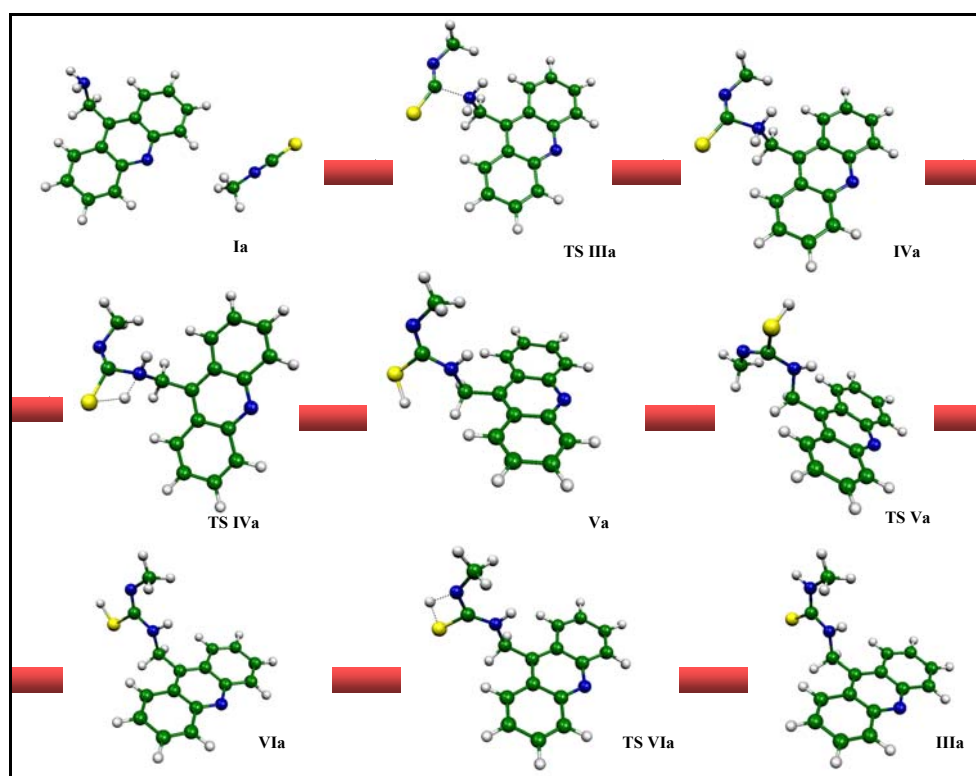


Figure 1.5 HF/6-31+G(d) stationary points on the reaction coordinate: addition to C=S bond of the $\text{CH}_3\text{-N=C=S}$

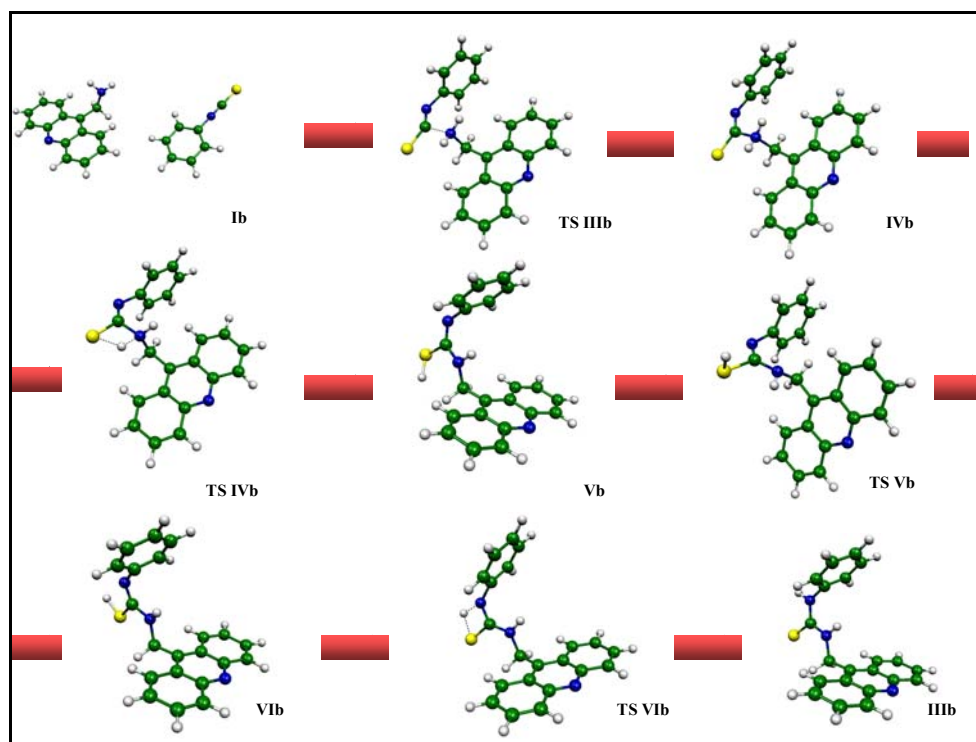


Figure 1.6 HF/6-31+G(d) stationary points on the reaction coordinate: addition to C=S bond of Ph-N=C=S

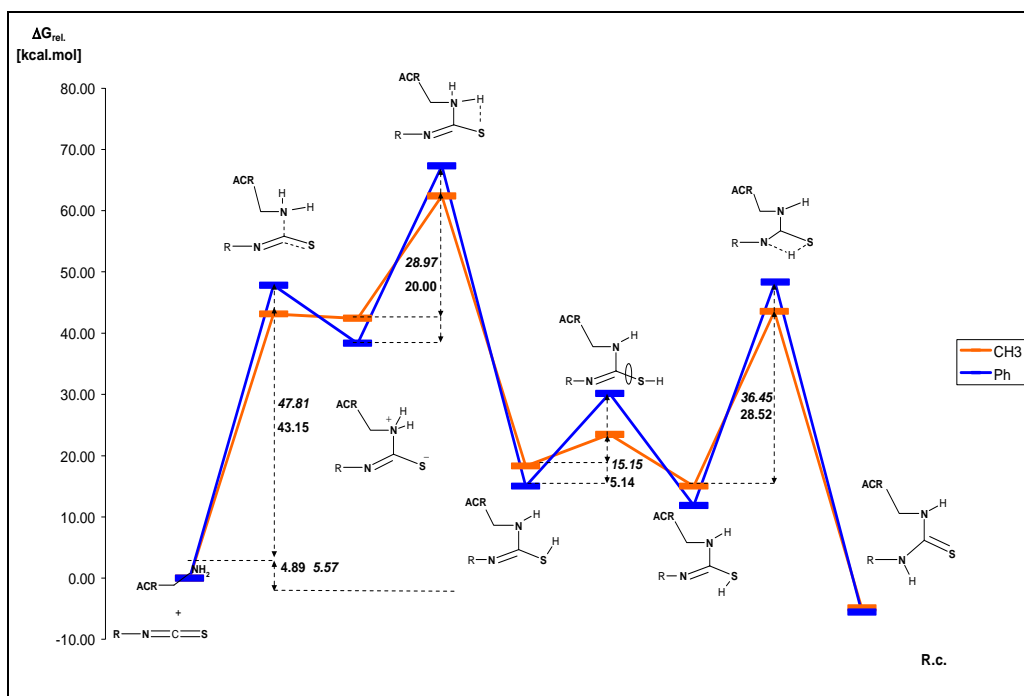


Figure 1.7 Addition to the C=S bond. Substituent effect on the energy reaction profile at HF/6-31+G(d) level. Values for the Phenyl substituent are displayed in *italic*.

R	CH ₃			Ph		
Process	ΔE^\ddagger	ΔH^\ddagger	ΔG^\ddagger	ΔE^\ddagger	ΔH^\ddagger	ΔG^\ddagger
I	0.0000	0.0000	0.0000	0.0000	0.0000	0.00
TS III	30.87	30.11	43.15	33.22	32.45	47.80
IV	30.97	30.21	43.47	24.88	24.34	38.34
TS IV	49.45	48.42	62.41	52.25	51.27	67.31
V	6.41	5.95	18.31	3.54	3.46	15.00
TS V	11.07	10.17	23.45	15.55	14.70	30.16
VI	2.91	2.38	15.02	-0.10	-0.26	11.87
TS VI	31.92	31.18	43.54	34.35	33.55	48.32
III	-16.76	-17.42	-4.89	-16.82	-17.13	-5.57

Table 1.3 Calculated relative energies (relative to separated reactants) including zero-point-energy correction (ZPE), ΔE_{rel} , and Gibbs free energies ΔG_{rel} on HF/6-31+G(d) level. All values are in kcal/mol.

R	CH ₃			Ph		
Process	ΔE^\ddagger	ΔH^\ddagger	ΔG^\ddagger	ΔE^\ddagger	ΔH^\ddagger	ΔG^\ddagger
I \rightarrow TS III	30.87	30.11	43.15	33.22	32.45	47.80
IV \rightarrow TS IV	22.45	18.20	19.99	32.88	26.93	28.96
V \rightarrow TS V	4.65	4.22	5.13	12.00	11.24	15.15
VI \rightarrow TS VI	29.00	28.80	28.52	34.45	33.82	36.45

Table 1.4 Computed activation energies ΔE^\ddagger (including ZPE), enthalpies ΔH^\ddagger and Gibbs free energies ΔG^\ddagger on HF/6-31+G(d) level. All values are in kcal/mol.

Comparison of the energy barriers (Table 1.4) revealed again that phenyl substitution leads to the higher activation energies compared to the reaction with methylisothiocyanate. Direct comparison of activation energies ΔE^\ddagger and Gibbs free energies ΔG^\ddagger can be used to address the question about most probable reaction mechanism. Results (Tables 1.2, 1.4) clearly show the preference for the nucleophilic addition of acridin-9-ylmethylamine to N=C bond of the studied isothiocyanates which is in agreement with the theoretical and experimental results for similar reactions of isothiocyanates and cyanates^{12, 22}.

1.7.3 The Effect of Electron Correlation

Two sources of uncertainty in the calculated reaction pathways and energetics consists in applying Hartree-Fock methods for the simulations of proton transfer (PT) and the non-inclusion of the solvent effects.

Hartree-Fock methods usually provide reasonably good agreement with the experimental structural parameters and relative energies of stable molecules^{1, 23}. However, the most significant drawback of the HF scheme is its neglect of the electron correlation making this method insufficient for quantitative predictions as well as for accurate modeling of processes like bond dissociation, dispersive effects and proton transfer²⁴.

Accurate calculations of proton transfer barriers still remain a challenge to quantum chemistry. To properly describe the proton transfer, methods including some effects of electron correlation are necessary. Density functional theory (DFT) and post-Hartree-Fock (e.g. MP2^{25, 26}) methods are known to give reliable geometric and thermodynamic properties for such systems²⁷.

It has to be also noted, that HF approach tends to overestimate the barrier heights for proton transfer transition states and the corresponding values would be probably significantly lower on other more appropriate level of theory (e.g. MP level)^{28, 29}. However, in some cases, HF methods are still able provide chemically meaningful results^{24, 30, 31} even for such theory-sensitive processes such as the proton transfer³²⁻³⁴. To verify that conclusions drawn from the HF calculations were not affected by the mentioned limitations, smaller model system was investigated – the reaction of the methylisothiocyanate with ammonia (Figure 1.8).

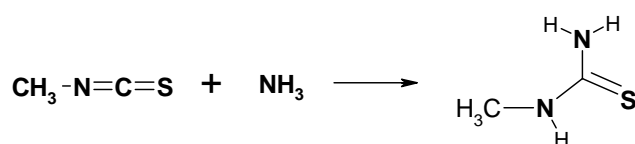


Figure 1.8 Model reaction for DFT calculations

To gain a deeper insight for the dependence of calculated proton transfer barriers on the level of theory employed, the calculations were performed both on HF/6-31++G(d,p)

level and with the Becke's three-parameter hybrid functional based on the correlation functional of Lee, Yang, and Parr (B3LYP³⁵) with the 6-31++G(d,p) basis set. All stationary points were fully optimized and verified by the vibrational analysis. Results of these calculations are shown in the Figures 1.9, 1.10, 1.11 and 1.12. Simulations on this level of theory showed similar reaction pathways to the HF calculations. However, **TsIII*** is a synchronous transition state corresponding to the simultaneous formation of the C \cdots N and S \cdots H bonds between methylisothiocyanate and ammonia, respectively. All attempts to find the intermediate similar to the **IVa** from the HF calculations led to the separation of both species. On the B3LYP level, the reaction across C=S bond is thus predicted to initiate via synchronous transition state **TsIII***.

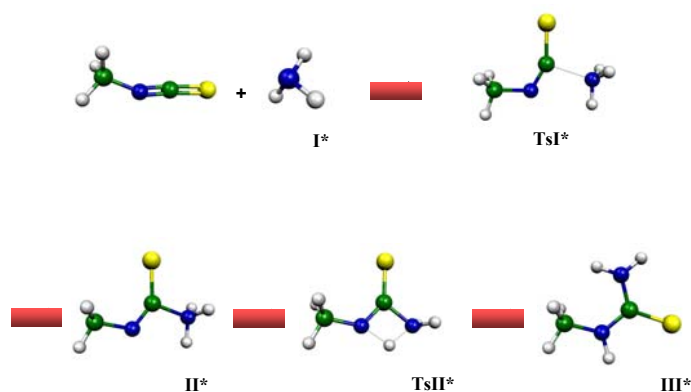


Figure 1.9 B3LYP/6-31++G(d,p) stationary points on the reaction coordinate: NH₃ addition to N=C bond of CH₃-N=C=S

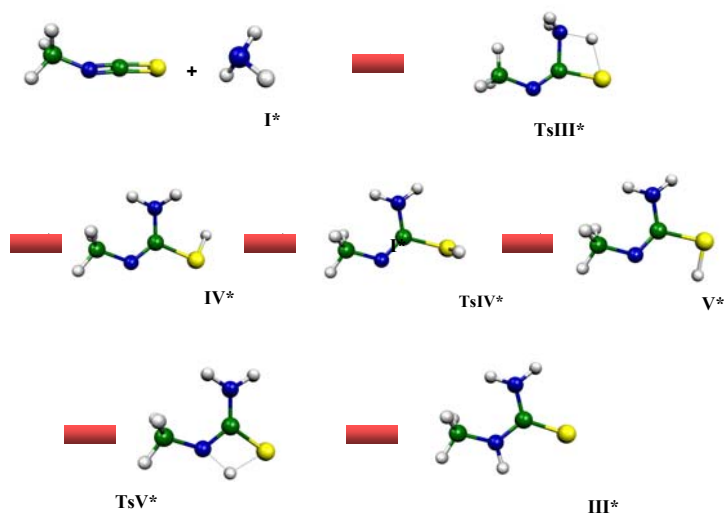


Figure 1.10 B3LYP/6-31++G(d,p) stationary points on the reaction coordinate: NH_3 addition to C=S bond of $\text{CH}_3\text{-N=C=S}$

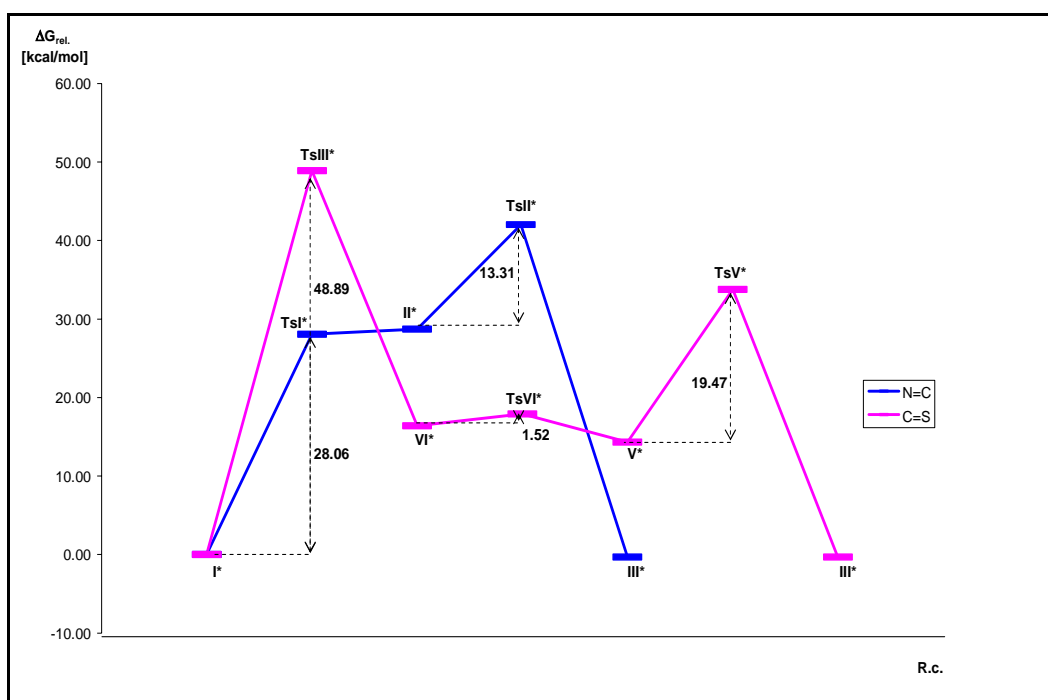


Figure 1.11 Addition to N=C and C=S bond. Comparison of reaction pathways at the B3LYP/6-31++G(d,p) level

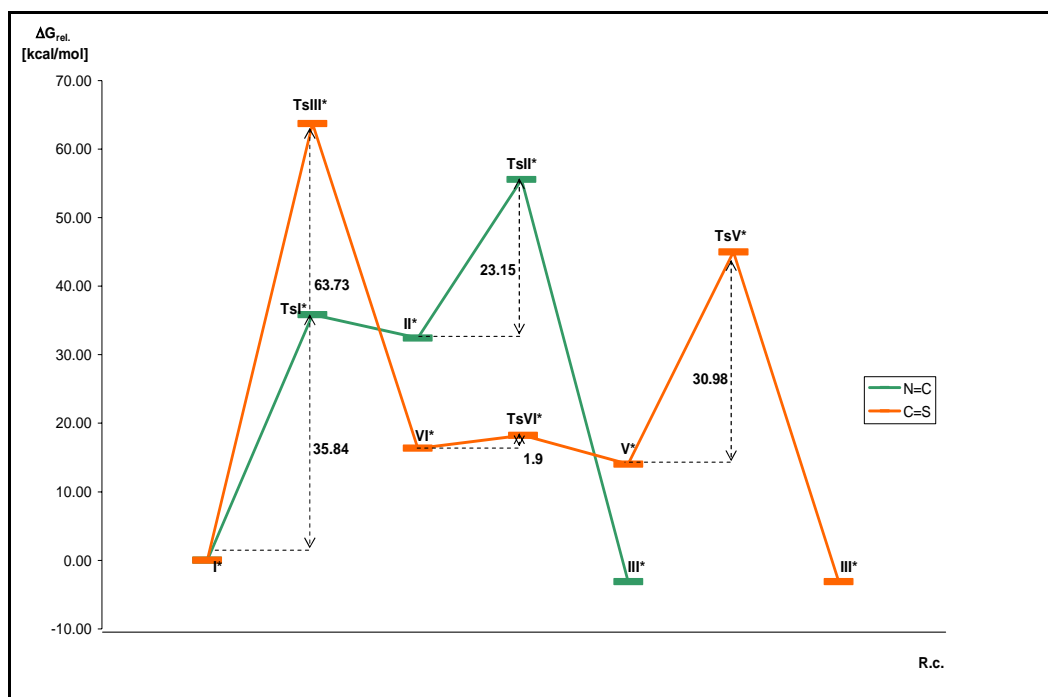


Figure 1.12 Addition to N=C and C=S bond. Comparison of reaction pathways at the HF/6-31++G(d,p) level.

Process	B3LYP/6-31++G(d,p)			HF/6-31++G(d,p)		
	ΔE^\ddagger	ΔH^\ddagger	ΔG^\ddagger	ΔE^\ddagger	ΔH^\ddagger	ΔG^\ddagger
I* \rightarrow Ts I*	18.25	17.04	28.05	26.38	25.14	35.84
II* \rightarrow Ts II*	13.17	12.82	13.31	22.97	22.69	23.15

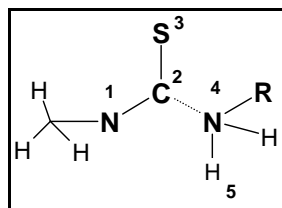
Table 1.5 Computed activation energies ΔE^\ddagger , enthalpies ΔH^\ddagger and Gibbs free energies ΔG^\ddagger on B3LYP/6-31++G(d,p) and HF/6-31++G(d,p) level for the N=C addition. All values are in kcal/mol.

Process	B3LYP/6-31++G(d,p)			HF/6-31++G(d,p)		
	ΔE^\ddagger	ΔH^\ddagger	ΔG^\ddagger	ΔE^\ddagger	ΔH^\ddagger	ΔG^\ddagger
I* \rightarrow Ts III*	37.35	35.51	48.89	52.86	51.00	63.73
IV* \rightarrow Ts IV*	1.15	0.79	1.51	1.55	1.18	1.90
V* \rightarrow Ts V*	19.68	19.56	19.46	31.06	30.90	30.98

Table 1.6 Computed activation energies ΔE^\ddagger (including ZPE), enthalpies ΔH^\ddagger and Gibbs free energies ΔG^\ddagger on B3LYP/6-31++G(d,p) and HF/6-31++G(d,p) level for the C=S addition. All values are in kcal/mol.

HF methods are known to overestimate heights of energy barriers²⁸. The results on both levels of theory indicate that HF barriers are too high by 5-7 kcal/mol for transition states

of C...N bond formation and approximately 10 kcal/mol for the proton transfer, respectively.



	Ts I		II		Ts II		III	
	HF	B3LYP	HF	B3LYP	HF	B3LYP	HF	B3LYP
N1-C2	1.210	1.244	1.251	1.293	1.287	1.328	1.340	1.358
C2-S3	1.644	1.640	1.707	1.670	1.667	1.647	1.692	1.684
C2-N4	2.012	1.952	1.522	1.560	1.485	1.513	1.338	1.365
N4-H5	1.003	1.017	1.008	1.025	1.281	1.263	-	-
N1-H5	-	-	-	-	1.331	1.358	0.995	1.009

Table 1.7 Characteristic geometry parameters of the “active site” stationary points optimized on HF/6-31+G(d) and B3LYP/6-31++G(d,p) level for addition to the N=C bond.

Calculations with the model system using density functional theory approach provided similar geometries of the “active part” of the system to those obtained by Hartree-Fock calculations (Table 1.7).

Comparison of the activation barriers (Tables 1.5 and 1.6) of this model reaction revealed again the preference for the addition to the N=C bond of the CH₃-N=C=S which agrees with conclusions from HF level, giving a confidence that despite known limitations, this approach can be used for the qualitative prediction of the reaction mechanism for this studied reaction.

1.7.4 Solvation Effects

All calculations considered so far were performed in the gas phase. However, solvent-solute interactions play a significant role in the chemical reactions. In the case of the reaction between isothiocyanates and acridin-9-ylmethylamine, solvent (chloroform, $\epsilon=4.8$) acts as a bulk medium but can still significantly affect the solute behaviour. The

continuum reaction field^{4, 36} models are usually used to describe the solution environment, because they have been proven quite successful in many applications^{37, 38}. The solvent effects were modeled using the Tomasi's polarized continuum model (PCM)^{39, 40} as implemented in Gaussian 03.⁴¹⁻⁴⁴ All stationary points were fully optimized in the field of chloroform applying PCM HF/6-31+G(d) method and verified by final frequency calculations at the same level of the theory.

Results confirmed again the preference for the addition across N=C bond of the isothiocyanates. Due to the similar reaction pathways to HF/DFT calculations and relevance for the further reaction course, only data for NC addition are presented (Table 1.8). The same trend of phenyl substitution on energy barriers after inclusion of solvent effect is observed (Figure 1.13). The calculated relative energies change most significantly for the intermediate **II** in the polar media (Tables 1.1 and 1.8). Zwitterionic species are traditionally very high on the PES in the gas phase.

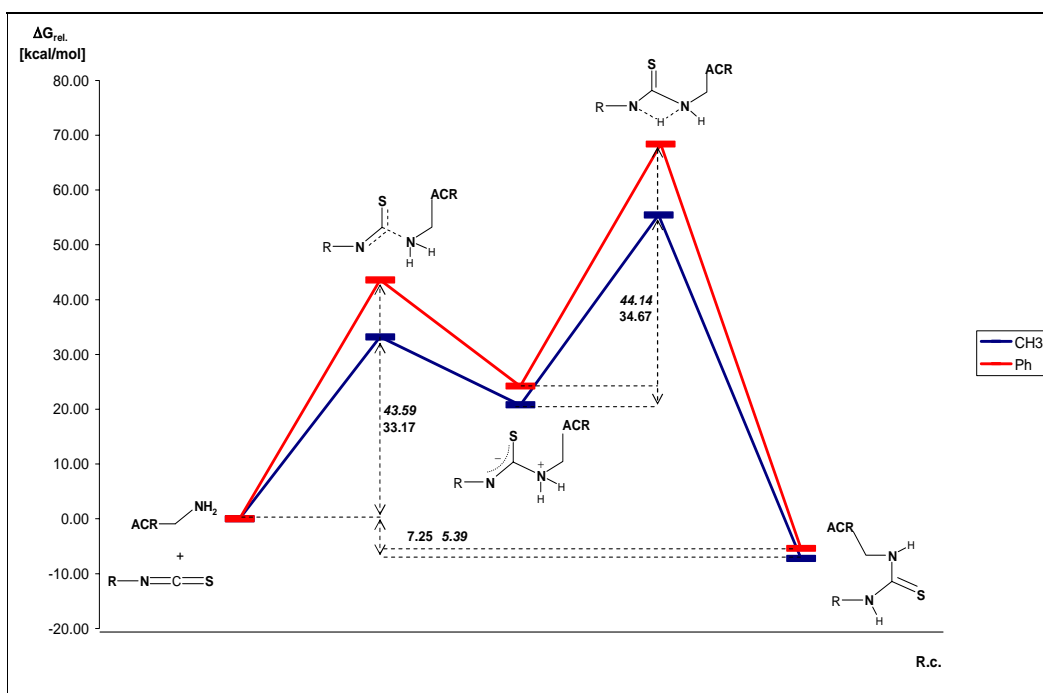


Figure 1.13 Addition to the N=C bond. Substituent effect on the energy reaction profile at PCM HF/6-31+G(d) level. Values for the Phenyl substituent are displayed in *italic*.

R	CH ₃			Ph		
Process	ΔE^\ddagger	ΔH^\ddagger	ΔG^\ddagger	ΔE^\ddagger	ΔH^\ddagger	ΔG^\ddagger
Is	0.00	0.00	0.00	0.00	0.00	0.00
TsIs	21.74	21.24	33.16	28.66	27.48	43.58

IIs	7.98	7.03	20.78	10.34	9.14	24.22
TsIIIs	42.53	41.45	55.45	52.01	50.32	68.36
IIIIs	-19.74	-20.57	-7.24	-18.06	-18.56	-5.39

Table 1.8 Calculated relative energies (relative to separated reactants) including zero-point-energy correction (ZPE), ΔE_{rel} , and Gibbs free energies ΔG_{rel} on PCM HF/6-31+G(d) level. All values are in kcal/mol.

The solute-solvent interactions stabilize such ionic intermediates in the polar solvents leading to the lower relative energies compared with gas phase calculations. PCM model also predicts thiourea derivatives **III** to be more stable in the solution environment (Tables 1.1 and 1.8). It is clear from activation barriers (Tables 1.9, 1.10) that solvent has only small effect on the barrier height of transition states **TS I**, whereas very strong solvent effect on the activation energy of proton transfer (**TS II**) has been observed. When going from gas phase to solution, the activation energy of proton transfer is increased by about 7 kcal/mol for the methyl and 9 kcal/mol for the phenyl substituent, respectively.

Process	$\epsilon=1.0$			$\epsilon=4.8$		
	ΔE^\ddagger	ΔH^\ddagger	ΔG^\ddagger	ΔE^\ddagger	ΔH^\ddagger	ΔG^\ddagger
I → TS I	22.56	22.05	33.49	21.74	21.24	33.16
II → TS II	26.94	26.89	26.65	34.55	34.42	34.67

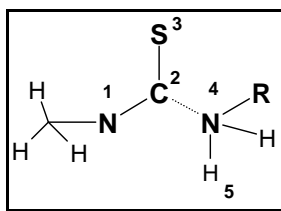
Table 1.9 Computed activation energies ΔE^\ddagger (including ZPE), enthalpies ΔH^\ddagger and Gibbs free energies ΔG^\ddagger in vacuo ($\epsilon=1.0$) and chloroform ($\epsilon=4.8$) for the reaction $\text{CH}_3\text{-N=C=S} + \text{ACR-CH}_2\text{-NH}_2$. Values are in kcal/mol.

Process	$\epsilon=1.0$			$\epsilon=4.8$		
	ΔE^\ddagger	ΔH^\ddagger	ΔG^\ddagger	ΔE^\ddagger	ΔH^\ddagger	ΔG^\ddagger
I → TS I	28.52	27.36	43.84	28.66	27.48	43.58
II → TS II	32.98	32.56	33.96	41.67	41.18	44.13

Table 1.10 Computed activation energies ΔE^\ddagger (including ZPE), enthalpies ΔH^\ddagger and Gibbs free energies ΔG^\ddagger in vacuo and solution (chloroform) for the reaction $\text{Ph-N=C=S} + \text{ACR-CH}_2\text{-NH}_2$. Values are in kcal/mol.

The main reason for the observed solvent effect is apparently the larger stabilization of the intermediate **II** in chloroform.

The geometry changes induced by the solvent continuum are small. Table 1.11 summarizes the characteristic geometry parameters in the gas phase and in the solution.



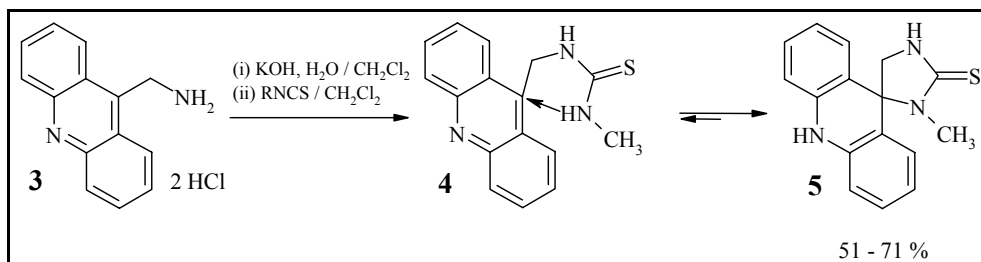
	R=CH ₃		Ts I		II		Ts II		III	
	ε=1.0	ε=4.8	ε=1.0	ε=4.8	ε=1.0	ε=4.8	ε=1.0	ε=4.8	ε=1.0	ε=4.8
N1-C2	1.210	1.203	1.251	1.249	1.287	1.284	1.340	1.329		
C2-S3	1.644	1.647	1.707	1.724	1.667	1.674	1.692	1.714		
C2-N4	2.012	2.060	1.522	1.508	1.485	1.477	1.338	1.332		
N4-H5	1.003	1.007	1.008	1.015	1.281	1.295	-	-		
N1-H5	-	-	-	-	1.331	1.329	0.995	0.996		

	R=Ph		Ts I		II		Ts II		III	
	ε=1.0	ε=4.8	ε=1.0	ε=4.8	ε=1.0	ε=4.8	ε=1.0	ε=4.8	ε=1.0	ε=4.8
N1-C2	1.210	1.210	1.256	1.251	1.288	1.288	1.348	1.337		
C2-S3	1.644	1.644	1.703	1.715	1.667	1.667	1.690	1.711		
C2-N4	2.011	2.010	1.526	1.515	1.484	1.484	1.334	1.329		
N4-H5	1.003	1.002	1.009	1.015	1.273	1.270	-	-		
N1-H5	-	-	-	-	1.326	1.328	0.996	1.005		

Table 1.11 Geometry parameters of the stationary points optimized in the gas phase and in the solution. Transition interatomic distances are in red.

1.8 Spirocyclisation of Acridin-9-ylmethyl thioureas

In the second part of this study, the spontaneous spirocyclisation of prepared thioureas was investigated (Scheme 10). The simulations of the reaction pathway were based on the experimental conditions and the monitoring of thiourea → final spirocompound conversion. The Table 1.12 and the Figure 1.14 show the overall reaction course and the ratio between the reactants, thiourea intermediate and the products.



Scheme 10

Time (min.)	3(%)	4(%)	5(%)
0	100.0	0	0
5	16.7	77.8	5.5
10	3.3	86.7	10.0
15	1.2	83.3	15.5
30	0	80.0	20.0
90	0	62.5	37.5
330	0	31.0	69.0
1440	0	16.7	83.3
2400	0	0	100

Table 1.12 Ratio (%) between the reactant, the intermediate and the product during the reaction course.

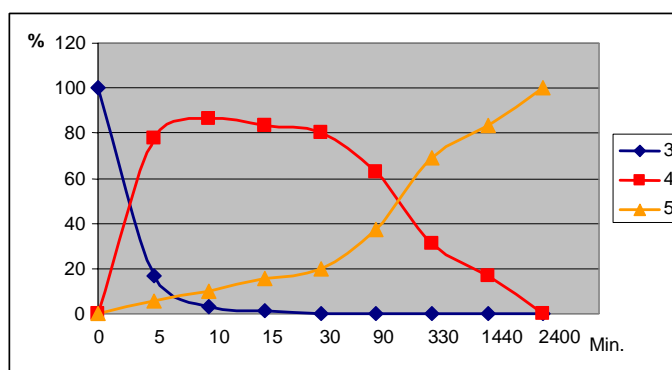
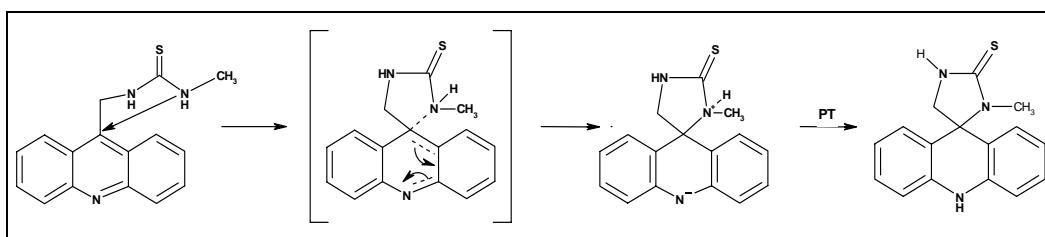


Figure 1.14 Conversion reactants → products

The experimental data presented in the Table 1.12 were provided by the collaborators from the Chemistry Department of the Pavol Jozef Safarik University. In proton NMR a signal of methylene group bound on acridine proved to be a valuable indicator of the

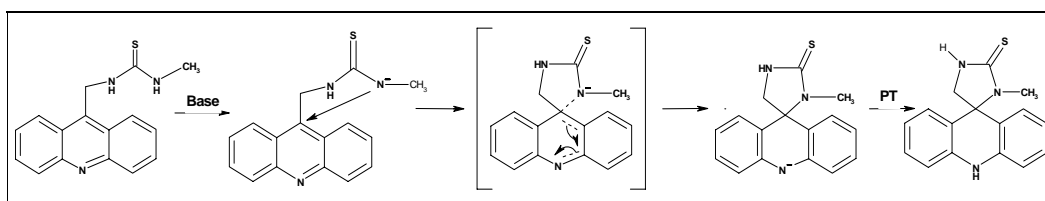
structure changing from a doublet in the case of thioureas **4** to a singlet of **5**. The transformation of thiourea **4** into **5** was monitored by NMR spectroscopy. The initial substance (Acridin-9-ylmethylamine) is consumed after 30 minutes (Table 1.12) and the reaction mixture contains 80% of thiourea and 20% of the product. As shown, the **4** is still left in the reaction mixture in a 16.7% content after 24 h standing in a NMR tube at room temperature. The conversion of thiourea intermediate to the product then continues and is accomplished after 40 hours. Considering these observations, following mechanisms were modeled:

1. Direct nucleophilic attack of the α -nitrogen of the thiourea:



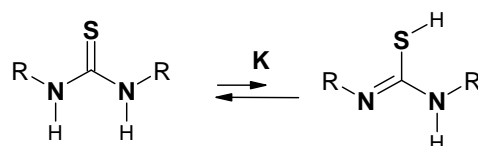
All attempts to find the corresponding stationary points failed and led back to the thiourea derivative. The observation could be explained by the insufficient nucleophilicity of the α -nitrogen of the thiourea.

2. Calculations with the negative charge on the α -nitrogen of the thiourea were more successful and all stationary points were found:

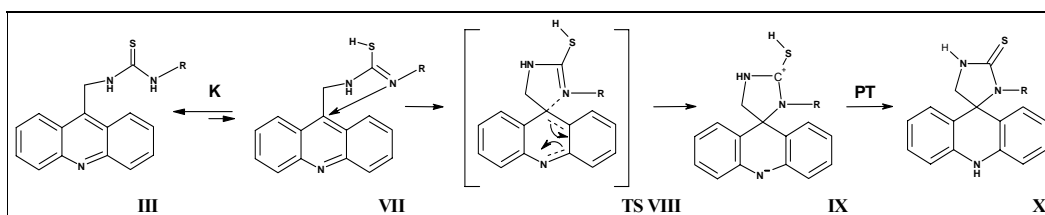


However, considering reaction condition (chloroform as a solvent) in the absence of the strong base, this conversion path seemed unlikely and was excluded from the consideration.

3. More promising were simulations with the thiol derivate of thiourea. Thiourea is known to exist in two tautomeric forms: thiourea and isothiurea:



The following mechanism was suggested, where the thiol tautomer of thiourea plays a key role in the conversion to the final product:



This hypothesis was further confirmed by experimental observations. The treatment of the reaction mixture after 30 minutes with sodium hydride and methyl bromoacetate yielded thiazolidinone **8** (Figure 1.15).

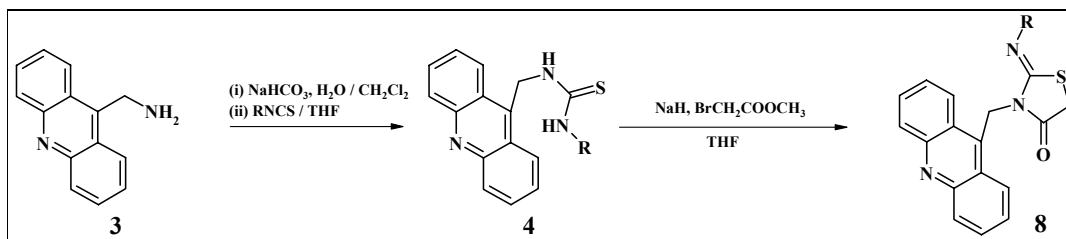


Figure 1.15 Reaction of Acridin-9-ylmethyl thioureas with methyl bromoacetate

It is assumed, that thiourea is formed during the reaction course. Based on previous studies^{45, 46}, the following mechanism was proposed, where the sulphur form the tautomeric form **4'** attacks α -carbon of methyl bromoacetate displacing the bromide ion

and forming the intermediate S-(methoxycarbonyl)methyl isothiurea **6** (Figure 1.16). Subsequent intramolecular nucleophilic attack by the nitrogen yields the product **8**.

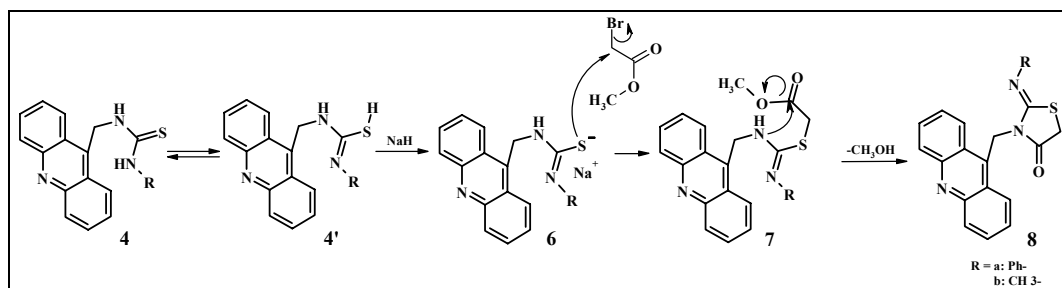


Figure 1.16 Suggested mechanism of the reaction between Acridin-9-ylmethyl thioureas and methyl bromoacetate

The proton transfer (PT) transition states were not modeled due to the already mentioned theoretical and computational limitations as well as uncertainties about the mechanism of this process. It has not been found out yet, how the proton is transferred from the imidazolidine ring to the acridine nitrogen. From the current knowledge of PT reactions⁴⁷⁻⁴⁹ and the geometry of the intermediate **IX** (Figure 1.17) it was assumed, that probably other molecule of acridine is involved in this proton transfer. Whether this process occurs in the concerted fashion via cyclic transition state, or gradually involving two mediator molecules, still remains unknown. Moreover, there is increasing evidence for the solvent assisted proton transfer reactions even for such weak H-donors as a chloroform^{50, 51}. It has been found that CH groups can act as proton donors in hydrogen-bonded systems⁵²⁻⁵⁴ and can interact with proton donors like O, N, π -systems, X^- (halogen anions) forming $CH...O$, $CH...N$, $CH... \pi$ and $CH...X^-$ interactions⁵¹. For example, $CH...O$ interactions possess all characteristics of hydrogen bond, including complex properties such as cooperativity within hydrogen bond arrays⁵⁵. Which of the above mentioned processes takes place in the final protonation of the spirocyclic product remains unanswered. However, these proton transfers are supposed to be much faster than the formation of the imidazolidine ring via **TS VIII** and therefore are not expected to be crucial for the description of the whole reaction mechanism.

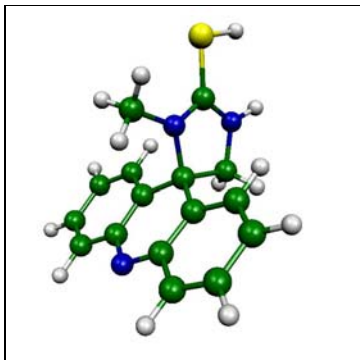


Figure 1.17 Intermediate IX

Simulations of this reaction pathway were performed both in the gas phase and solution (chloroform) on the HF/6-31+G (d) level. Figures 1.18 and 1.19 display the reaction profiles in the gas phase and chloroform. Crucial for this conversion is the formation of the imidazolidine ring **XI**. The inclusion of the solvent effects lowers the activation energy of this process (Table 1.15) which can be assigned to the more appropriate description of the transition state **TS VIII** in the solution environment. From Figures 1.18 and 1.19 is again apparent the stabilization effect of the polar medium on the zwitterionic intermediate **IX**. The intermediate **II** seems to play a crucial role in the whole transformation, since there are two ways of its stabilization: intramolecular proton transfer to the nitrogen atom or terminal sulphur atom of the isothiocyanate moiety, leading to the thiourea **III** or its tautomer isothioureia **VII** in the latter case (Figure 1.20). Calculated electrostatic potential suggested the possibility of such process (Figure 1.21).

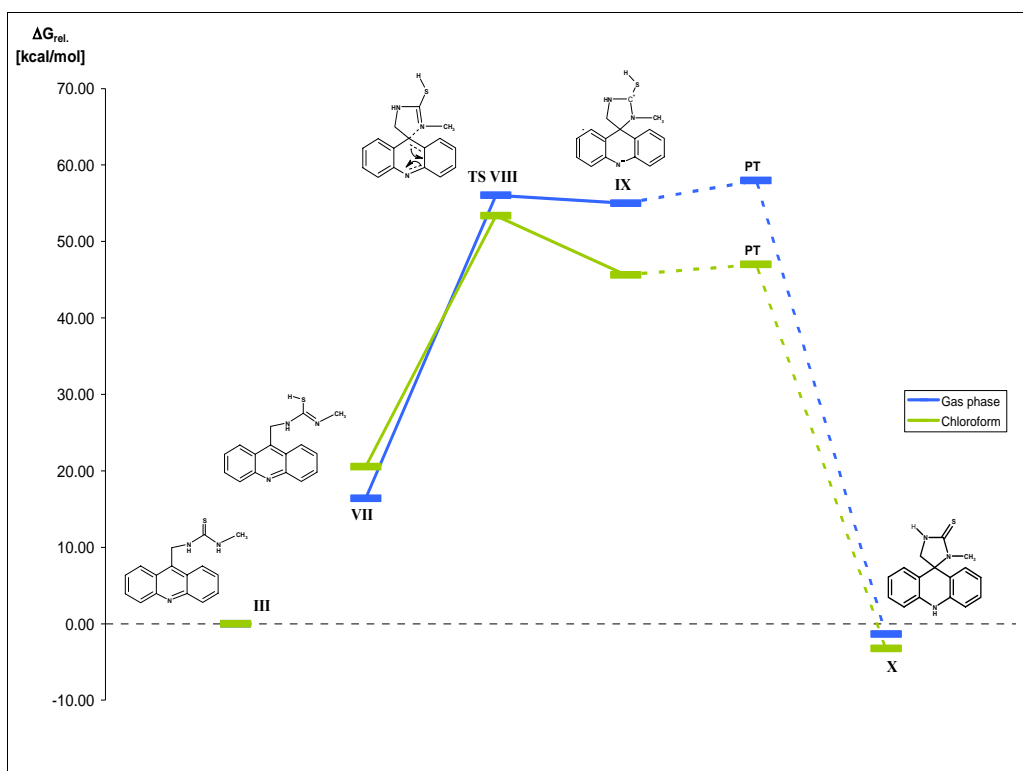


Figure 1.18 Spirocyclisation of the methyl isothiurea derivate.

R= CH ₃	$\epsilon=1.0$			$\epsilon=4.8$		
	ΔE^\ddagger	ΔH^\ddagger	ΔG^\ddagger	ΔE^\ddagger	ΔH^\ddagger	ΔG^\ddagger
III	0.00	0.00	0.00	0.00	0.00	0.00
VII	16.49	16.71	16.40	19.99	19.90	20.54
TS VIII	54.15	53.76	56.04	50.99	50.37	53.36
IX	53.36	53.20	55.00	44.74	44.63	45.63
X	-3.52	-4.13	-1.32	-4.89	-5.34	-3.23

Table 1.13 Calculated relative energies (relative to the thiourea derivate III) including zero-point-energy correction (ZPE), ΔE_{rel} , and Gibbs free energies ΔG_{rel} in the gas phase and chloroform on HF/6-31+G(d) level

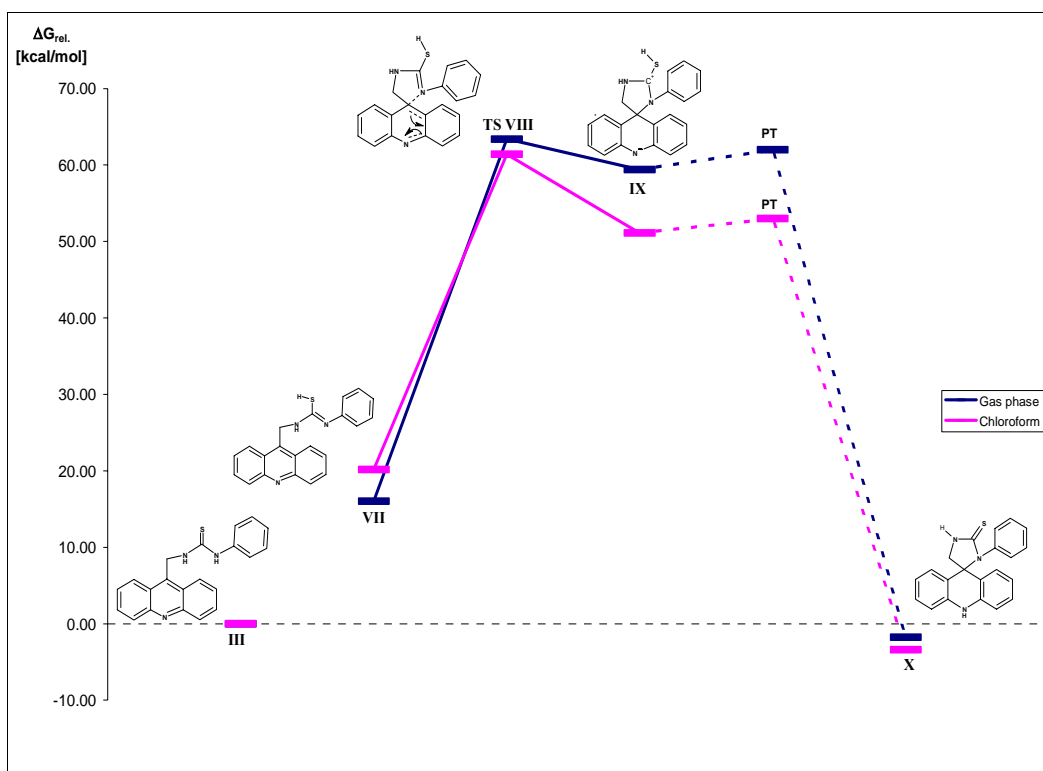


Figure 1.19 Spirocyclisation of the phenyl isothiourea derivate.

R= Ph	$\epsilon=1.0$			$\epsilon=4.8$		
Process	ΔE^\ddagger	ΔH^\ddagger	ΔG^\ddagger	ΔE^\ddagger	ΔH^\ddagger	ΔG^\ddagger
III	0.00	0.00	0.00	0.00	0.00	0.00
VII	15.05	15.22	16.02	17.55	16.85	20.16
TS VIII	58.88	58.14	63.40	56.79	55.76	61.41
IX	56.40	56.29	59.41	49.03	48.79	51.10
X	-3.43	-3.95	-1.77	-4.91	-4.48	-3.44

Table 1.14 Calculated relative energies (relative to the thiourea derivate III) including zero-point-energy correction (ZPE), ΔE_{rel} , and Gibbs free energies ΔG_{rel} in the gas phase and chloroform on HF/6-31+G(d) level.

R	CH ₃				Ph			
	$\epsilon=1.0$		$\epsilon=4.8$		$\epsilon=1.0$		$\epsilon=4.8$	
	ΔH^\ddagger	ΔG^\ddagger	ΔH^\ddagger	ΔG^\ddagger	ΔH^\ddagger	ΔG^\ddagger	ΔH^\ddagger	ΔG^\ddagger
VII → TS VIII	37.04	39.64	30.46	32.81	42.92	47.38	38.90	41.25

Table 1.15 Computed activation enthalpies ΔH^\ddagger (including ZPE) and Gibbs free energies ΔG^\ddagger in vacuo and solution (chloroform).

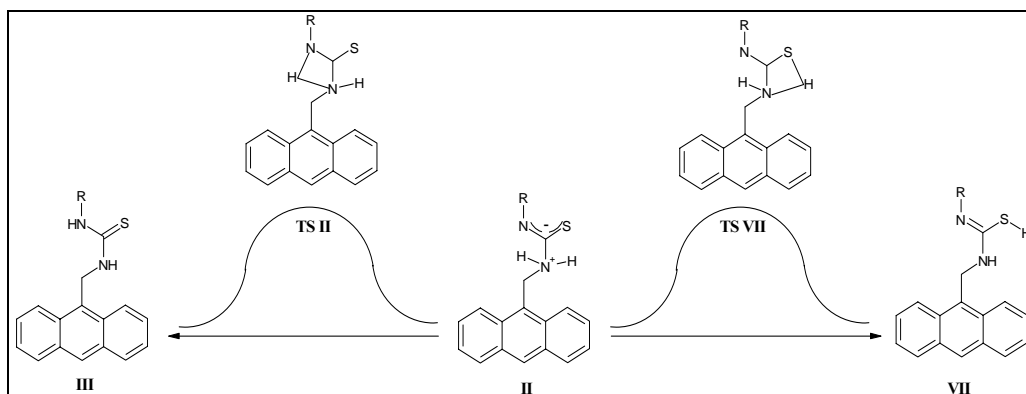


Figure 1.20 Reaction mechanisms leading to thione and thiol tautomeric form of thiourea.

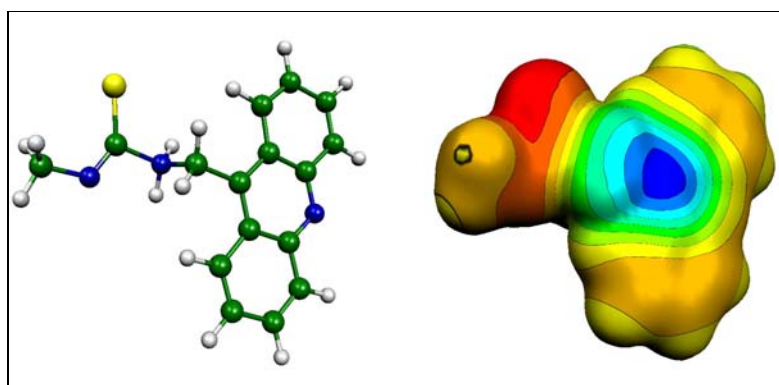


Figure 1.21 Intermediate II: Electrostatic potential mapped to the electron density. Red color corresponds to the negative electrostatic potential.

Modeling based on this assumption led indeed to the new transition state **TS VII** (Figure 1.22).

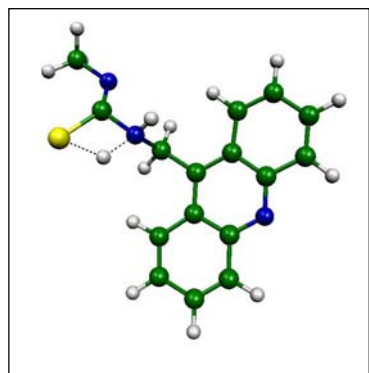


Figure 1.22 Transition state geometry TS VIIa

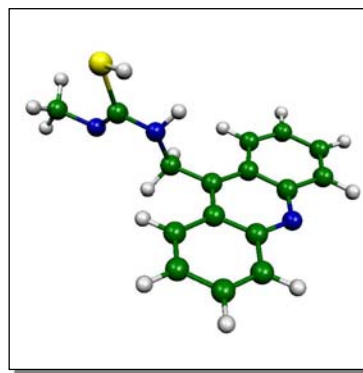


Figure 1.23 Thiol tautomer VIIa of thiourea

The reaction can proceed in two directions producing thione or thiol thiourea tautomer, respectively. Interestingly, calculations showed that both processes have essentially the same activation enthalpies and Gibbs free energies for the methyl derivate (Table 1.16, Figure 1.24) and the reaction should proceed with the same rate in both directions. In the case of Phenyl isothiocyanate is the situation different. The values of computed activation barriers support the hypothesis about the preference of the “thiol branch” of the reaction (Table 1.16) – activation enthalpies for **II**→**TS VII** are lower in both environments compared to **II**→**TS II** process. Despite the fact, that thione tautomer **III** is more stable (Figure 1.24), considering the transformation to the final spirocompound **X**, the reaction is in both cases exothermic and also spontaneous (Tables 1.13, 1.14).

R	CH ₃				Ph			
	ε=1.0		ε=4.8		ε=1.0		ε=4.8	
	ΔH [‡]	ΔG [‡]	ΔH [‡]	ΔG [‡]	ΔH [‡]	ΔG [‡]	ΔH [‡]	ΔG [‡]
II → TS VII	26.59	26.50	36.20	35.84	25.88	26.07	36.91	37.94
II → TS II	26.89	26.65	34.42	34.67	32.56	33.96	41.18	44.13

Table 1.26 Comparison of activation energies ΔE[‡] (including ZPE) and Gibbs free energies for the concurrent reaction pathways on HF/6-31+G(d) level.

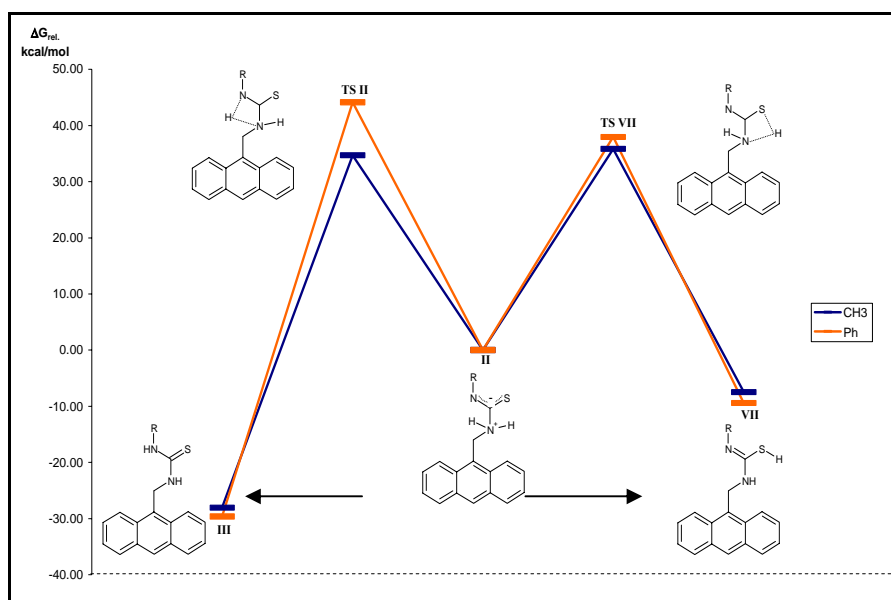


Figure 1.24 Thione ↔ thiol reaction course suggested by PCM HF/6-31+G(d) calculations.

This process drew more attention and transition states **TS II**, **TS VII** and local minima **II**, **III** and **VII** were also calculated in the gas phase on B3LYP/6-31+G* level to obtain more reliable thermochemistry informations, since the accuracy of desired parameters (rate constant *k* and equilibrium constant *K*) strongly depend on the accuracy of the method used for free energy computation⁵⁶.

The rate constants have been modeled using the following equation from the transition state theory²⁰:

$$k(T) = \frac{k_B T}{h} e^{-\frac{\Delta G^\ddagger}{RT}}$$

where k_B is the Boltzmann constant, h Planck's constant, R is the gas constant, T is temperature and ΔG^\ddagger is the change in the free energy of activation.

Computed enthalpies of activation are virtually the same (Table 1.17); this result can explain the detection of the spirocyclic product in the early stages of the reaction (Figure 1.13).

R	CH ₃			Ph			
	Process	ΔH^\ddagger	ΔG^\ddagger	<i>k</i>	ΔH^\ddagger	ΔG^\ddagger	<i>k</i>
	II→TS II	15.61	16.76	3.20	15.77	17.05	1.96
	II→TS VII	15.59	15.26	40.04	15.78	16.43	5.53

Table 1.17 Rate constants in the gas phase on B3LYP/6-31+G(d) at 298.15 K. Rate constants are in s⁻¹, ΔH and ΔG are in kcal/mol.

To investigate the equilibrium between thiourea **III**, intermediate **II** and isothiourea **VII**, the equilibrium constant *K* has also been calculated using the formula (Table 1.18):

$$K = e^{-\Delta G / RT}$$

Presented kinetic data show that the reaction proceeds faster towards the thiol tautomer. On the other hand, the thione tautomer is energetically more stable and the values of equilibrium constants show the preference for the thione thiourea tautomer relative to the thiol one, respectively (Table 1.18). However, the thiourea intermediate **III** is not reactive

and represents the ‘dead end’ of the reaction. Only its thiol form seems to be reactive enough to facilitate the final spirocyclisation. Whether this tautomerism occurs via the intermediate **II** or some other process takes place, remains unknown and would require further investigation.

R	CH ₃			Ph		
	ΔH	ΔG	K	ΔH	ΔG	K
VII ↔ III	-58.89	-51.85	1.22 × 10 ⁹	-48.33	-43.60	4.36 × 10 ⁷

Table 1.18 Equilibrium constants in the gas phase on B3LYP/6-31+G(d) at 298.15 K. ΔH and ΔG values are in kJ/mol.

As the reaction advances and final ring closure occurs, the formed spirocyclic compound becomes energetically more stable and is the product of this reaction (Figure 1.25).

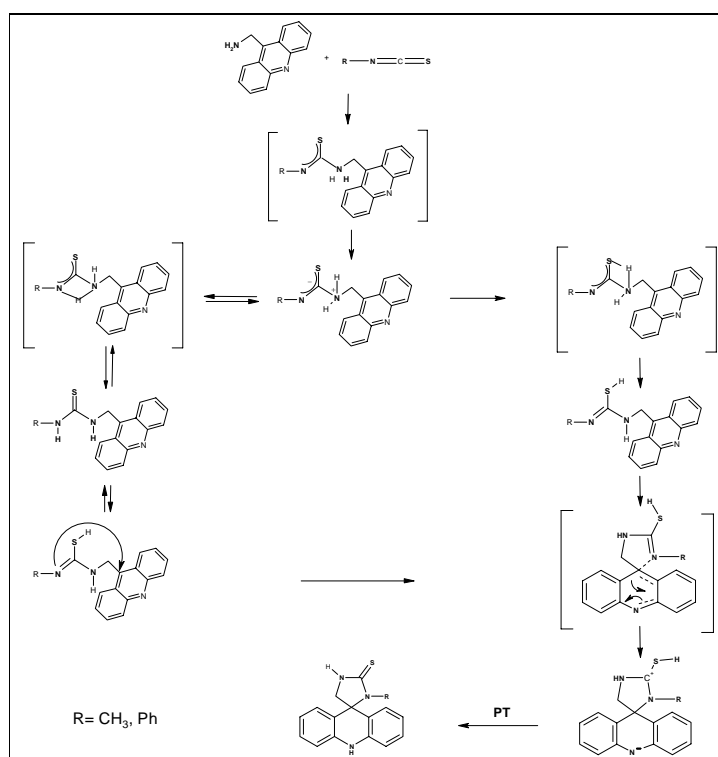


Figure 1.25 Suggested reaction scheme

1.9 Summary

In the light of experimental observations and theoretical calculations it is possible to draw the following conclusions about the reaction mechanism:

1. Initial nucleophilic addition of acridin-9-ylmethylamine occurs across the N=C bond of the corresponding isothiocyanate.
2. Reaction proceeds via the zwitterionic intermediate **II**, which can be stabilized by the proton transfer to the nitrogen or sulphur atom of the isothiocyanate moiety, producing thione or thiol tautomer of (acridin-9-ylmethyl)-3-methyl (phenyl) thiourea, respectively.
3. Only thiol intermediate is reactive enough and can further undergo cyclization yielding the spirocyclic product (spiro[dihydroacridine-9(10H),5'-imidazoline]-2'-thiones). The driving force of this transformation is the higher thermodynamic stability of the product relative to the concurrent thiourea intermediate (Figure 1.24, 1.19).

2 Computational Investigation of Thymine Dimers Incorporated into the DNA double strand

2.1 DNA Structure

Deoxyribonucleic acid (DNA) is a nucleic acid, which is capable of carrying genetic instructions for the biological development of all cellular forms of life and many viruses. Nucleic acid, so called because of its prevalence in cellular nuclei, is a generic name of a family of biopolymers. The monomers are called nucleotides, and each consists of three components: a nitrogenous heterocyclic base (either a purine or a pyrimidine), a pentose sugar, and a phosphate group. The two basic types of nucleic acids differ in the specific sugar found in their chain (e.g. DNA or deoxyribonucleic acid contains 2-deoxyriboses). The nitrogenous bases occurring in the two nucleic acids can also be diverse: adenine, cytosine, and guanine are found both in RNA and DNA, while thymine occurs exclusively in DNA and uracil in RNA.

The sugars and phosphates in nucleic acids are connected to each other in an alternating chain through shared oxygens (forming a phosphodiester functional group). Using the conventional nomenclature, the carbons to which the phosphate groups are attached are the 3' and the 5' carbons. The bases extend from a glycosidic linkage to the 1' carbon of the pentose ring.

Nucleic acids may be single-stranded or double-stranded. DNA is usually double-stranded, though some viruses have single-stranded DNA as their genome. A double-stranded nucleic acid consists of two single-stranded nucleic acids held together by non-covalent interactions such as hydrogen bonds, electrostatics and base stacking interactions. The electrostatic interactions are due to the negatively charged phosphate groups, which repel each other. These are partially neutralized by the presence of cations such as Na^+ , K^+ , and Mg^{2+} . There are three H-bonds between the G-C base pair and 2 H-bonds between the A-T base pair (Figure 2.1). They contribute to the overall net stabilization of the DNA structure. The interactions between the aromatic rings of the bases (π -stacking) play a crucial role in the overall net stabilization of the double strand.

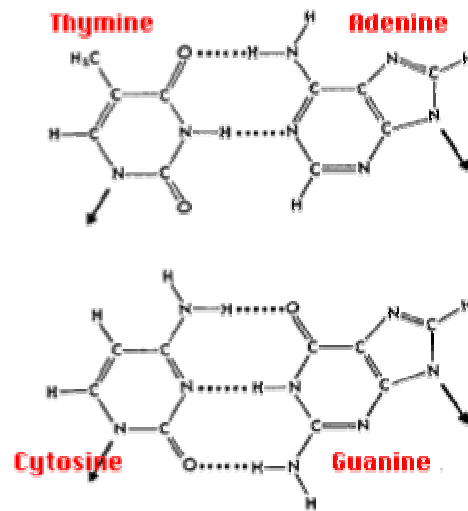


Figure 2.1

The spatial structure of the DNA resembles that of a ladder, twisted into a double helix form (Figure 2.2).



Figure 2.2

The DNA helix can assume one of three slightly different geometries, of which the "B" form described by James D. Watson and Francis Crick is believed to predominate in cells. The two other known double-helical forms of DNA, called A and Z, differ slightly in their geometries and dimensions. The A form is likely to occur only in dehydrated samples of DNA. Segments of DNA methylated by cells for regulatory purposes may adopt the Z geometry, in which the strands turn about the helical axis like a mirror image of the B form⁵⁷ (Figure 2.3).

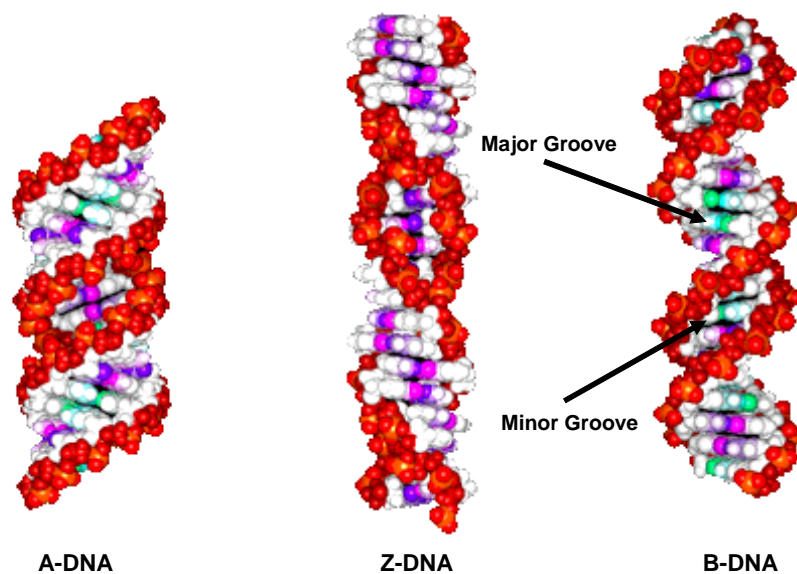


Figure 2.3 DNA conformations

The glycosidic bonds of a DNA base pair are the boundaries to define major and minor grooves. The major groove covers a larger angle than the minor groove. In B-DNA, the major groove is the richer of the two grooves of the duplex DNA, both in the information content, and in its ability to facilitate the discrimination of different DNA sequences. The latter property is essential for the recognition of appropriate sequences by proteins. Thus, the major groove is generally the site of direct information readout. The minor groove is an important target for a few regulatory and structural proteins, especially those that are able to deform DNA so that the minor groove becomes greatly expanded.

2.2 Structural Analysis of the DNA

Owing to a large number of base pairs constituting the genome (over two billion in the case of a human DNA), the DNA is subject to many modifications. Some examples of these modifications are methylation, strand scission, depurination, and photodimerization⁵⁸. Such damages compromise the genetic information and lead to cell death in most cases.

It is very important to maintain the integrity of the genetic material to ensure the survival of the cell. In order to understand the deformations, it is necessary to define different motions of the base-pairs relative to each other. These motions have been defined by Dickerson⁵⁹. Base pairs are presented in a schematic way in order to simplify the analysis. They are presented as rigid blocks and six parameters are required to describe exactly the position and orientation of one of them relative to another. The two sets of local parameters are commonly used for a nucleic acid conformation analysis: step parameters, which relate sequential base pairs and the two complementary base pair parameters (Figure 2.4). The first three step parameters (Shift, Slide and Rise) describe the movements of the two conjugated base-pairs simultaneously; the other three step parameters correspond to the rotations of the base-pairs relative to the consecutive base-pairs (Tilt, Roll and Twist). Buckle and Propeller Twist are base pair parameters that define the rotations of the complementary bases relative to each other. In general, the six torsional angles are necessary to properly describe the sugar-phosphate backbone of the nucleic acids (Figure 2.5).

Two types of DNA deformations are described in this work: general deformations imposed to the curvature of the DNA and local deformations of the base pairs. Two programs are used to analyze the deformation of DNA strands and nucleotides movements: CURVES⁶⁰ and X3DNA⁶¹. CURVES and X3DNA generate step parameters and helical parameters. X3DNA generates a block representation of base-pairs whereas CURVES only gives numerical values. An average structure of the DNA can be extracted from the trajectory files with the use of the PTRAJ program. With an average structure at hand, one can then proceed to the analysis of the DNA deformations.

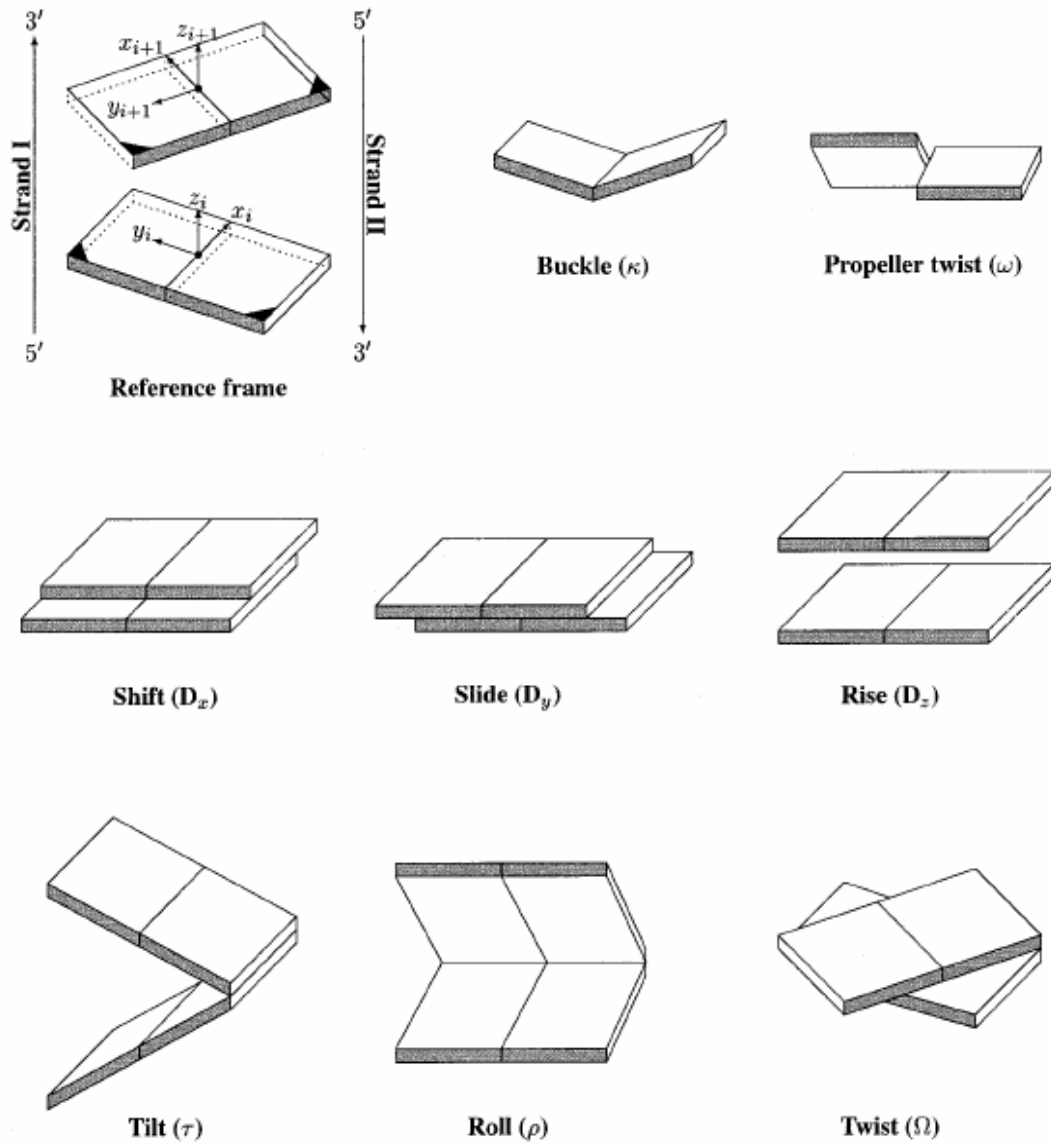


Figure 2.4 Step parameters and complementary base pair parameters

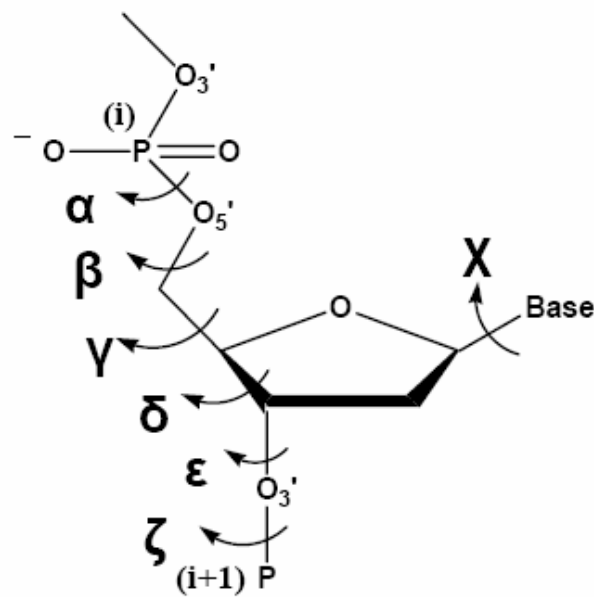
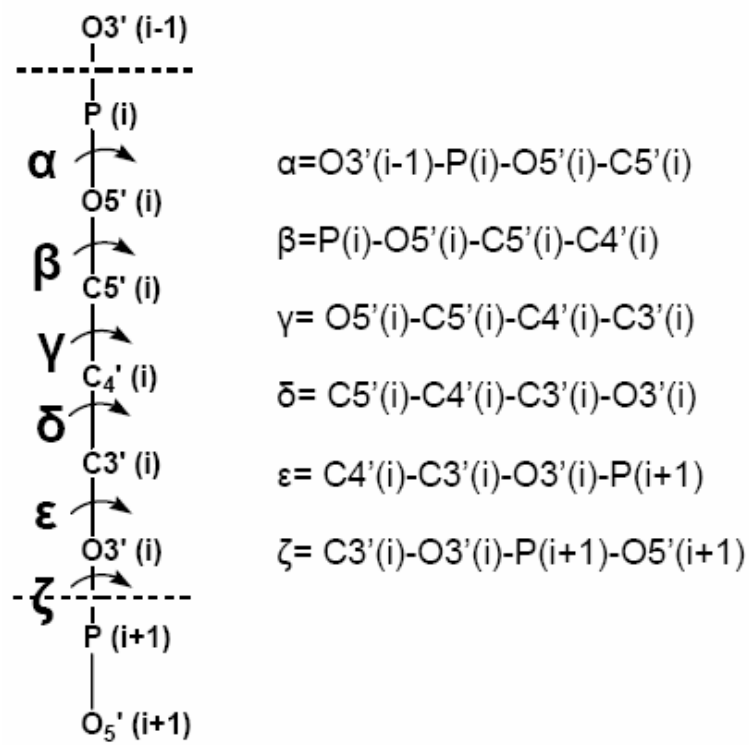


Figure 2.5 Definition of the torsional angles

2.3 Excess Electron Transport through DNA

Over the last years, the group of Prof. Bernd Giese has been concerned with a charge transfer through a variety of DNA and peptide systems. One of the interesting research topics I had an opportunity to take part in was the investigation of a negative charge (an extra electron) transport through the DNA double helix. Recent experiments have suggested that electrons are able to travel through the DNA pyrimidine bases^{62, 63}. The experimental study of the charge transfer through the DNA depends on the injection system, particularly on its reduction potential, and the detection system used. The condition for the detection system is that the charge detection has to be the fastest step of the whole process. To study the process of an electron transfer through the DNA, the group of Prof. Bernd Giese synthesized DNA double strands with the new injection system and the open-backboned thymine dimer detection system⁶⁴ (Figure 2.6). The injection system introduces an extra electron into the DNA double strand upon irradiation. The electron moves through the thymine bases and it is eventually captured by the detection system, which leads to the cycloreversion and a strand break (Figure 2.7).

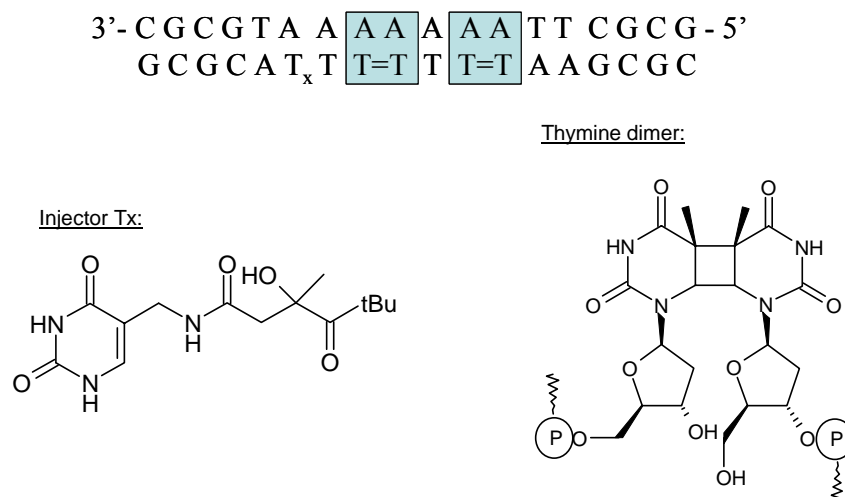


Figure 2.6 Structure of the thymine dimer and the injector

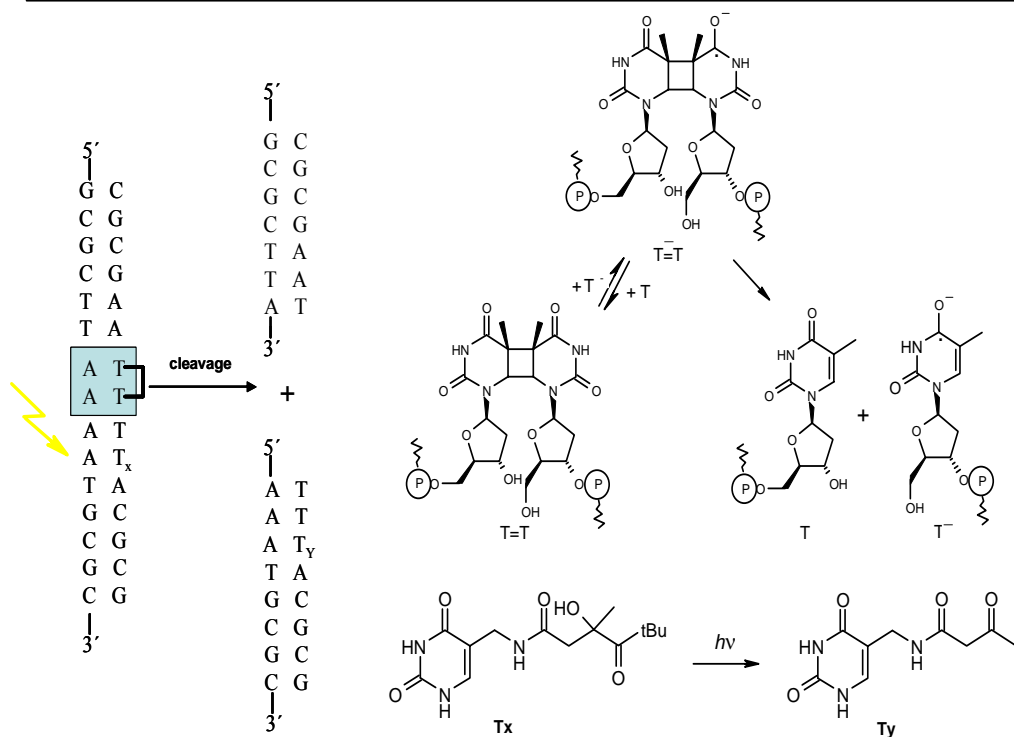


Figure 2.7 Process of the cycloreversion

The cleavage yielded two shorter DNA strands in a 1:1 ratio. To study how the thymine dimer cleavage competes with an electron transfer, the new double strand containing two thymine dimers was prepared (Figure 2.8) and used for the subsequent irradiation experiments. Contradictory to the suggested mechanism, when the distal dimer is cleaved *only* after the cycloreversion of the proximal dimer and thus cleavage yields are in a 1:1 ratio, the experiments revealed more than double cleavage (11%) of the distal dimer in comparison with the proximal dimer cleavage (4.5%). These results indicate that the electron can migrate to the distal site without cleaving the proximal thymine dimer.

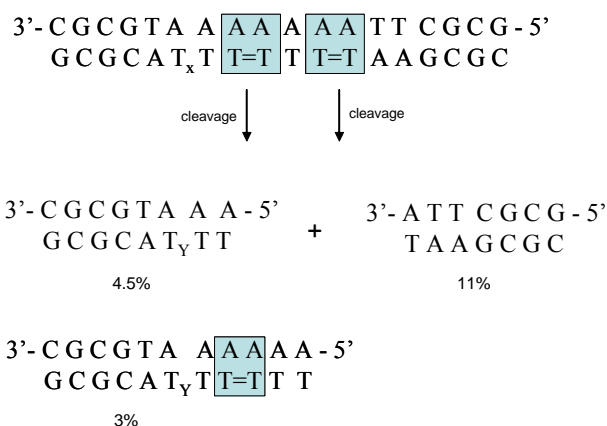


Figure 2.8 Cleavage at the proximal and distal thymine dimer site

This theory was supported by the detection of the double strand, where the proximal dimer remained intact (Figure 2.8). But the reason why does an electron move preferentially in one direction is still debatable.

Molecular modeling was chosen as a tool for the investigation of the observed phenomenon. The molecular dynamics was the straightforward choice because of the direct access to the trajectories after simulation and its broad use for simulations of large systems like DNA and proteins.

2.4 Empirical Force Field methods

Force field (also known as molecular mechanics) refers to computational techniques, which use classical mechanics to analyze the structure and dynamics of molecular systems such as biological macromolecules, organic compounds, polymers, and materials. Molecular mechanics is usually used to perform calculations on systems containing large numbers of atoms. These systems are composed of atoms, the interactions of which are described by classical potential energy functions. Force field methods ignore the electronic motions and calculate the energy of a given system as a function of the positions of individual nuclei. A force field method can, in some cases, reach the minimum potential energy of a specific system as accurate as the highest level quantum chemical calculation in a fraction of computer time. However, molecular mechanics does not provide any electronic information about the molecular system.

Molecular mechanics is based on a rather simple model of interactions within the system with contributions from processes such as bond stretching, angle bending, the rotations around single bonds and non-bonded interactions (Figure 2.9).

$$E_p = E_{\text{bond}} + E_{\text{non-bond}}$$

One of the energy expression commonly used in force field methods has the following form¹:

$$E_p = \sum_{\text{bonds}} \frac{K_i}{2} (l_i - l_{i,0})^2 + \sum_{\text{angles}} \frac{K}{2} (\phi_i - \phi_{i,0})^2 + \sum_{\text{torsions}} \frac{V_n}{2} (1 + \cos(n\omega - \gamma))$$

$$+ \sum_{i=1}^N \sum_{j=i+1}^N \left(4\epsilon_{ij} \left[\left(\frac{\sigma}{r_{ij}} \right)^{12} - \left(\frac{\sigma}{r_{ij}} \right)^6 \right] + \frac{q_i q_j}{4\pi\epsilon_0 r_{ij}} \right)$$

where E_p stands for the potential energy. The first three terms describe the interaction between the pairs of bonded atoms (bonded interactions) as a harmonic potential: bonds, angles and dihedrals. K_i and V_n are constants, which are defined for each type of atom; l_0 , ϕ_0 , and γ are the reference values (equilibrium values) for each type of atom in the system. The fourth term represents the non-bonded interactions: van der Waals and electrostatic interactions, with ϵ_{ij} being the well depth, σ the collision diameter (the separation for which the energy is equal to zero), r the actual distance between the two atoms i and j , q_i , q_j are the atom charges, ϵ_0 the dielectric constant and r_{ij} the distance between the atoms i and j . The determination of the potential energy is performed by summing all energy terms in the potential energy form for the current configuration of the system. In order to define a force field, one needs to specify not only the functional form but also the parameters (i.e. constants such as K_i and V_n and σ). Parameterization plays a crucial role in molecular mechanics. A good parameter set should reproduce the experimental data and the parameter set should be complete and self-consistent.

The force fields used in molecular modeling are primarily designed to reproduce structural and other properties (i.e. molecular spectra) and are accordingly parameterized in order to correctly reproduce the experimental data. If the experimental data are

difficult to obtain, the quantum chemical calculations are increasingly used to provide the missing data.

Another important feature of a force field is the transferability of the functional form and parameters. “Transferability” means that the same set of parameters can be used to model a series of related molecules, rather than having to develop a new set of parameters for each individual molecule.

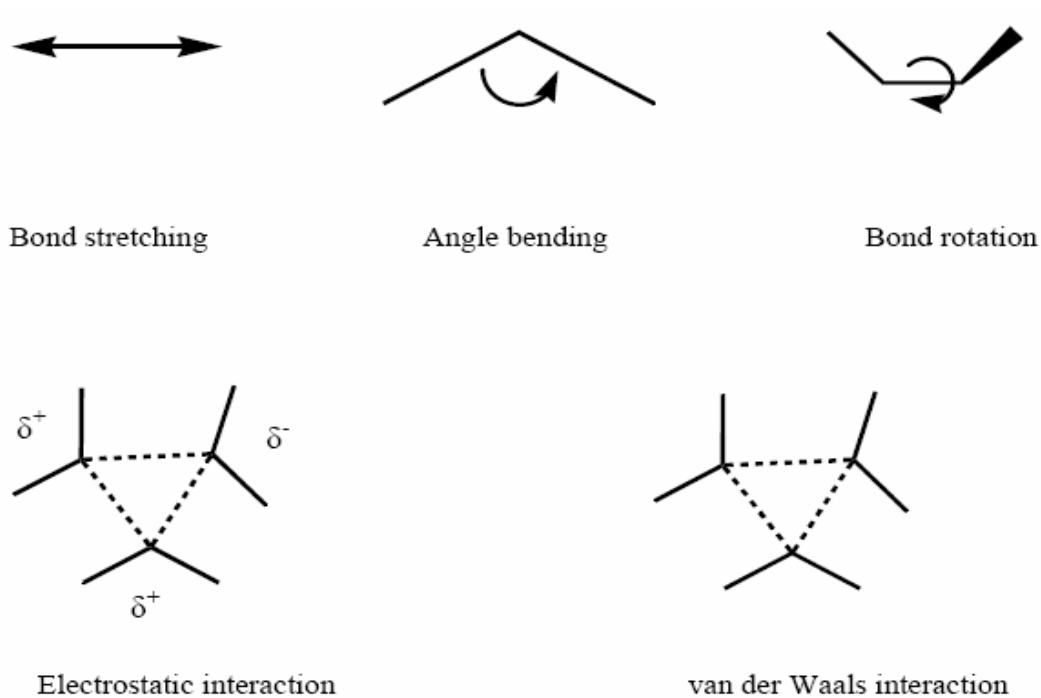


Figure 2.9 Schematic representation of the key contributions to a force field

A concept common to most force fields is that of an atom type. Besides the initial configuration of the system, it is usually necessary to specify an atom type for each atom in the system. The atom type usually contains the information about the hybridization state and sometimes the neighboring environment of an atom. Most force fields distinguish between sp^3 (tetrahedral geometry), sp^2 (trigonal geometry) and sp -hybridized (linear geometry) carbon atoms. For example, the reference angle ϕ_0 for the tetrahedral atom would be approximately 109.5° and that for a trigonal carbon would be near 120° . Force fields, which are designed for modeling specific classes of molecules (such as

proteins and nucleic acids); usually use more specific atom types than the general-purpose force fields.

2.4.1 Amber Force Field

Molecular mechanics force fields are a key component underlying many investigations of protein-ligand interactions, drug design and other tasks¹. The use of empirical parameters enables them to model conformational changes and non-covalent interaction energies relatively accurately.

The basic tool in this study used for a simulation of a modified b-DNA is the program package called AMBER⁶⁵. "AMBER (an acronym for Assisted Model Building and Energy Refinement)" stands for two things: it is a force field for the molecular dynamics originally developed by Peter Kollman's group in the University of California, San Francisco^{66, 67}. AMBER is also the name for the molecular dynamics simulation package associated with this force field, now coordinated by David A. Case at Scripps Research Institute.

The AMBER force field was originally designed for small organic components of proteins and nucleic acids. Later, it has been extended to other systems such as polymers, proteins and DNA^{68, 69}. The AMBER force field has been extensively applied for the simulations of proteins and DNA and it proved to be more reliable for longer simulation times than other force fields (CHARMM)^{70, 71}.

2.4.2 Molecular Dynamics

One important application of the force fields is the molecular dynamics (MD), which simulates the motion of particles in a system by numerically solving the Newton's equations of motion to obtain information about time-dependent properties of the system. Newton's laws of motions:

1. A body's center of mass remains at rest, or moves in a straight line (at a constant velocity, v), unless acted upon by a net outside force

$$\frac{dv}{dt} = 0$$

2. The rate of change in momentum is proportional to the net force acting on the object and takes place in the direction of the force

$$F = m \frac{dv}{dt} = ma$$

3. Whenever one body exerts force upon a second body, the second body exerts an equal and opposite force upon the first body

The result of the integration of the Newton's equations is the trajectory that describes how the positions of the particles vary time. The trajectory is obtained by solving the following differential equation:

$$F_i = m_i \frac{dr_i^2}{d^2t} = -\nabla V(r_1, r_2, r_3 \dots r_N) \quad i = 1, \dots, N$$

This equation describes the motion of the particle i with F_i being the force acting upon this particle. From these calculations, the accelerations and velocities of each particle in the system can be derived. The total energy of the system (E) is the sum of the kinetic (E_k) and the potential energy (E_p), where E_p has one of the force field functional forms¹. An important aspect is the conservation of the total energy. During the MD simulation, the total energy is expected to be constant (microcanonical or NVE ensemble). In practice, the energy fluctuates around the constant value.

In general, the MD simulation run can be divided into four stages:

- I. Initialization of the positions and velocities of the particles:

The initial configuration of the system is usually provided by the user after the previous geometry optimization.

The initial velocities are assigned by random selection from a Maxwell Boltzmann distribution at the specified temperature (Figure 2.10):

$$p(v_i) = \left(\frac{m_i}{2\pi kT} \right)^{1/2} \exp \left[-\frac{1}{2} \frac{m_i v_i^2}{kT} \right]$$

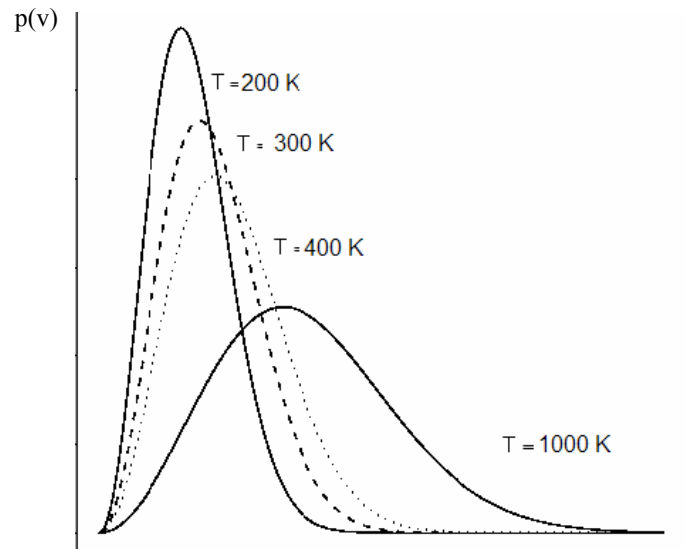


Figure 2.10 Maxwell Boltzmann distribution

II. Equilibration around the desired temperature – velocity scaling

Atomic velocities are multiplied by a factor that creates the target temperature. The temperature of the system is related to the average kinetic energy by the following relationship:

$$\frac{1}{2} \sum m_i v_i^2 = \frac{3}{2} NkT$$

The scaling procedure can be described as follows:

- a) Run MD for n steps
- b) Calculate kinetic energy each step $\Rightarrow T_i$
- c) Form time average

$$\langle T \rangle = \frac{1}{n} \sum T_i$$

- d) Compare $\langle T \rangle$ with the desired T
- e) Form

$$\frac{\langle T \rangle}{\langle T \rangle_{desired}} = 1 \pm \lambda$$

- f) Rescale the velocities: $v_{i,scal.} = \lambda v_i$

III. Production phase, the accumulation of data

During the MD simulation, the atoms move according to the force acting upon them. Force is calculated at each step by differentiating the potential energy function. The trajectories are obtained by integrating the equations of motion using *finite difference methods*. The basic idea is that the equations of motion are turned into differential equations that can be solved iteratively. One among many integration schemes that is commonly used in MD simulation programs is the Velocity Verlet algorithm. The velocity Verlet method is commonly applied as a four-step procedure. The goal is to determine the new positions x_{i+1} , velocities v_{i+1} and accelerations a_{i+1} at time $t+\Delta t$, coming from the initial positions r_i , velocities v_i and accelerations a_i at time t .

- a) The positions at time $t+\Delta t$ are calculated according to the following equation:

$$r_{i+1} = r_i + v_i \Delta t + \frac{1}{2} a_i \Delta t^2$$

b) Velocities at time $t + \frac{1}{2}\Delta t$ are then determined:

$$v_{i+\frac{1}{2}} = v_i + \frac{1}{2}a_i\Delta t^2$$

c) Forces are calculated from the new positions (by differentiating the potential energy function) giving the accelerations a_{i+1} at $t+\Delta t$:

$$f_{i+1} = -\nabla V(x_{i+1}) = ma_{i+1}$$

d) Finally, the velocities at time $t+\Delta t$ are computed:

$$v_{i+1} = v_{i+\frac{1}{2}} + \frac{1}{2}a_{i+1}\Delta t$$

IV. Data analysis

MD produces a set of configurations along the trajectory, which can be used to create “movies”. The visualization of the trajectories provides the user with the ‘real-time’ picture of the particles movements over the simulation run, hence giving a better insight into the process of interest.

Besides the trajectories, MD provides other important macroscopic (total energy, heat capacity, pressure, temperature etc.) as well as microscopic properties (diffusion function, thermal conductivity, infrared spectra etc.).

A disadvantage of conventional molecular dynamics procedures is that they can only tackle simulations with a relatively short time scale - few nanoseconds is the approximate upper limit with current computers. In this study, the molecular dynamics simulations were carried out on the department cluster BoB (220 pentium processors) at the Notre Dame University. The high performance of this cluster allowed for the simulation time scale up to four nanoseconds.

2.5 Molecular Dynamic Simulation of the Modified DNA Structure

The model of the B-DNA double strand with two CPD sites and the injector was generated with the InsightII program (Figure 2.11).

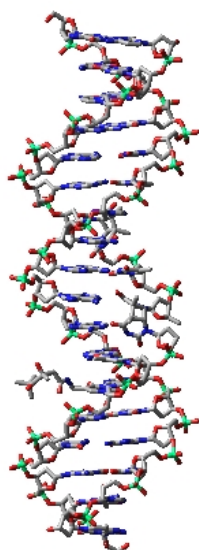
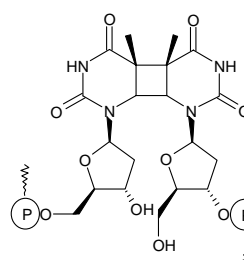


Figure 2.11 Model of the B-DNA with two CPD lesions and an injector site

5'			
I			
1	G	C	36
2	C	G	35
3	G	C	34
4	C	G	33
5	T	A	32
6	T	A	31
7	A	T	30
8	A	T	29
9	A	T	28
10	A	T	27
11	A	T	26
12	A	T	25
13	A	T _x	24
14	T	A	23
15	G	C	22
16	C	G	21
17	G	C	20
18	C	G	19
I			
3'			

Figure 2.12 Sequence and the notation of the nucleotides in the DNA strand

CPD:



The injector

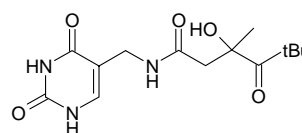


Figure 2.13 Structure of the CPD site and the injector system

The created file in the pdb format was imported to the “Xleap” module of the AMBER 7 package. The missing atom types and charges of the CPD were taken from the ab-initio calculations of Kollman *et al.*⁷² (Figure 2.14). The new charges for the free hydroxyl groups of the CPD units were obtained from additional calculations on the B3LYP density functional level (B3LYP/6-31+G*) using CHelpG partitioning scheme⁷³.

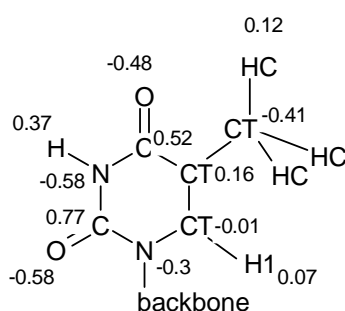


Figure 2.14 CPD parameters

The final file was then used to create the input topology (prmtop) and coordinate (inpcrd) files. MD simulations with the model of 18 base pairs surrounded by water molecules (TIP3 model) and 32 Na⁺ counterions (box size ~ 48*47*87 Å) were then performed using the AMBER7 package for time of 4 nanoseconds.

The molecular dynamic calculations were carried out at constant temperature T=300K and constant pressure for the periodic boundary conditions (1 bar). For the treatment of the long-range electrostatic interactions, the Particle Ewald Mesh (PME) method⁷⁴ was used. The PME method is based on the Ewald summation method, in which the particle interacts with other particles in the simulation box and all of their images in an infinite array of periodic cells. The Ewald method divides the charge-charge contribution to the potential energy into two rapidly converging series – the summation in the ‘real’ and ‘reciprocal’ space and two correction terms. There are numbers of modifications of the Ewald method, which implement the fast Fourier transformation in order to speed up the calculation. These methods replace the point charges with their continuous coordinates by a grid charge distribution. Proceeding from this gridded charge density, one can calculate the potential at each of the particles using the fast Fourier transformation.

The Ewald sum is probably the best method developed up to date to accurately model long-range interaction in the simulation. It has been successfully used in the simulations of highly charged systems as well as large polar molecular systems such as DNA and proteins.

2.5.1 Computational Methodology

An important part of every molecular dynamics simulation is the equilibrium phase. Before a free molecular dynamics run can commence, a careful equilibration is often necessary. The aim of the equilibration phase is to eliminate any strain from the starting structure, which is usually imposed during the construction of the initial configuration of the system. Especially in the case of inhomogeneous systems, an equilibration process is desired, during which the solvent molecules are allowed to equally distribute around the solute (e.g. simulations of the DNA in the aqueous solutions).

In this study, we used the following equilibration strategy: in the first minimisation procedure, all surrounding water molecules were allowed to relax in order to better adapt to the potential of the solute (DNA double strand). During this minimisation, all heavy atoms of the DNA were ‘frozen’ using the constraint of 5000 kcal/mol. The molecule of DNA was then relaxed with the special attention paid to the region surrounding the CPD sites. The four adjacent base pairs (T_5-A_{32} , T_6-A_{32} , $A_{12}-T_{25}$, $A_{13}-T_{24}$) and the base pair between the two CPD units (A_9-T_{28}) were frozen using the constraint of 50 kcal/mol. This constraint was then gradually removed in four subsequent minimisation steps (Figure 2.15). The same procedure of freezing base pairs surrounding the CPD lesions was used in the short consecutive MD equilibration simulations for time period of 100ps (Figure 2.16). The only difference was the longer simulation time of 1ns for the solvent relaxation phase.

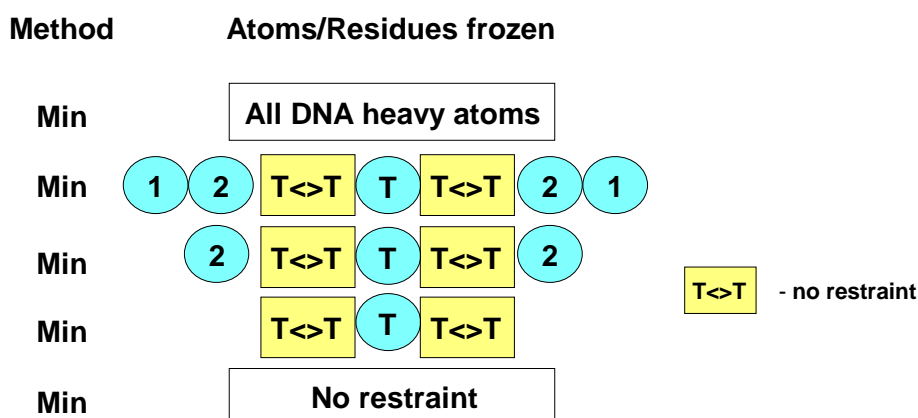


Figure 2.15 Description of the minimisation procedure

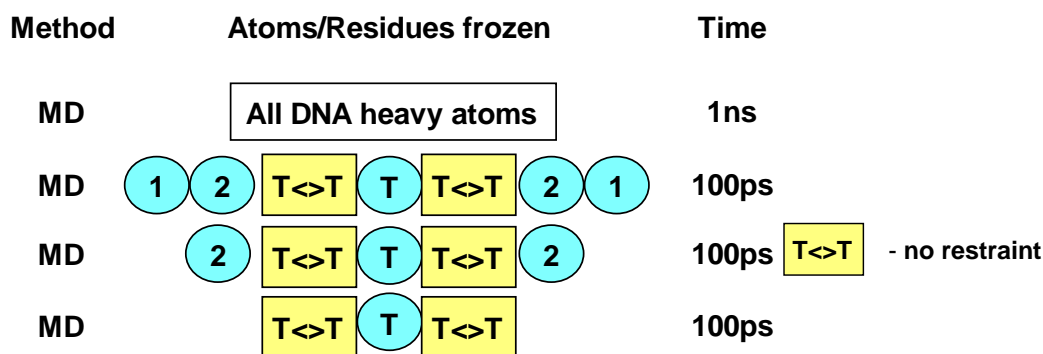


Figure 2.16 Description of the MD equilibration procedure

The thoroughly equilibrated structure of the modified B-DNA was then finally used as an input for the production phase of the simulation for time period of 4 nanoseconds.

2.5.2 MD simulation

After a molecular dynamics simulation, it is always necessary to check if the calculation was stable and no errors occurred. There are several so called control parameters which provide the information about the behaviour of the system during the simulation. The density informs about the distribution of the solvent molecules (water in this case) around

the solute (DNA molecule). The density value close to one indicates a good uniform distribution of water molecules around the DNA molecule. The variation of the density over the simulation can be visualized by plotting the immediate density values against time. The density plot in the Figure 2.17 showed very small fluctuations around 1.06 ± 0.01 what corresponds to an isotropic solvent distribution.

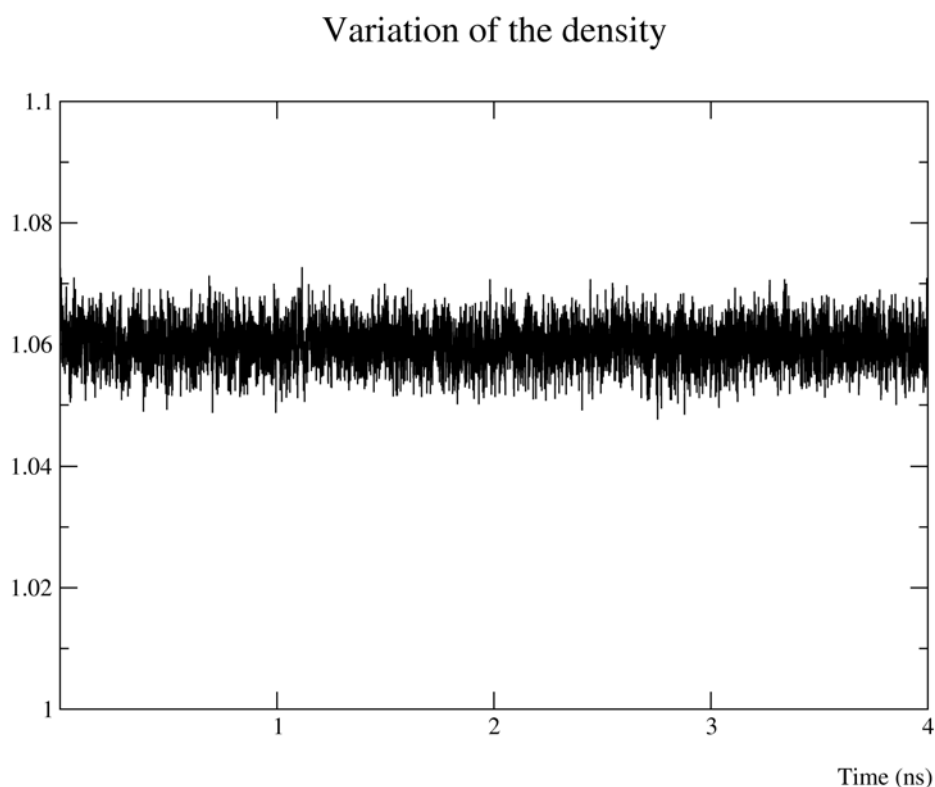


Figure 2.17 Variation of the density during the production phase

Another useful indicator of the convergence is the total energy of the system. The total energy is the sum of the kinetic and the potential energy and is expected to fluctuate around a constant value (Figure 2.18).

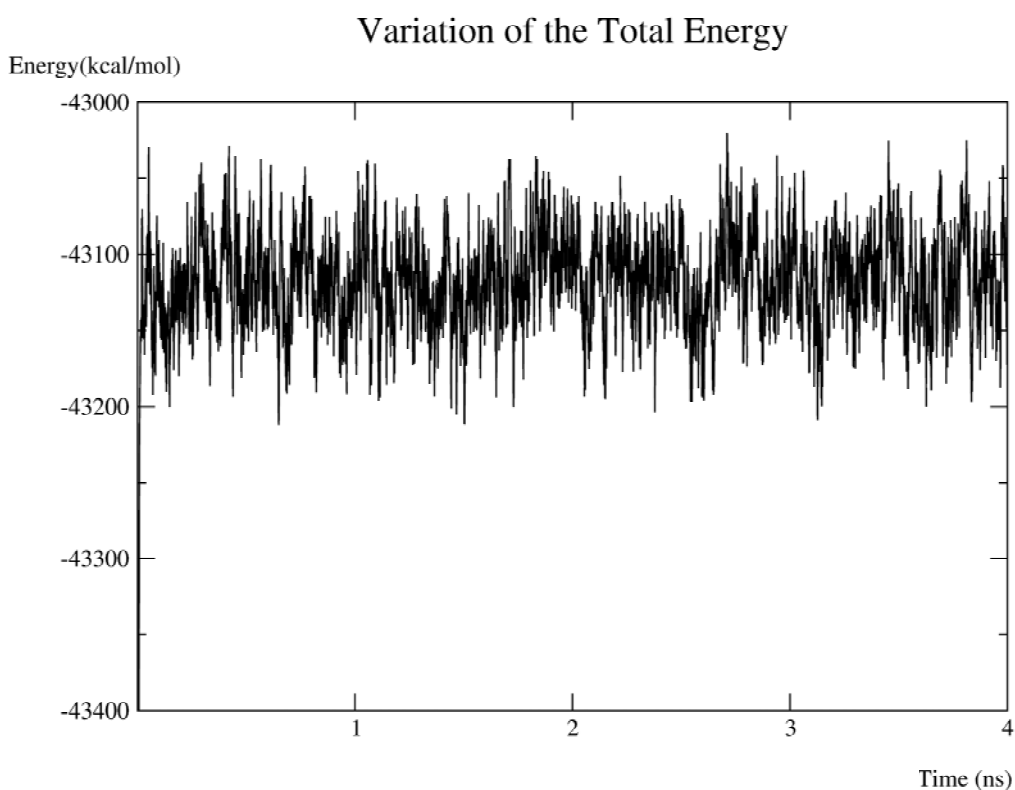


Figure 2.18 Variation of the total energy during the production phase

During the production phase, the total energy of the entire system (DNA, counterions, water molecules) remained stable at -43100 ± 100 kcal/mol. Considering the size of the system ($\sim 14\,100$ atoms), the simulation was assumed to be stable.

The root mean square deviation (RMSD) is a useful indicator of the extent, to which we have drifted during the dynamics. The RMSD reflects the deviation of each frame in the trajectory compared to the first frame in the trajectory, thus indicating any major structural changes (e.g. conformational changes, $B \leftrightarrow A$ transitions of the DNA, denaturation, unfolding of the proteins). The plot of RMSD variation during the dynamics run showed only small fluctuations (the largest RMSD was 4.5 \AA) for DNA double strand containing 1168 atoms (Figure 2.19).

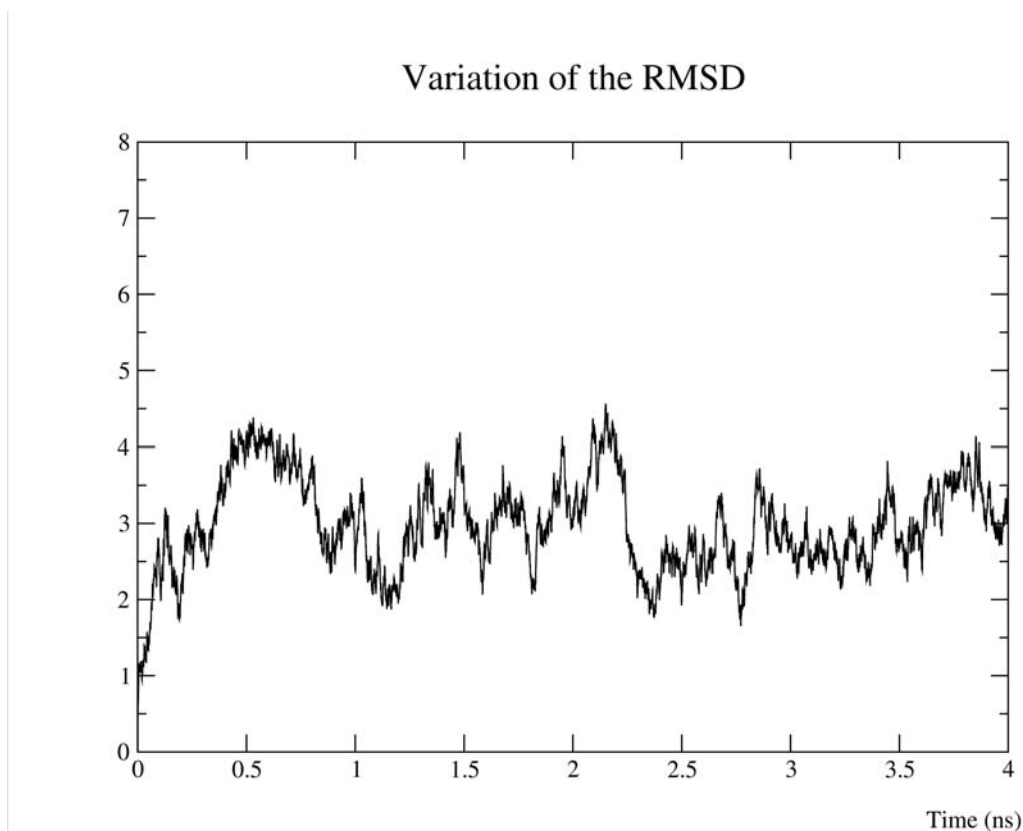


Figure 2.19 Variation of the RMSD during the production phase

From the observed RMS deviations during the simulation can be concluded that the structure was reasonably converging.

2.5.3 Structural Analysis

The aim of this MD simulation was to investigate the structural changes at the CPD sites and the deformations of the adjacent base pairs. In order to study the deformed DNA structure, an average structure was extracted from the trajectory files after the production run (Figure 2.20). With an average DNA structure at hand, it was possible to proceed to a more detailed analysis of global and local deformations of the B-DNA double strand caused by two CPD units. In the Figure 2.21, an average structure from the simulation is compared with the standard B-DNA (Dickerson dodecamer⁵⁹). A strong effect of CPD sites on the general curvature of the DNA double strand is obvious from the displayed

structure. According to the previous X-Ray, NMR and theoretical studies⁷⁵⁻⁷⁷ with only one CPD, the incorporation of the thymine dimer results in a sharper bend and the kink of the helical axis.

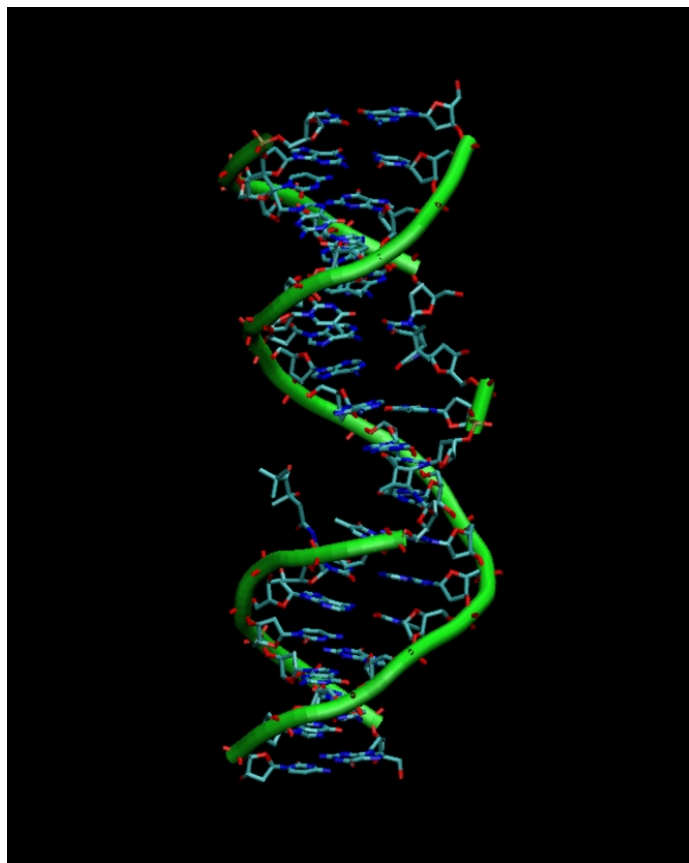


Figure 2.20 Average structure of the DNA after 4ns MD simulation

This deformation is even more pronounced in the step representation created with the X3DNA program (Figure 2.22).

In the next phase, the local deformations in the CPD region were investigated. The analysis of the central segment of the DNA strand revealed considerable changes in helical as well as local base pair parameters. The Figure 2.22 shows the local base pair parameters obtained from the X3DNA program.

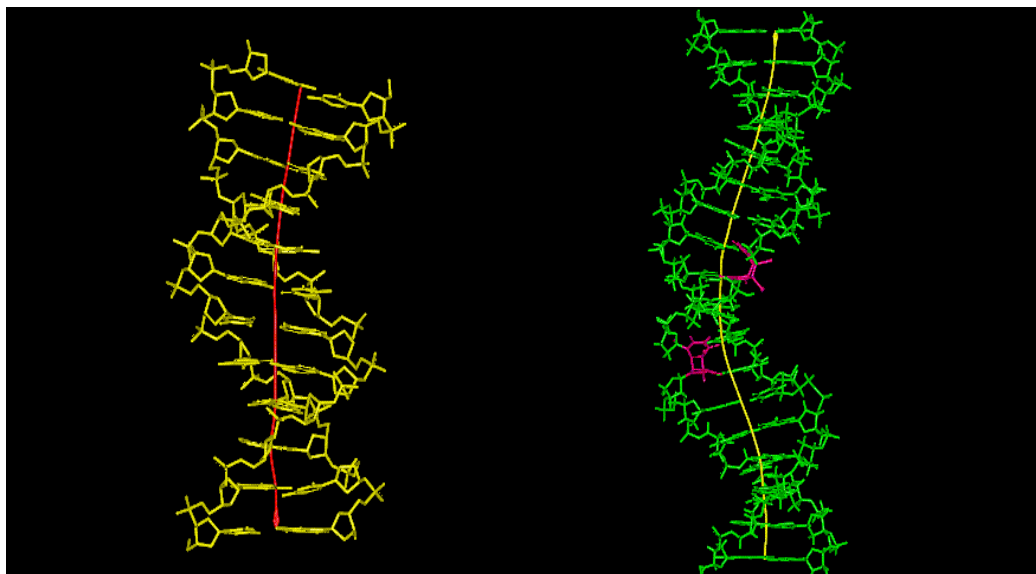


Figure 2.21 Comparison of the standard and the modified B-DNA

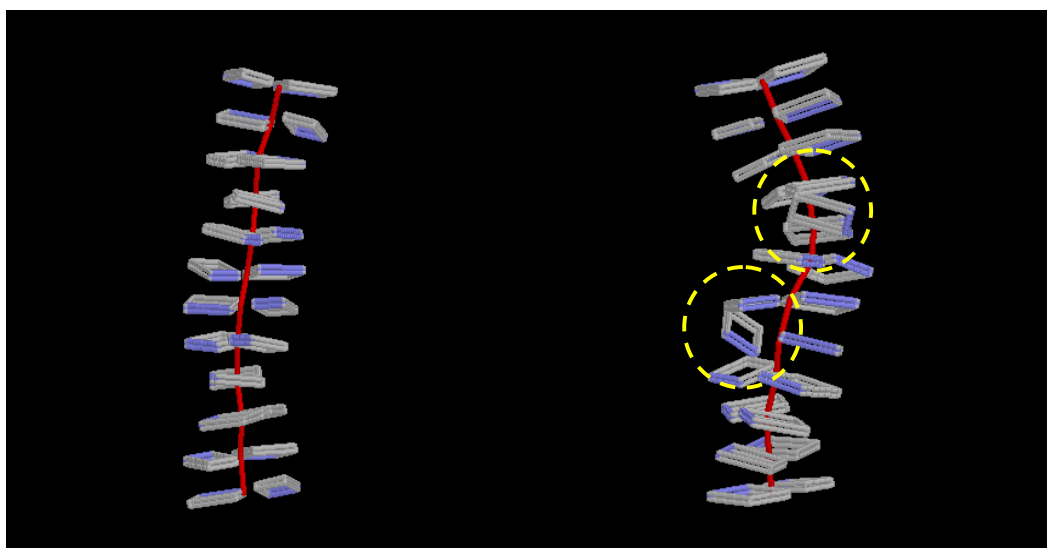
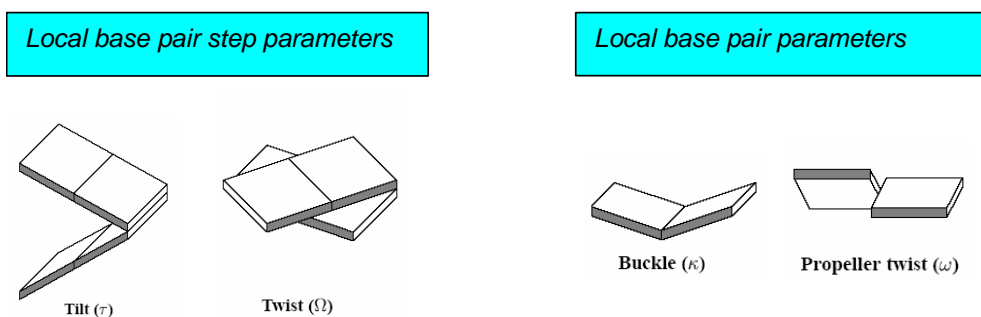


Figure 2.22 Step representations of the standard B-DNA (left) and the modified DNA (right)



Modified B-DNA		
Base pairs	Tilt	Twist
T5/T6	2.7	22.7
T6/A7	-8.8	41.3
A7/A8	23.3	15.3
A8/A9	-18.0	35.3
A9/A10	-7.3	35.0
A10/A11	23.8	15.3
A11/A12	-18.9	39.2
A12/A13	-2.1	37.1
Dickerson Dodecamer		
Base pairs	Tilt	Twist
A/T	2.8	34.2
A/A	1.8	34.8
T/T	3.0	35.4

Figure 2.23 Parameters for the base pairs around the CPD region

From the Figure

Modified B-DNA			
B. number	Base pair	Buckle	Propeller
5 -- 32	T -- A	-3.8	-8.0
6 -- 31	T -- A	7.7	-14.5
7 -- 30	A -- T	13.8	-2.4
8 -- 29	A -- T	-24.0	-19.2
9 -- 28	A -- T	11.6	-14.1
10 -- 27	A -- T	15.0	-4.8
11 -- 26	A -- T	-21.9	-23.0
12 -- 25	A -- T	6.2	-19.1
13 -- 24	A -- Tx	-3.3	-20.8
Dickerson Dodecamer			
Base pair	Buckle	Propeller	
A -- T	5.0	-16.4	

Figure 2.23 is evident that both CPD units induce very similar deformation to the adjacent base pairs. The parameter change on both sides of thymine dimers is of particular interest. The propeller angles of the A₇-T₃₀ and A₁₀-T₂₇ base pairs, which are on the 3' side of the dimers, show reduced angles of -2.4° and -4.8°, respectively. On the other hand, the values of the buckle angles indicate greater distortion in the alignment of the A – T bases on the 5' side of the CPD sites. This deformation is reflected in an unfavourable geometry of the corresponding hydrogen bonds. The analysis of the hydrogen bonds in the CPD lesion indeed revealed the loss of the hydrogen bonding on 5' sides of both thymine dimers. While 3' thymines maintain normal hydrogen bonds with complementary bases (Table 2.1), the hydrogen bonds on the 5' side are longer than normal H-bonds and their orientation vectors are not in the proper plane (Figure 2.24), which is in agreement with the studies with one CPD⁵⁷.

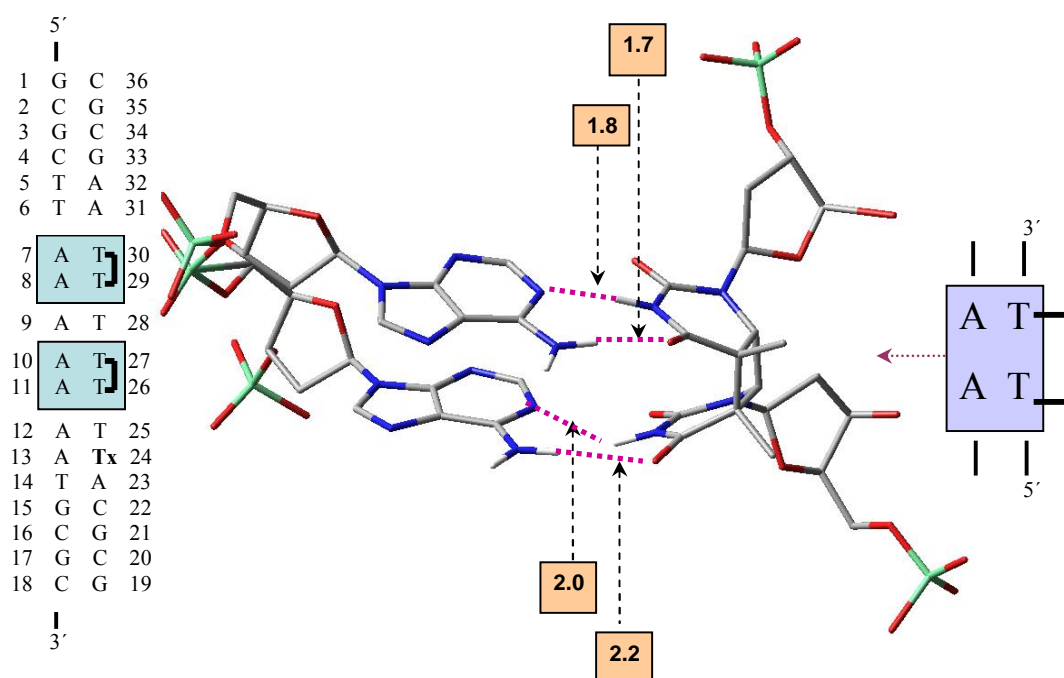


Figure 2.24 Detail of the CPD site

Base pair	<i>H-Bond</i>	<i>H-Bond</i>
	N--H--N	O--H—NH
A₇ – T₃₀	1.8	1.7
A₈ – T₂₉	2.0	2.2
A₉ – T₂₈	1.7	1.8
A₁₀ – T₂₇	1.8	1.7
A₁₁ – T₂₆	2.0	2.0

Table 2.1 Hydrogen bonds in the CPD sites

This was an important observation since it can help to explain the unequal cleavage of the modified double strand upon irradiation. It is known that hydrogen bonds have a positive effect on the radical anion stability. In the light of this fact, it is reasonable to assume that the radical anions formed after the irradiation will prefer to stay at the 3' thymine, where they are stabilized by the corresponding hydrogen bonds. An additional explanation for the observed phenomenon could be a different distance between the central thymine T₂₈ and the closest thymine of both CPD units (T₂₇ and T₂₉). The investigation of the

corresponding distances revealed that thymine T₂₈ is closer to the thymine T₂₉ than to the T₂₇ (Figure 2.25).

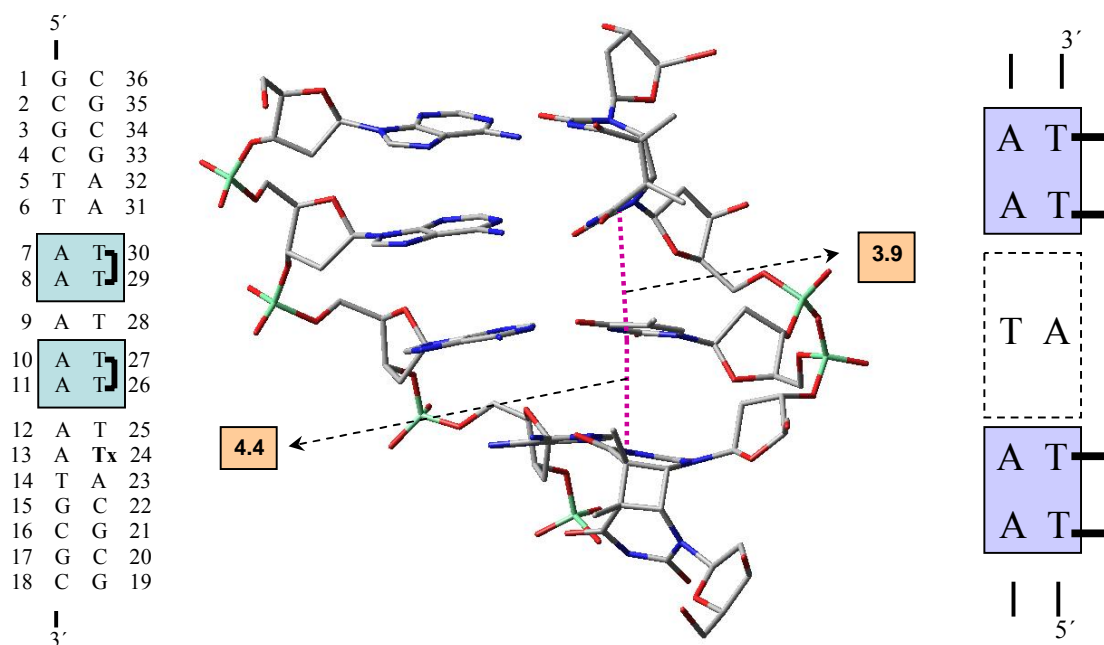


Figure 2.25 π - π interaction

Bases	Distance (Å)
T ₂₈ --T ₂₉	3.9
T ₂₈ --T ₂₇	4.4

Table 2.2 Distances between the central thymine and the thymine of both CPD units

This result can be interpreted in the following way. An electron released upon irradiation does not necessarily cleave the proximal dimer and is able to migrate to the central thymine T₂₈. Due to the shorter distance to T₂₉, it will then move preferentially in the 3' direction towards the T₂₉, where it finally cleaves the distal thymine dimer. After the cleavage, the corresponding thymine radical anion is formed on the 3' side. The result of this process is thus a higher cleavage yield at the distal site.

2.6 Summary

The structural influence of two thymine dimers on B-DNA double strand was investigated by carrying out molecular dynamic simulation with the Amber7 software package. The structural analysis of the final average DNA structure helped to shed light on the experimentally observed cleavage yields. The phenomenon of the unequal cleavage on the proximal and distal dimer sites can be explained in terms of local deformations of the DNA double strand. An electron formed after the irradiation of the DNA strand travels through the A:T base pairs until it is eventually trapped by the detection system (thymine dimer). After the cleavage of the cyclobutane ring of the thymine dimer, it will preferentially form a thymine radical anion on the 3' position of the CPD site, due to the stabilizing effect of the hydrogen bonds between the complementary bases.

In the case of two thymine dimers, an electron does not necessarily have to cleave the proximal dimer first but it can migrate to the thymine between the CDP sites and then move with the higher probability in the 3' direction due to the shorter distance to the distal thymine dimer. The subsequent cleavage yields the thymine radical anion on the 3' position and induces the strand cleavage. The whole process hence leads to the higher cleavage yield at the distal 3' site.

3 Summary of the work

The goal of this PhD work was the application of tools of computational chemistry in various research areas of chemistry.

The first chapter deals with the mechanism of the unusual spontaneous cyclization of Acridin-9-ylmethyl thioureas observed during the attempted synthesis of new spirocompounds based on the acridine skeleton. The reaction path simulations were performed using ab initio quantum chemistry methods. The new reaction mechanism was suggested, in which the thione tautomer of thiourea intermediate plays a crucial role and determines the course of the whole reaction.

In the second part, structural aspects of the modified DNA double strand were investigated by means of molecular dynamics. Simulations shed light on the behaviour of the deformed double strand upon irradiation. The observed phenomena can be explained in terms of local deformations caused by two CPD units, which cause the preference of the electron transfer in one direction.

The goal of this theoretical study was to attempt to find answers to particular questions emerging during the practical experiments. In this regard, it was successful. I see it as a nice example of combining the experimental work with theoretical models in pursuing the common objective. As the science advances, more sophisticated problems are emerging. To address these questions, more complex approaches are required. And in my opinion, the computational chemistry has already established its firm and undisputable position as a powerful tool in the modern era of multi-disciplinary projects.

Appendix

Hardware:

The calculations were performed on a variety of computer platforms:

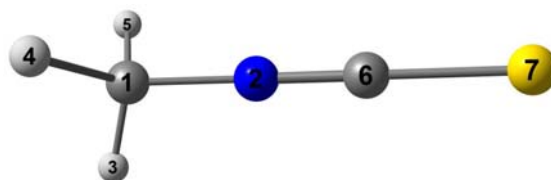
Xeon Dual PC (2 x 1.7 GHz, Linux RedHat 8.0)

Compaq XP1000 AlphaStation (500 MHz, Digital UNIX 4.0E)

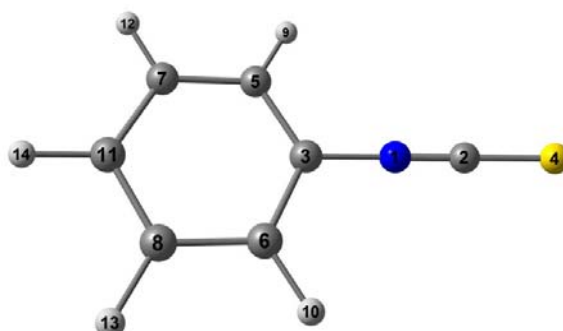
Linux Beowulf Cluster (Master 2 x 2.4 GHz Xeon CPUs, 36 Nodes 2 x 2.4 GHz Xeon CPUs, 16 Nodes 2 x 2.0 GHz Opteron CPUs, 8 Nodes 2 x 2.2 GHz Opteron CPUs, Linux RedHat 8.0) hosted by “Universitätsrechnungszentrum (URZ)” at the University of Basel
NEC SX-5 (16 CPUs, theoretical peak performance of 128 GFlops, Super-UX R13.1)
and HP-Cluster with 3 HP-N4000 (8 x 360 MHz, HP-UX 11.00) hosted by “Swiss Center of Scientific Computing (CSCS) in Manno, Switzerland

BoB Beowulf Cluster (106 Nodes 2 x 2x 1.7 GHz Xeon CPUs), High Performance Computing Cluster (HPCC) (128 Nodes 2 x 3.06 GHz Xeon CPUs, 16 Nodes 2 x 2.2 GHz AMD Opteron CPUs) hosted by “Office of Information Technology” at the Notre Dame University, USA

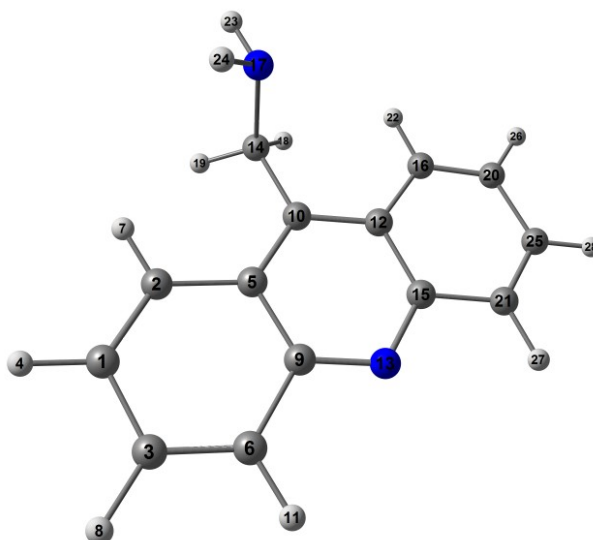
Interatomic parameter tables

**Methylisothiocyanate**

R(1-2)	1.426	A(2-1-3)	109.2	A(4-1-5)	109.8
R(1-3)	1.081	A(2-1-4)	109.2	A(2-6-7)	179.9
R(1-4)	1.081	A(2-1-5)	109.2		
R(1-5)	1.081	A(1-2-6)	179.9		
R(2-6)	1.147	A(3-1-4)	109.8		
R(6-7)	1.617	A(3-1-5)	109.8		

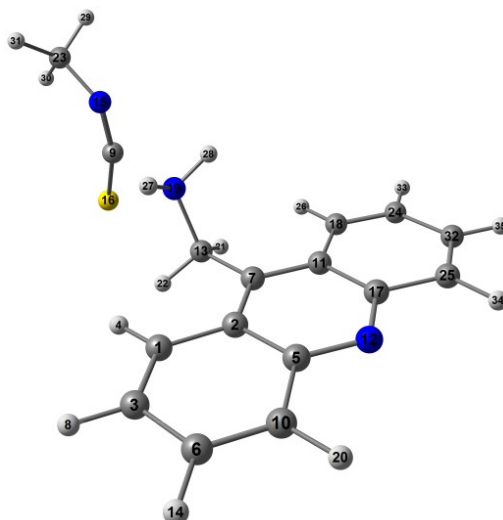
**Phenylisothiocyanate**

R(1-2)	1.15	A(2-1-3)	179.9	A(6-8-13)	119.5
R(1-3)	1.388	A(1-2-4)	180	A(11-7-12)	120.2
R(2-4)	1.61	A(1-3-5)	119.3	A(7-11-8)	120
R(3-5)	1.388	A(1-3-6)	119.3	A(7-11-14)	120
R(3-6)	1.388	A(5-3-6)	121.4	A(11-8-13)	120.2
R(5-7)	1.385	A(3-5-7)	119	A(8-11-14)	120
R(5-9)	1.075	A(3-5-9)	119.9		
R(6-8)	1.385	A(3-6-8)	119		
R(6-10)	1.075	A(3-6-10)	119.9		
R(7-11)	1.388	A(7-5-9)	121.1		
R(7-12)	1.075	A(5-7-11)	120.3		
R(8-11)	1.388	A(5-7-12)	119.5		
R(8-13)	1.075	A(8-6-10)	121.1		
R(11-14)	1.075	A(6-8-11)	120.3		



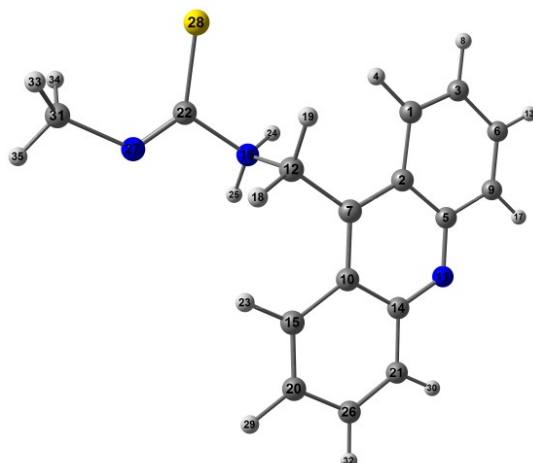
Acridin-9-ylmethyl amine

R(1-2)	1.35	A(2-1-3)	120.6	A(12-16-20)	121
R(1-3)	1.431	A(2-1-4)	120.1	A(12-16-22)	119.3
R(1-4)	1.075	A(1-2-5)	121.3	A(13-15-21)	117.7
R(2-5)	1.441	A(1-2-7)	118.9	A(17-14-18)	108
R(2-7)	1.072	A(3-1-4)	119.3	A(17-14-19)	113.1
R(3-6)	1.348	A(1-3-6)	120.3	A(14-17-23)	110.1
R(3-8)	1.076	A(1-3-8)	119.3	A(14-17-24)	110.9
R(5-9)	1.428	A(5-2-7)	119.8	A(18-14-19)	105.7
R(5-10)	1.4	A(2-5-9)	117.7	A(15-21-25)	120.7
R(6-9)	1.437	A(2-5-10)	124.1	A(15-21-27)	117.5
R(6-11)	1.074	A(6-3-8)	120.4	A(20-16-22)	119.6
R(9-13)	1.321	A(3-6-9)	120.8	A(16-20-25)	120.6
R(10-12)	1.402	A(3-6-11)	121.9	A(16-20-26)	120.1
R(10-14)	1.518	A(9-5-10)	118.2	A(23-17-24)	106.8
R(12-15)	1.423	A(5-9-6)	119.3	A(25-20-26)	119.3
R(12-16)	1.438	A(5-9-13)	123.2	A(20-25-21)	120.4
R(13-15)	1.325	A(5-10-12)	118.1	A(20-25-28)	119.3
R(14-17)	1.459	A(5-10-14)	121.6	A(25-21-27)	121.9
R(14-18)	1.082	A(9-6-11)	117.3	A(21-25-28)	120.3
R(14-19)	1.083	A(6-9-13)	117.5		
R(15-21)	1.436	A(9-13-15)	118.8		
R(16-20)	1.351	A(12-10-14)	120.3		
R(16-22)	1.072	A(10-12-15)	118.5		
R(17-23)	1.003	A(10-12-16)	123.4		
R(17-24)	1.003	A(10-14-17)	110.8		
R(20-25)	1.431	A(10-14-18)	109		
R(20-26)	1.075	A(10-14-19)	110		
R(21-25)	1.349	A(15-12-16)	118.1		
R(21-27)	1.075	A(12-15-13)	123		
R(25-28)	1.076	A(12-15-21)	119.2		



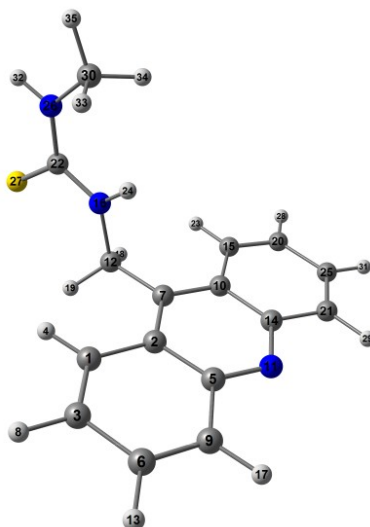
TS Ia

R(1-2)	1.441	R(23-30)	1.083	A(7-11-17)	118.2
R(1-3)	1.351	R(23-31)	1.082	A(7-11-18)	124
R(1-4)	1.074	R(24-32)	1.432	A(7-13-19)	113.8
R(2-5)	1.426	R(24-33)	1.077	A(7-13-21)	110.8
R(2-7)	1.402	R(25-32)	1.349	A(7-13-22)	110.7
R(3-6)	1.432	R(25-34)	1.076	A(15-9-16)	153.1
R(3-8)	1.077	R(32-35)	1.077	A(9-15-23)	123
R(5-10)	1.437	A(2-1-3)	121.2	A(17-11-18)	117.8
R(5-12)	1.324	A(2-1-4)	120.2	A(11-17-12)	123
R(6-10)	1.349	A(1-2-5)	117.7	A(11-17-25)	119.3
R(6-14)	1.077	A(1-2-7)	124	A(11-18-24)	121.2
R(7-11)	1.402	A(3-1-4)	118.6	A(11-18-26)	120.1
R(7-13)	1.521	A(1-3-6)	120.6	A(12-17-25)	117.6
R(9-15)	1.203	A(1-3-8)	120	A(19-13-21)	107.8
R(9-16)	1.647	A(5-2-7)	118.2	A(19-13-22)	107.8
R(10-20)	1.076	A(2-5-10)	119.3	A(13-19-27)	112.1
R(11-17)	1.426	A(2-5-12)	123	A(13-19-28)	112.1
R(11-18)	1.441	A(2-7-11)	118.5	A(21-13-22)	105.7
R(12-17)	1.324	A(2-7-13)	120.7	A(15-23-29)	108.3
R(13-19)	1.463	A(6-3-8)	119.3	A(15-23-30)	112.2
R(13-21)	1.078	A(3-6-10)	120.3	A(15-23-31)	108.3
R(13-22)	1.078	A(3-6-14)	119.3	A(17-25-32)	120.8
R(15-23)	1.459	A(10-5-12)	117.6	A(17-25-34)	117.4
R(17-25)	1.437	A(5-10-6)	120.8	A(24-18-26)	118.7
R(18-24)	1.351	A(5-10-20)	117.4	A(18-24-32)	120.6
R(18-26)	1.074	A(5-12-17)	119	A(18-24-33)	120
R(19-27)	1.007	A(10-6-14)	120.4	A(27-19-28)	106.1
R(19-28)	1.007	A(6-10-20)	121.8	A(29-23-30)	109.7
R(23-29)	1.082	A(11-7-13)	120.8	A(29-23-31)	108.4

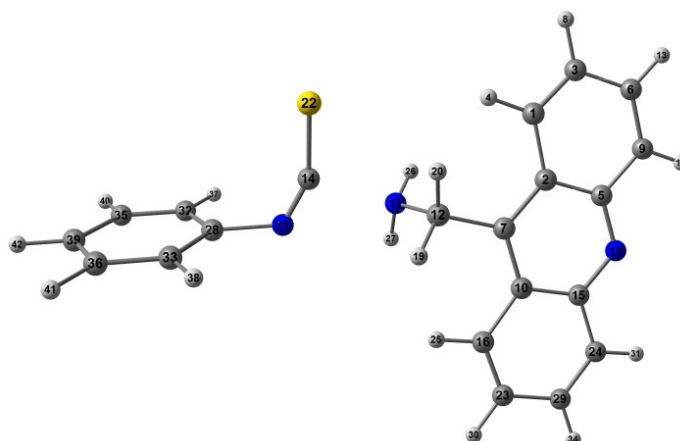


IIa

R(1-2)	1.441	R(20-29)	1.077	A(5-9-17)	117.5
R(1-3)	1.351	R(21-26)	1.349	A(5-11-14)	119.5
R(1-4)	1.074	R(21-30)	1.076	A(9-6-13)	120.5
R(2-5)	1.427	R(22-27)	1.249	A(6-9-17)	121.9
R(2-7)	1.4	R(22-28)	1.724	A(10-7-12)	120.7
R(3-6)	1.432	R(26-32)	1.077	A(7-10-14)	117.8
R(3-8)	1.077	R(27-31)	1.449	A(7-10-15)	124.5
R(5-9)	1.437	R(31-33)	1.085	A(7-12-16)	111.5
R(5-11)	1.323	R(31-34)	1.085	A(7-12-18)	112.4
R(6-9)	1.349	R(31-35)	1.082	A(7-12-19)	112.2
R(6-13)	1.077	A(2-1-3)	121	A(14-10-15)	117.7
R(7-10)	1.4	A(2-1-4)	120.4	A(10-14-11)	122.9
R(7-12)	1.514	A(1-2-5)	117.8	A(10-14-21)	119.4
R(9-17)	1.076	A(1-2-7)	124.3	A(10-15-20)	121.1
R(10-14)	1.428	A(3-1-4)	118.6	A(10-15-23)	120.4
R(10-15)	1.441	A(1-3-6)	120.8	A(11-14-21)	117.7
R(11-14)	1.323	A(1-3-8)	119.9	A(16-12-18)	106.3
R(12-16)	1.501	A(5-2-7)	117.9	A(16-12-19)	106.6
R(12-18)	1.077	A(2-5-9)	119.4	A(12-16-22)	112.9
R(12-19)	1.076	A(2-5-11)	122.8	A(12-16-24)	110.6
R(14-21)	1.437	A(2-7-10)	119.2	A(12-16-25)	110.6
R(15-20)	1.351	A(2-7-12)	120.1	A(18-12-19)	107.4
R(15-23)	1.074	A(6-3-8)	119.3	A(14-21-26)	120.7
R(16-22)	1.508	A(3-6-9)	120.3	A(14-21-30)	117.4
R(16-24)	1.015	A(3-6-13)	119.2	A(20-15-23)	118.5
R(16-25)	1.015	A(9-5-11)	117.7	A(15-20-26)	120.8
R(20-26)	1.432	A(5-9-6)	120.7	A(15-20-29)	119.9
A(22-16-24)	108.5	A(21-26-32)	120.5	A(33-31-34)	107.9
A(22-16-25)	107.2	A(27-22-28)	134.8	A(33-31-35)	109
A(16-22-27)	110.9	A(22-27-31)	118.9	A(34-31-35)	109
A(16-22-28)	114.4	A(20-26-21)	120.2	A(27-31-33)	111.2
A(24-16-25)	106.7	A(20-26-32)	119.3	A(27-31-34)	111.1
A(26-20-29)	119.3	A(26-21-30)	121.9	A(27-31-35)	108.7

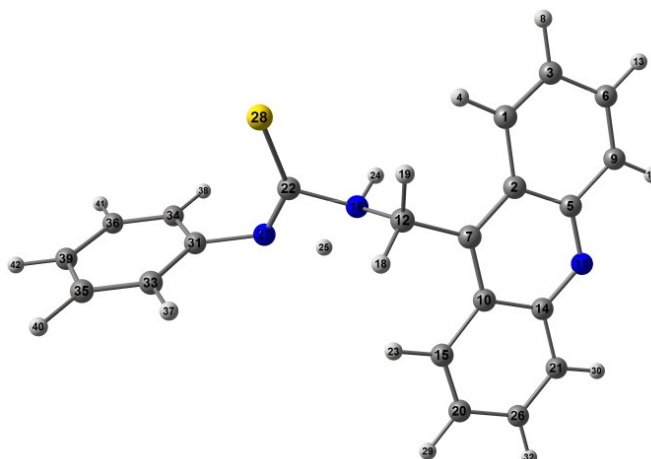
**IIIa**

R(1-2)	1.441	R(30-33)	1.085	A(14-10-15)	117.9
R(1-3)	1.351	R(30-34)	1.085	A(10-14-11)	122.9
R(1-4)	1.074	R(30-35)	1.08	A(10-14-21)	119.3
R(2-5)	1.427	A(2-1-3)	121	A(10-15-20)	121
R(2-7)	1.401	A(2-1-4)	120	A(10-15-23)	120
R(3-6)	1.433	A(1-2-5)	117.9	A(11-14-21)	117.7
R(3-8)	1.077	A(1-2-7)	124.1	A(16-12-18)	109.6
R(5-9)	1.437	A(3-1-4)	119	A(16-12-19)	109.6
R(5-11)	1.324	A(1-3-6)	120.7	A(12-16-22)	125
R(6-9)	1.349	A(1-3-8)	120	A(12-16-24)	116.4
R(6-13)	1.077	A(5-2-7)	118.1	A(18-12-19)	106.4
R(7-10)	1.401	A(2-5-9)	119.3	A(14-21-25)	120.7
R(7-12)	1.517	A(2-5-11)	122.9	A(14-21-29)	117.5
R(9-17)	1.076	A(2-7-10)	118.8	A(20-15-23)	119
R(10-14)	1.427	A(2-7-12)	120.6	A(15-20-25)	120.7
R(10-15)	1.441	A(6-3-8)	119.3	A(15-20-28)	120
R(11-14)	1.324	R(26-30)	1.451	A(22-16-24)	118.6
R(12-16)	1.461	R(26-32)	1.002	A(16-22-26)	117.5
R(12-18)	1.078	A(3-6-9)	120.4	A(16-22-27)	122.2
R(12-19)	1.078	A(3-6-13)	119.2	A(25-20-28)	119.3
R(14-21)	1.437	A(9-5-11)	117.8	A(20-25-21)	120.4
R(15-20)	1.351	A(5-9-6)	120.7	A(20-25-31)	119.2
R(15-23)	1.074	A(5-9-17)	117.5	A(25-21-29)	121.8
R(16-22)	1.332	A(5-11-14)	119.2	A(21-25-31)	120.4
R(16-24)	0.996	A(9-6-13)	120.4	A(26-22-27)	120.3
R(20-25)	1.433	A(6-9-17)	121.8	A(22-26-30)	126.3
R(20-28)	1.077	A(10-7-12)	120.6	A(22-26-32)	115.5
R(21-25)	1.349	A(7-10-14)	118	A(30-26-32)	118.2
R(21-29)	1.076	A(7-10-15)	124.1	A(26-30-33)	111.5
R(22-26)	1.329	A(7-12-16)	109.5	A(26-30-34)	111.5
R(22-27)	1.714	A(7-12-18)	110.8	A(26-30-35)	107.8
R(25-31)	1.077	A(7-12-19)	110.8	A(33-30-34)	109.5



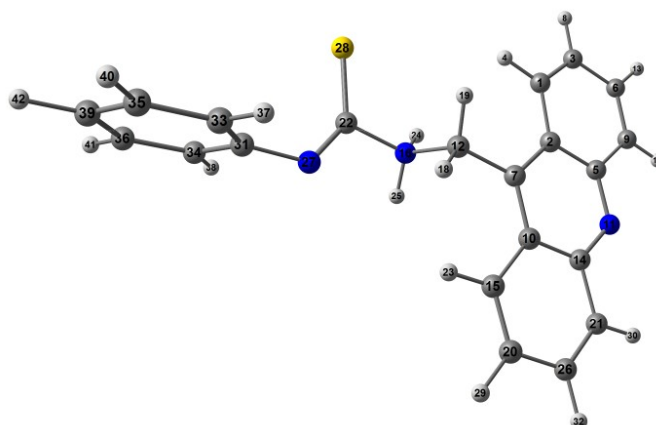
Ts Ib

R(1-2)	1.441	R(32-35)	1.405	A(7-12-20)	110.9
R(1-3)	1.35	R(32-37)	1.104	A(15-10-16)	117.7
R(1-4)	1.073	R(33-36)	1.405	A(10-15-11)	123.1
R(2-5)	1.427	R(33-38)	1.103	A(10-15-24)	119.3
R(2-7)	1.401	R(35-39)	1.404	A(10-16-23)	121.1
R(3-6)	1.432	R(35-40)	1.104	A(10-16-25)	120.1
R(3-8)	1.075	R(36-39)	1.404	A(11-15-24)	117.6
R(5-9)	1.437	R(36-41)	1.103	A(17-12-19)	107.6
R(5-11)	1.321	R(39-42)	1.104	A(17-12-20)	107.4
R(6-9)	1.348	A(2-1-3)	121	A(12-17-26)	111.2
R(6-13)	1.075	A(2-1-4)	120.1	A(12-17-27)	112
R(7-10)	1.401	A(1-2-5)	117.8	A(19-12-20)	106.3
R(7-12)	1.518	A(1-2-7)	124.1	A(21-14-22)	152.7
R(9-18)	1.074	A(3-1-4)	118.8	A(14-21-28)	121.4
R(10-15)	1.426	A(1-3-6)	120.8	A(15-24-29)	120.8
R(10-16)	1.441	A(1-3-8)	119.9	A(15-24-31)	117.1
R(11-15)	1.322	A(5-2-7)	118.1	A(23-16-25)	118.8
R(12-17)	1.466	A(2-5-9)	119.3	A(16-23-29)	120.8
R(12-19)	1.079	A(2-5-11)	123.1	A(16-23-30)	119.9
R(12-20)	1.078	A(2-7-10)	118.6	A(26-17-27)	108.5
R(14-21)	1.21	A(2-7-12)	120.5	A(21-28-32)	120
R(14-22)	1.644	A(6-3-8)	119.4	A(21-28-33)	119.9
R(15-24)	1.436	A(3-6-9)	120.3	A(29-23-30)	119.3
R(16-23)	1.35	A(3-6-13)	119.3	A(23-29-24)	120.3
R(16-25)	1.073	A(9-5-11)	117.6	A(23-29-34)	119.3
R(17-26)	1.003	A(5-9-6)	120.7	A(29-24-31)	122.1
R(17-27)	1.003	A(5-9-18)	117.2	A(24-29-34)	120.4
R(21-28)	1.5	A(5-11-15)	119.1	A(32-28-33)	120
R(23-29)	1.431	A(9-6-13)	120.4	A(28-32-35)	120
R(23-30)	1.076	A(6-9-18)	122.1	A(28-32-37)	120
R(24-29)	1.348	A(10-7-12)	120.9	A(28-33-36)	120
R(24-31)	1.074	A(7-10-15)	118.1	A(28-33-38)	120
R(28-32)	1.404	A(7-10-16)	124.2	A(35-32-37)	120
R(28-33)	1.405	A(7-12-17)	113.5	A(32-35-39)	120
R(29-34)	1.075	A(7-12-19)	110.9	A(32-35-40)	120

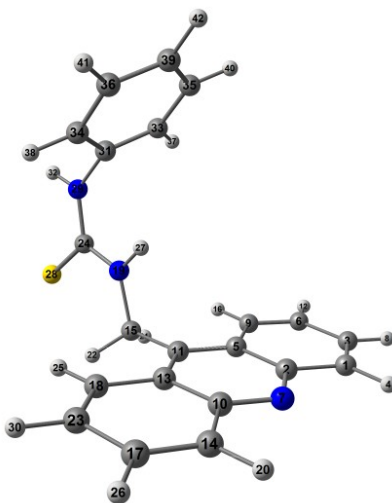


Ts IIb

R(1-2)	1.441	R(31-34)	1.405	A(7-12-16)	110.6
R(1-3)	1.35	R(33-35)	1.404	A(7-12-18)	111.5
R(1-4)	1.074	R(33-37)	1.104	A(7-12-19)	111.5
R(2-5)	1.427	R(34-36)	1.404	A(14-10-15)	117.8
R(2-7)	1.4	R(34-38)	1.103	A(10-14-11)	123.1
R(3-6)	1.433	R(35-39)	1.405	A(10-14-21)	119.3
R(3-8)	1.075	R(35-40)	1.104	A(10-15-20)	121.1
R(5-9)	1.437	R(36-39)	1.404	A(10-15-23)	120.1
R(5-11)	1.321	R(36-41)	1.104	A(11-14-21)	117.6
R(6-9)	1.347	R(39-42)	1.104	A(16-12-18)	107.4
R(6-13)	1.075	A(2-1-3)	121	A(16-12-19)	108.9
R(7-10)	1.401	A(2-1-4)	120.2	A(12-16-22)	116.2
R(7-12)	1.514	A(1-2-5)	117.8	A(12-16-24)	110.8
R(9-17)	1.074	A(1-2-7)	124.2	A(18-12-19)	106.7
R(10-14)	1.426	A(3-1-4)	118.8	A(14-21-26)	120.7
R(10-15)	1.44	A(1-3-6)	120.8	A(14-21-30)	117.2
R(11-14)	1.321	A(1-3-8)	119.9	A(20-15-23)	118.9
R(12-16)	1.474	A(5-2-7)	118	A(15-20-26)	120.8
R(12-18)	1.079	A(2-5-9)	119.3	A(15-20-29)	119.9
R(12-19)	1.078	A(2-5-11)	123	A(22-16-24)	110.3
R(14-21)	1.437	A(2-7-10)	118.8	A(16-22-27)	98.1
R(15-20)	1.349	A(2-7-12)	120.2	A(16-22-28)	125.1
R(15-23)	1.073	A(6-3-8)	119.3	A(26-20-29)	119.3
R(16-22)	1.484	A(3-6-9)	120.3	A(20-26-21)	120.3
R(16-24)	1.006	A(3-6-13)	119.3	A(20-26-32)	119.4
R(20-26)	1.432	A(9-5-11)	117.7	A(26-21-30)	122.1
R(20-29)	1.075	A(5-9-6)	120.7	A(21-26-32)	120.4
R(21-26)	1.348	A(5-9-17)	117.2	A(27-22-28)	136.8
R(21-30)	1.073	A(5-11-14)	119.2	A(22-27-31)	124.4
R(22-27)	1.288	A(9-6-13)	120.4	A(27-31-33)	120
R(22-28)	1.667	A(6-9-17)	122.1	A(27-31-34)	120
R(26-32)	1.075	A(10-7-12)	121	A(33-31-34)	120
R(27-31)	1.5	A(7-10-14)	118	A(31-33-35)	120
R(31-33)	1.405	A(7-10-15)	124.2	A(31-33-37)	120

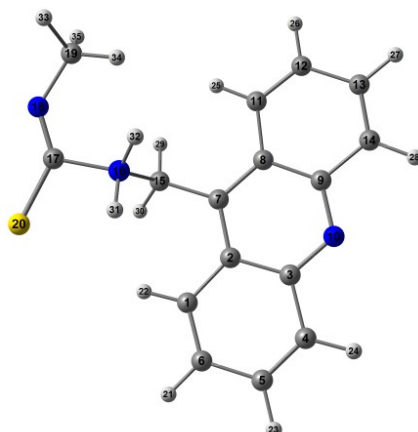
**IIb**

R(1-2)	1.441	R(31-34)	1.388	A(7-12-18)	112.1
R(1-3)	1.351	R(33-35)	1.387	A(7-12-19)	112.2
R(1-4)	1.073	R(33-37)	1.077	A(14-10-15)	117.7
R(2-5)	1.427	R(34-36)	1.389	A(10-14-11)	122.9
R(2-7)	1.4	R(34-38)	1.077	A(10-14-21)	119.4
R(3-6)	1.433	R(35-39)	1.39	A(10-15-20)	121.1
R(3-8)	1.077	R(35-40)	1.077	A(10-15-23)	120.5
R(5-9)	1.437	R(36-39)	1.387	A(11-14-21)	117.7
R(5-11)	1.323	R(36-41)	1.077	A(16-12-18)	106.2
R(6-9)	1.349	R(39-42)	1.077	A(16-12-19)	106.6
R(6-13)	1.077	A(2-1-3)	121	A(12-16-22)	112.1
R(7-10)	1.4	A(2-1-4)	120.4	A(12-16-24)	110.8
R(7-12)	1.514	A(1-2-5)	117.8	A(12-16-25)	110.6
R(9-17)	1.076	A(1-2-7)	124.4	A(18-12-19)	107.5
R(10-14)	1.427	A(3-1-4)	118.6	A(14-21-26)	120.7
R(10-15)	1.441	A(1-3-6)	120.8	A(14-21-30)	117.4
R(11-14)	1.323	A(1-3-8)	119.9	A(20-15-23)	118.5
R(12-16)	1.502	A(5-2-7)	117.8	A(15-20-26)	120.8
R(12-18)	1.077	A(2-5-9)	119.4	A(15-20-29)	119.9
R(12-19)	1.076	A(2-5-11)	122.9	A(22-16-24)	108.6
R(14-21)	1.437	A(2-7-10)	119.2	A(22-16-25)	107.6
R(15-20)	1.351	A(2-7-12)	120.4	A(16-22-27)	110.1
R(15-23)	1.074	A(6-3-8)	119.3	A(16-22-28)	113.8
R(16-22)	1.515	A(3-6-9)	120.3	A(24-16-25)	107
R(16-24)	1.014	A(3-6-13)	119.2	A(26-20-29)	119.3
R(16-25)	1.015	A(9-5-11)	117.7	A(20-26-21)	120.2
R(20-26)	1.432	A(5-9-6)	120.7	A(20-26-32)	119.3
R(20-29)	1.077	A(5-9-17)	117.4	A(26-21-30)	121.9
R(21-26)	1.349	A(5-11-14)	119.5	A(21-26-32)	120.5
R(21-30)	1.076	A(9-6-13)	120.5	A(27-22-28)	136.1
R(22-27)	1.251	A(6-9-17)	121.9	A(22-27-31)	121.4
R(22-28)	1.715	A(10-7-12)	120.5	A(27-31-33)	120.1
R(26-32)	1.077	A(7-10-14)	117.8	A(27-31-34)	120.1
R(27-31)	1.412	A(7-10-15)	124.5	A(33-31-34)	119.6
R(31-33)	1.392	A(7-12-16)	111.8	A(31-33-35)	120.1



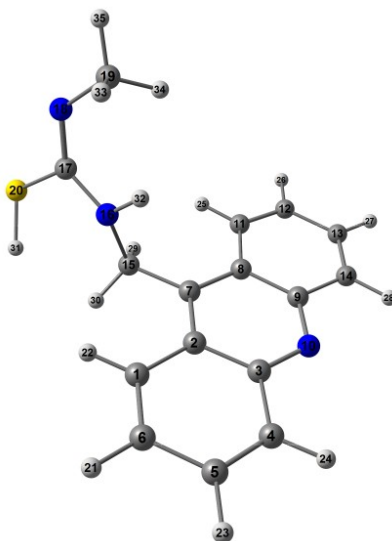
IIIb

R(1-2)	1.437	R(24-29)	1.337	A(5-11-13)	118.8
R(1-3)	1.349	R(29-31)	1.43	A(5-11-15)	120.6
R(1-4)	1.076	R(29-32)	1.005	A(9-6-12)	120
R(2-5)	1.427	R(31-33)	1.389	A(6-9-16)	119
R(2-7)	1.324	R(31-34)	1.389	A(7-10-13)	123
R(3-6)	1.433	R(33-35)	1.388	A(7-10-14)	117.7
R(3-8)	1.077	R(33-37)	1.077	A(13-10-14)	119.3
R(5-9)	1.441	R(34-36)	1.388	A(10-13-11)	118
R(5-11)	1.4	R(34-38)	1.077	A(10-13-18)	117.9
R(6-9)	1.351	R(35-39)	1.389	A(10-14-17)	120.7
R(6-12)	1.077	R(35-40)	1.077	A(10-14-20)	117.5
R(7-10)	1.324	R(36-39)	1.389	A(13-11-15)	120.6
R(9-16)	1.074	R(36-41)	1.077	A(11-13-18)	124.1
R(10-13)	1.427	R(39-42)	1.077	A(11-15-19)	109.4
R(10-14)	1.437	A(2-1-3)	120.7	A(11-15-21)	110.8
R(11-13)	1.401	A(2-1-4)	117.5	A(11-15-22)	110.8
R(11-15)	1.517	A(1-2-5)	119.3	A(13-18-23)	121
R(13-18)	1.441	A(1-2-7)	117.7	A(13-18-25)	120
R(14-17)	1.349	A(3-1-4)	121.8	A(17-14-20)	121.8
R(14-20)	1.076	A(1-3-6)	120.3	A(14-17-23)	120.4
R(15-19)	1.46	A(1-3-8)	120.4	A(14-17-26)	120.4
R(15-21)	1.078	A(5-2-7)	123	A(19-15-21)	109.7
R(15-22)	1.078	A(2-5-9)	117.9	A(19-15-22)	109.7
R(17-23)	1.433	A(2-5-11)	118	A(15-19-24)	125.1
R(17-26)	1.077	A(2-7-10)	119.2	A(15-19-27)	117.1
R(18-23)	1.351	A(6-3-8)	119.2	A(21-15-22)	106.4
R(18-25)	1.074	A(3-6-9)	120.7	A(23-17-26)	119.2
R(19-24)	1.329	A(3-6-12)	119.3	A(17-23-18)	120.7
R(19-27)	0.997	A(9-5-11)	124	A(17-23-30)	119.3
R(23-30)	1.077	A(5-9-6)	121	A(23-18-25)	119
R(24-28)	1.711	A(5-9-16)	120	A(18-23-30)	120



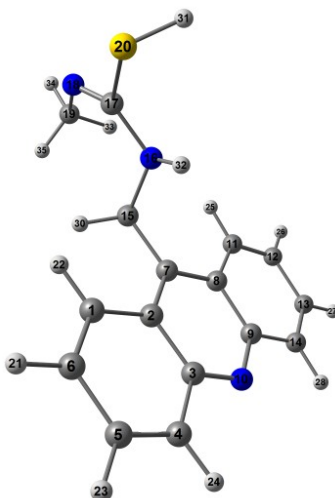
IVa

R(1-2)	1.441	R(19-34)	1.092	A(9-14-13)	120.8
R(1-6)	1.35	R(19-35)	1.085	A(9-14-28)	117.1
R(1-22)	1.074	A(2-1-6)	120.7	A(12-11-25)	118.5
R(2-3)	1.427	A(2-1-22)	120.6	A(11-12-13)	120.9
R(2-7)	1.401	A(1-2-3)	118	A(11-12-26)	119.8
R(3-4)	1.436	A(1-2-7)	124.1	A(13-12-26)	119.3
R(3-10)	1.322	A(6-1-22)	118.7	A(12-13-14)	120.1
R(4-5)	1.348	A(1-6-5)	121	A(12-13-27)	119.3
R(4-24)	1.074	A(1-6-21)	119.6	A(14-13-27)	120.5
R(5-6)	1.432	A(3-2-7)	117.8	A(13-14-28)	122.1
R(5-23)	1.075	A(2-3-4)	119.4	A(16-15-29)	107.1
R(6-21)	1.075	A(2-3-10)	122.9	A(16-15-30)	106
R(7-8)	1.401	A(2-7-8)	119.1	A(15-16-17)	112.7
R(7-15)	1.513	A(2-7-15)	119.8	A(15-16-31)	109.5
R(8-9)	1.428	A(4-3-10)	117.7	A(15-16-32)	110.4
R(8-11)	1.441	A(3-4-5)	120.6	A(29-15-30)	107.4
R(9-10)	1.32	A(3-4-24)	117.2	A(17-16-31)	103.6
R(9-14)	1.437	A(3-10-9)	119.4	A(17-16-32)	112.4
R(11-12)	1.35	A(5-4-24)	122.2	A(16-17-18)	118.1
R(11-25)	1.073	A(4-5-6)	120.3	A(16-17-20)	108.8
R(12-13)	1.432	A(4-5-23)	120.4	A(31-16-32)	107.9
R(12-26)	1.075	A(6-5-23)	119.3	A(18-17-20)	133.1
R(13-14)	1.348	A(5-6-21)	119.4	A(17-18-19)	128.5
R(13-27)	1.075	A(8-7-15)	121.1	A(18-19-33)	108.9
R(14-28)	1.074	A(7-8-9)	117.7	A(18-19-34)	116.4
R(15-16)	1.495	A(7-8-11)	124.7	A(18-19-35)	109
R(15-29)	1.076	A(7-15-16)	111.3	A(33-19-34)	107.6
R(15-30)	1.077	A(7-15-29)	112.4	A(33-19-35)	107.2
R(16-17)	1.581	A(7-15-30)	112.2	A(34-19-35)	107.4
R(16-31)	1.007	A(9-8-11)	117.6		
R(16-32)	1.006	A(8-9-10)	123		
R(17-18)	1.241	A(8-9-14)	119.4		
R(17-20)	1.712	A(8-11-12)	121.2		
R(18-19)	1.435	A(8-11-25)	120.3		
R(19-33)	1.084	A(10-9-14)	117.5		



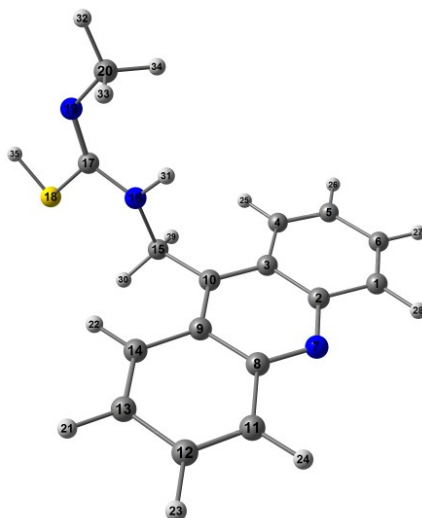
Va

R(1-2)	1.44	R(18-19)	1.446	A(9-8-11)	117.8
R(1-6)	1.35	R(19-33)	1.09	A(8-9-10)	123.1
R(1-22)	1.073	R(19-34)	1.091	A(8-9-14)	119.3
R(2-3)	1.426	R(19-35)	1.081	A(8-11-12)	121.1
R(2-7)	1.4	R(20-31)	1.326	A(8-11-25)	119.9
R(3-4)	1.437	A(2-1-6)	121	A(10-9-14)	117.6
R(3-10)	1.322	A(2-1-22)	119.6	A(9-14-13)	120.7
R(4-5)	1.348	A(1-2-3)	118	A(9-14-28)	117.2
R(4-24)	1.074	A(1-2-7)	123.9	A(12-11-25)	119
R(5-6)	1.432	A(6-1-22)	119.3	A(11-12-13)	120.8
R(5-23)	1.075	A(1-6-5)	120.7	A(11-12-26)	119.9
R(6-21)	1.075	A(1-6-21)	120	A(13-12-26)	119.3
R(7-8)	1.4	A(3-2-7)	118.1	A(12-13-14)	120.3
R(7-15)	1.517	A(2-3-4)	119.3	A(12-13-27)	119.3
R(8-9)	1.427	A(2-3-10)	123	A(14-13-27)	120.4
R(8-11)	1.441	A(2-7-8)	118.6	A(13-14-28)	122.1
R(9-10)	1.322	A(2-7-15)	120.4	A(16-15-29)	111.1
R(9-14)	1.437	A(4-3-10)	117.7	A(16-15-30)	110.4
R(11-12)	1.35	A(3-4-5)	120.7	A(15-16-17)	124.8
R(11-25)	1.073	A(3-4-24)	117.2	A(15-16-32)	114.2
R(12-13)	1.432	A(3-10-9)	119.1	A(29-15-30)	106.4
R(12-26)	1.075	A(5-4-24)	122.1	A(17-16-32)	113.6
R(13-14)	1.348	A(4-5-6)	120.4	A(16-17-18)	126.8
R(13-27)	1.075	A(4-5-23)	120.4	A(16-17-20)	118.2
R(14-28)	1.074	A(6-5-23)	119.3	A(18-17-20)	115
R(15-16)	1.461	A(5-6-21)	119.3	A(17-18-19)	120.2
R(15-29)	1.08	A(8-7-15)	121	A(17-20-31)	98.7
R(15-30)	1.082	A(7-8-9)	118	A(18-19-33)	111.8
R(16-17)	1.379	A(7-8-11)	124.2	A(18-19-34)	112.8
R(16-32)	0.995	A(7-15-16)	110.1	A(18-19-35)	108.6
R(17-18)	1.253	A(7-15-29)	110	A(33-19-34)	108.3
R(17-20)	1.786	A(7-15-30)	108.8	A(33-19-35)	107.5



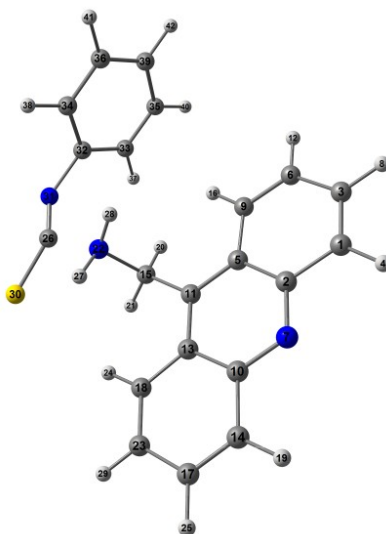
Ts Va

R(1-2)	1.441	R(19-33)	1.087	A(8-9-14)	119.3
R(1-6)	1.35	R(19-34)	1.082	A(8-11-12)	121
R(1-22)	1.073	R(19-35)	1.086	A(8-11-25)	119.6
R(2-3)	1.427	R(20-31)	1.329	A(10-9-14)	117.7
R(2-7)	1.4	A(2-1-6)	121.1	A(9-14-13)	120.7
R(3-4)	1.437	A(2-1-22)	119.9	A(9-14-28)	117.2
R(3-10)	1.321	A(1-2-3)	117.8	A(12-11-25)	119.4
R(4-5)	1.348	A(1-2-7)	124.2	A(11-12-13)	120.7
R(4-24)	1.074	A(6-1-22)	119	A(11-12-26)	120
R(5-6)	1.432	A(1-6-5)	120.8	A(13-12-26)	119.3
R(5-23)	1.075	A(1-6-21)	119.9	A(12-13-14)	120.4
R(6-21)	1.075	A(3-2-7)	118	A(12-13-27)	119.3
R(7-8)	1.4	A(2-3-4)	119.3	A(14-13-27)	120.4
R(7-15)	1.517	A(2-3-10)	123.1	A(13-14-28)	122.1
R(8-9)	1.425	A(2-7-8)	118.6	A(16-15-29)	110.7
R(8-11)	1.44	A(2-7-15)	121.1	A(16-15-30)	110.6
R(9-10)	1.322	A(4-3-10)	117.6	A(15-16-17)	121.7
R(9-14)	1.437	A(3-4-5)	120.8	A(15-16-32)	112.1
R(11-12)	1.35	A(3-4-24)	117.1	A(29-15-30)	106.4
R(11-25)	1.073	A(3-10-9)	119	A(17-16-32)	111.9
R(12-13)	1.432	A(5-4-24)	122.1	A(16-17-18)	129.4
R(12-26)	1.075	A(4-5-6)	120.3	A(16-17-20)	113.5
R(13-14)	1.348	A(4-5-23)	120.4	A(18-17-20)	117.1
R(13-27)	1.075	A(6-5-23)	119.3	A(17-18-19)	122.9
R(14-28)	1.074	A(5-6-21)	119.3	A(17-20-31)	95.7
R(15-16)	1.466	A(8-7-15)	120.3	A(18-19-33)	112.6
R(15-29)	1.078	A(7-8-9)	118.2	A(18-19-34)	107.7
R(15-30)	1.082	A(7-8-11)	123.9	A(18-19-35)	111.9
R(16-17)	1.39	A(7-15-16)	110.2	A(33-19-34)	108.2
R(16-32)	0.995	A(7-15-29)	108.9	A(33-19-35)	108.8
R(17-18)	1.248	A(7-15-30)	109.9	A(34-19-35)	107.4
R(17-20)	1.815	A(9-8-11)	118		
R(18-19)	1.449	A(8-9-10)	123		



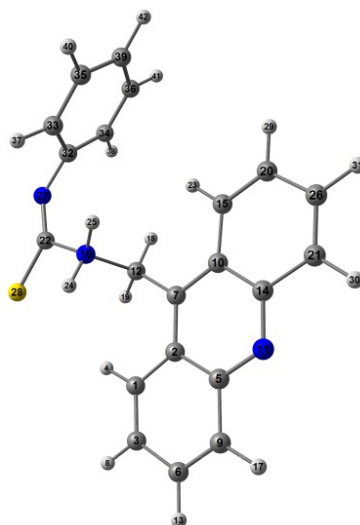
VIa

R(1-2)	1.438	R(18-35)	1.324	A(8-11-24)	117.2
R(1-6)	1.348	R(19-20)	1.447	A(10-9-14)	123.9
R(1-28)	1.074	R(20-32)	1.081	A(9-10-15)	120.4
R(2-3)	1.427	R(20-33)	1.09	A(9-14-13)	120.9
R(2-7)	1.321	R(20-34)	1.091	A(9-14-22)	119.7
R(3-4)	1.441	A(2-1-6)	120.8	A(10-15-16)	110
R(3-10)	1.4	A(2-1-28)	117.1	A(10-15-29)	110.1
R(4-5)	1.349	A(1-2-3)	119.3	A(10-15-30)	109.2
R(4-25)	1.073	A(1-2-7)	117.6	A(12-11-24)	122.1
R(5-6)	1.432	A(6-1-28)	122.1	A(11-12-13)	120.4
R(5-26)	1.075	A(1-6-5)	120.3	A(11-12-23)	120.4
R(6-27)	1.075	A(1-6-27)	120.4	A(13-12-23)	119.3
R(7-8)	1.323	A(3-2-7)	123.1	A(12-13-14)	120.7
R(8-9)	1.425	A(2-3-4)	117.7	A(12-13-21)	119.3
R(8-11)	1.436	A(2-3-10)	118	A(14-13-21)	119.9
R(9-10)	1.4	A(2-7-8)	119.1	A(13-14-22)	119.3
R(9-14)	1.439	A(4-3-10)	124.3	A(16-15-29)	111.6
R(10-15)	1.517	A(3-4-5)	121.1	A(16-15-30)	109.5
R(11-12)	1.348	A(3-4-25)	119.9	A(15-16-17)	124.9
R(11-24)	1.074	A(3-10-9)	118.7	A(15-16-31)	115.4
R(12-13)	1.432	A(3-10-15)	120.9	A(29-15-30)	106.4
R(12-23)	1.075	A(5-4-25)	119	A(17-16-31)	115
R(13-14)	1.35	A(4-5-6)	120.8	A(16-17-18)	114.7
R(13-21)	1.075	A(4-5-26)	119.9	A(16-17-19)	126.8
R(14-22)	1.073	A(6-5-26)	119.3	A(18-17-19)	118.5
R(15-16)	1.457	A(5-6-27)	119.3	A(17-18-35)	93.9
R(15-29)	1.082	A(7-8-9)	123	A(17-19-20)	119.4
R(15-30)	1.08	A(7-8-11)	117.7	A(19-20-32)	108.6
R(16-17)	1.372	A(9-8-11)	119.3	A(19-20-33)	112.2
R(16-31)	0.995	A(8-9-10)	118.1	A(19-20-34)	112.4
R(17-18)	1.787	A(8-9-14)	118	A(32-20-33)	107.8
R(17-19)	1.256	A(8-11-12)	120.7	A(32-20-34)	107.4



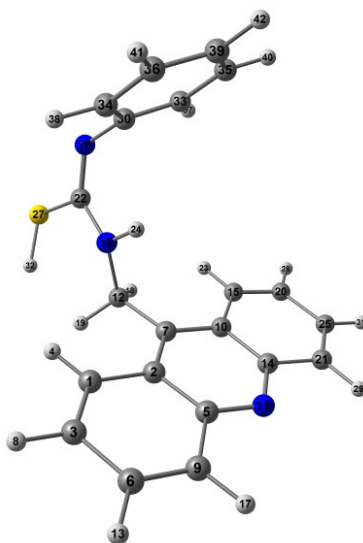
Ts IIIb

R(1-2)	1.438	R(31-32)	1.5	A(6-9-16)	118.5
R(1-3)	1.347	R(32-33)	1.404	A(7-10-13)	123
R(1-4)	1.074	R(32-34)	1.404	A(7-10-14)	117.7
R(2-5)	1.426	R(33-35)	1.405	A(13-10-14)	119.4
R(2-7)	1.321	R(33-37)	1.103	A(10-13-11)	118
R(3-6)	1.431	R(34-36)	1.405	A(10-13-18)	117.9
R(3-8)	1.075	R(34-38)	1.103	A(10-14-17)	120.6
R(5-9)	1.441	R(35-39)	1.404	A(10-14-19)	117.2
R(5-11)	1.401	R(35-40)	1.104	A(13-11-15)	120.1
R(6-9)	1.35	R(36-39)	1.405	A(11-13-18)	124.1
R(6-12)	1.075	R(36-41)	1.103	A(11-15-20)	111.6
R(7-10)	1.322	R(39-42)	1.103	A(11-15-21)	111.4
R(9-16)	1.072	A(2-1-3)	120.8	A(11-15-22)	112.3
R(10-13)	1.427	A(2-1-4)	117.1	A(13-18-23)	120.8
R(10-14)	1.436	A(1-2-5)	119.4	A(13-18-24)	120.4
R(11-13)	1.4	A(1-2-7)	117.5	A(17-14-19)	122.2
R(11-15)	1.516	A(3-1-4)	122.2	A(14-17-23)	120.4
R(13-18)	1.441	A(1-3-6)	120.2	A(14-17-25)	120.4
R(14-17)	1.347	A(1-3-8)	120.5	A(20-15-21)	106.9
R(14-19)	1.073	A(5-2-7)	123.1	A(20-15-22)	107.7
R(15-20)	1.077	A(2-5-9)	117.6	A(21-15-22)	106.6
R(15-21)	1.078	A(2-5-11)	117.9	A(15-22-27)	110.2
R(15-22)	1.481	A(2-7-10)	119.3	A(15-22-28)	110.9
R(17-23)	1.432	A(6-3-8)	119.3	A(23-17-25)	119.2
R(17-25)	1.076	A(3-6-9)	120.8	A(17-23-18)	120.9
R(18-23)	1.35	A(3-6-12)	119.3	A(17-23-29)	119.3
R(18-24)	1.074	A(9-5-11)	124.5	A(23-18-24)	118.8
R(22-27)	1.005	A(5-9-6)	121.2	A(18-23-29)	119.8
R(22-28)	1.004	A(5-9-16)	120.3	A(27-22-28)	107.6
R(23-29)	1.075	A(5-11-13)	118.8	A(30-26-31)	140
R(26-30)	1.685	A(5-11-15)	121.1	A(26-31-32)	132.7
R(26-31)	1.218	A(9-6-12)	119.9	A(31-32-33)	120



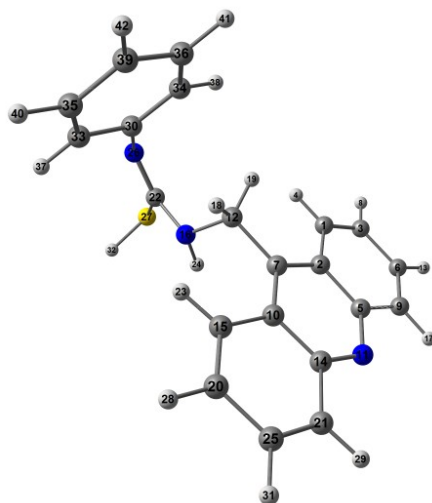
IVb

R(1-2)	1.441	R(26-31)	1.075	A(9-6-13)	120.4
R(1-3)	1.35	R(27-32)	1.399	A(6-9-17)	122.2
R(1-4)	1.074	R(32-33)	1.395	A(10-7-12)	120.8
R(2-5)	1.427	R(32-34)	1.395	A(7-10-14)	117.7
R(2-7)	1.4	R(33-35)	1.389	A(7-10-15)	124.5
R(3-6)	1.432	R(33-37)	1.077	A(7-12-16)	111.2
R(3-8)	1.075	R(34-36)	1.385	A(7-12-18)	112.3
R(5-9)	1.436	R(34-38)	1.075	A(7-12-19)	112.2
R(5-11)	1.321	R(35-39)	1.385	A(14-10-15)	117.8
R(6-9)	1.348	R(35-40)	1.076	A(10-14-11)	123
R(6-13)	1.075	R(36-39)	1.39	A(10-14-21)	119.4
R(7-10)	1.4	R(36-41)	1.076	A(10-15-20)	121
R(7-12)	1.513	R(39-42)	1.075	A(10-15-23)	120.5
R(9-17)	1.074	A(2-1-3)	120.7	A(11-14-21)	117.6
R(10-14)	1.427	A(2-1-4)	120.5	A(16-12-18)	106.8
R(10-15)	1.44	A(1-2-5)	118	A(16-12-19)	106.1
R(11-14)	1.321	A(1-2-7)	124.3	A(12-16-22)	112.7
R(12-16)	1.5	A(3-1-4)	118.7	A(12-16-24)	109.4
R(12-18)	1.077	A(1-3-6)	121	A(12-16-25)	109.7
R(12-19)	1.076	A(1-3-8)	119.6	A(18-12-19)	107.9
R(14-21)	1.437	A(5-2-7)	117.7	A(14-21-26)	120.7
R(15-20)	1.35	A(2-5-9)	119.4	A(14-21-30)	117.1
R(15-23)	1.073	A(2-5-11)	122.9	A(20-15-23)	118.5
R(16-22)	1.558	A(2-7-10)	119.1	A(15-20-26)	120.9
R(16-24)	1.007	A(2-7-12)	120	A(15-20-29)	119.7
R(16-25)	1.009	A(6-3-8)	119.3	A(22-16-24)	105.2
R(20-26)	1.432	A(3-6-9)	120.3	A(22-16-25)	111.1
R(20-29)	1.075	A(3-6-13)	119.3	A(16-22-27)	117.1
R(21-26)	1.348	A(9-5-11)	117.7	A(16-22-28)	110.5
R(21-30)	1.074	A(5-9-6)	120.6	A(24-16-25)	108.6
R(22-27)	1.251	A(5-9-17)	117.2	A(26-20-29)	119.4
R(22-28)	1.701	A(5-11-14)	119.4	A(20-26-21)	120.2

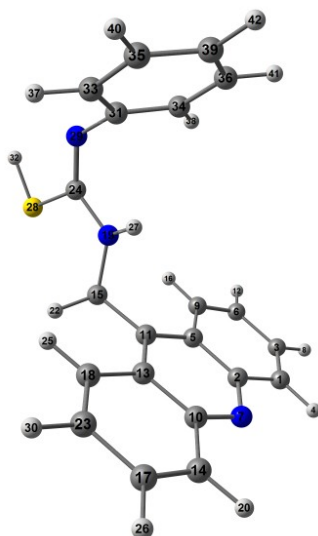


Vb

R(1-2)	1.44	R(26-30)	1.41	A(9-6-13)	120.4
R(1-3)	1.35	R(27-32)	1.325	A(6-9-17)	122.1
R(1-4)	1.073	R(30-33)	1.392	A(10-7-12)	121.1
R(2-5)	1.425	R(30-34)	1.393	A(7-10-14)	117.9
R(2-7)	1.4	R(33-35)	1.387	A(7-10-15)	124.3
R(3-6)	1.432	R(33-37)	1.075	A(7-12-16)	110.2
R(3-8)	1.075	R(34-36)	1.387	A(7-12-18)	110
R(5-9)	1.437	R(34-38)	1.076	A(7-12-19)	108.6
R(5-11)	1.322	R(35-39)	1.387	A(14-10-15)	117.8
R(6-9)	1.348	R(35-40)	1.076	A(10-14-11)	123.1
R(6-13)	1.075	R(36-39)	1.387	A(10-14-21)	119.3
R(7-10)	1.399	R(36-41)	1.076	A(10-15-20)	121.1
R(7-12)	1.517	R(39-42)	1.075	A(10-15-23)	119.9
R(9-17)	1.074	A(2-1-3)	121	A(11-14-21)	117.6
R(10-14)	1.427	A(2-1-4)	119.7	A(16-12-18)	111.1
R(10-15)	1.441	A(1-2-5)	118	A(16-12-19)	110.4
R(11-14)	1.321	A(1-2-7)	123.9	A(12-16-22)	125.6
R(12-16)	1.459	A(3-1-4)	119.3	A(12-16-24)	115.2
R(12-18)	1.08	A(1-3-6)	120.7	A(18-12-19)	106.6
R(12-19)	1.082	A(1-3-8)	120	A(14-21-25)	120.8
R(14-21)	1.437	A(5-2-7)	118.1	A(14-21-29)	117.1
R(15-20)	1.349	A(2-5-9)	119.3	A(20-15-23)	119
R(15-23)	1.073	A(2-5-11)	123	A(15-20-25)	120.8
R(16-22)	1.37	A(2-7-10)	118.7	A(15-20-28)	119.9
R(16-24)	0.997	A(2-7-12)	120.2	A(22-16-24)	113.3
R(20-25)	1.432	A(6-3-8)	119.3	A(16-22-26)	126.6
R(20-28)	1.075	A(3-6-9)	120.3	A(16-22-27)	119.2
R(21-25)	1.348	A(3-6-13)	119.3	A(25-20-28)	119.3
R(21-29)	1.074	A(9-5-11)	117.7	A(20-25-21)	120.3
R(22-26)	1.258	A(5-9-6)	120.7	A(20-25-31)	119.3
R(22-27)	1.783	A(5-9-17)	117.2	A(25-21-29)	122.1
R(25-31)	1.075	A(5-11-14)	119.1	A(21-25-31)	120.4

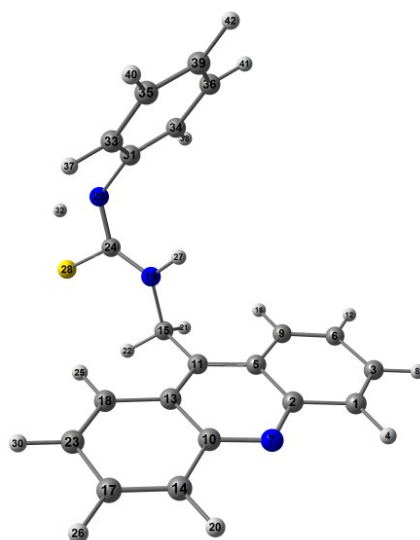
**Ts Vb**

R(1-2)	1.44	R(27-32)	1.329	A(10-7-12)	120.3
R(1-3)	1.35	R(30-33)	1.404	A(7-10-14)	118.2
R(1-4)	1.073	R(30-34)	1.404	A(7-10-15)	123.8
R(2-5)	1.428	R(33-35)	1.405	A(7-12-16)	110.2
R(2-7)	1.4	R(33-37)	1.104	A(7-12-18)	108.9
R(3-6)	1.432	R(34-36)	1.405	A(7-12-19)	109.9
R(3-8)	1.075	R(34-38)	1.104	A(14-10-15)	117.9
R(5-9)	1.436	R(35-39)	1.404	A(10-14-11)	123
R(5-11)	1.321	R(35-40)	1.103	A(10-14-21)	119.3
R(6-9)	1.348	R(36-39)	1.405	A(10-15-20)	121
R(6-13)	1.076	R(36-41)	1.103	A(10-15-23)	119.6
R(7-10)	1.399	R(39-42)	1.103	A(11-14-21)	117.7
R(7-12)	1.517	A(2-1-3)	121.1	A(16-12-18)	110.7
R(9-17)	1.075	A(2-1-4)	119.9	A(16-12-19)	110.6
R(10-14)	1.425	A(1-2-5)	117.8	A(12-16-22)	121.7
R(10-15)	1.44	A(1-2-7)	124.2	A(12-16-24)	112.2
R(11-14)	1.323	A(3-1-4)	119	A(18-12-19)	106.4
R(12-16)	1.466	A(1-3-6)	120.8	A(14-21-25)	120.6
R(12-18)	1.078	A(1-3-8)	119.9	A(14-21-29)	117.3
R(12-19)	1.082	A(5-2-7)	118	A(20-15-23)	119.4
R(14-21)	1.437	A(2-5-9)	119.3	A(15-20-25)	120.7
R(15-20)	1.35	A(2-5-11)	123.1	A(15-20-28)	120
R(15-23)	1.073	A(2-7-10)	118.6	A(22-16-24)	111.9
R(16-22)	1.39	A(2-7-12)	121.1	A(16-22-26)	129.4
R(16-24)	0.995	A(6-3-8)	119.4	A(16-22-27)	113.4
R(20-25)	1.432	A(3-6-9)	120.3	A(25-20-28)	119.2
R(20-28)	1.076	A(3-6-13)	119.3	A(20-25-21)	120.4
R(21-25)	1.348	A(9-5-11)	117.6	A(20-25-31)	119.3
R(21-29)	1.073	A(5-9-6)	120.7	A(25-21-29)	122.1
R(22-26)	1.248	A(5-9-17)	117.2	A(21-25-31)	120.3
R(22-27)	1.814	A(5-11-14)	119.1	A(26-22-27)	117.1
R(25-31)	1.076	A(9-6-13)	120.4	A(22-26-30)	122.9
R(26-30)	1.5	A(6-9-17)	122.1	A(22-27-32)	95.7



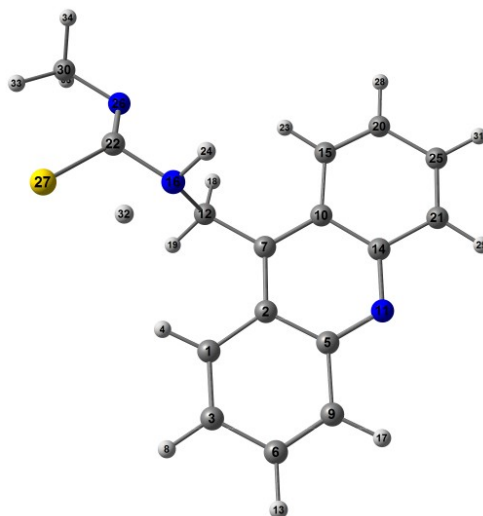
VIb

R(1-2)	1.436	R(28-32)	1.324	A(9-6-12)	120
R(1-3)	1.348	R(29-31)	1.411	A(6-9-16)	119.3
R(1-4)	1.074	R(31-33)	1.392	A(7-10-13)	123.1
R(2-5)	1.425	R(31-34)	1.393	A(7-10-14)	117.6
R(2-7)	1.323	R(33-35)	1.387	A(13-10-14)	119.3
R(3-6)	1.432	R(33-37)	1.075	A(10-13-11)	118
R(3-8)	1.075	R(34-36)	1.387	A(10-13-18)	117.8
R(5-9)	1.439	R(34-38)	1.076	A(10-14-17)	120.8
R(5-11)	1.4	R(35-39)	1.387	A(10-14-20)	117.1
R(6-9)	1.35	R(35-40)	1.076	A(13-11-15)	120.9
R(6-12)	1.075	R(36-39)	1.387	A(11-13-18)	124.3
R(7-10)	1.321	R(36-41)	1.076	A(11-15-19)	110.1
R(9-16)	1.073	R(39-42)	1.075	A(11-15-21)	109.2
R(10-13)	1.428	A(2-1-3)	120.7	A(11-15-22)	110.1
R(10-14)	1.437	A(2-1-4)	117.2	A(13-18-23)	121.1
R(11-13)	1.399	A(1-2-5)	119.3	A(13-18-25)	119.9
R(11-15)	1.517	A(1-2-7)	117.7	A(17-14-20)	122.1
R(13-18)	1.441	A(3-1-4)	122.1	A(14-17-23)	120.3
R(14-17)	1.347	A(1-3-6)	120.3	A(14-17-26)	120.4
R(14-20)	1.074	A(1-3-8)	120.4	A(19-15-21)	109.6
R(15-19)	1.456	A(5-2-7)	123	A(19-15-22)	111.5
R(15-21)	1.08	A(2-5-9)	118	A(15-19-24)	125.3
R(15-22)	1.082	A(2-5-11)	118.1	A(15-19-27)	116.5
R(17-23)	1.432	A(2-7-10)	119.1	A(21-15-22)	106.4
R(17-26)	1.075	A(6-3-8)	119.3	A(23-17-26)	119.3
R(18-23)	1.349	A(3-6-9)	120.7	A(17-23-18)	120.8
R(18-25)	1.073	A(3-6-12)	119.3	A(17-23-30)	119.3
R(19-24)	1.363	A(9-5-11)	123.9	A(23-18-25)	119
R(19-27)	0.997	A(5-9-6)	121	A(18-23-30)	119.9
R(23-30)	1.075	A(5-9-16)	119.7	A(24-19-27)	114.8
R(24-28)	1.784	A(5-11-13)	118.7	A(19-24-28)	114.9
R(24-29)	1.261	A(5-11-15)	120.4	A(19-24-29)	127



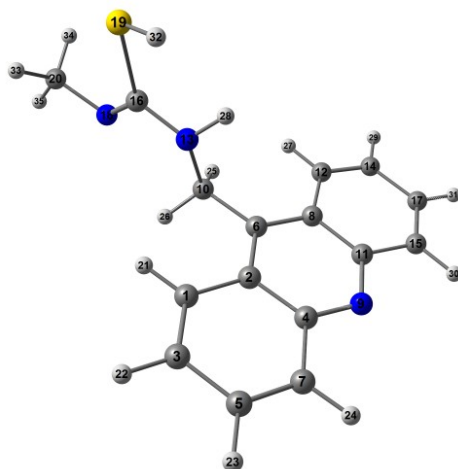
Ts VIb

R(1-2)	1.436	R(29-31)	1.5	A(6-9-16)	119
R(1-3)	1.345	R(31-33)	1.404	A(7-10-13)	123
R(1-4)	1.074	R(31-34)	1.404	A(7-10-14)	117.7
R(2-5)	1.426	R(33-35)	1.405	A(13-10-14)	119.3
R(2-7)	1.321	R(33-37)	1.104	A(10-13-11)	118.1
R(3-6)	1.432	R(34-36)	1.405	A(10-13-18)	118
R(3-8)	1.075	R(34-38)	1.103	A(10-14-17)	120.7
R(5-9)	1.441	R(35-39)	1.405	A(10-14-20)	117.1
R(5-11)	1.398	R(35-40)	1.104	A(13-11-15)	120.3
R(6-9)	1.347	R(36-39)	1.404	A(11-13-18)	124
R(6-12)	1.075	R(36-41)	1.103	A(11-15-19)	110.3
R(7-10)	1.322	R(39-42)	1.103	A(11-15-21)	110.7
R(9-16)	1.073	A(2-1-3)	120.8	A(11-15-22)	110.5
R(10-13)	1.424	A(2-1-4)	117	A(13-18-23)	120.9
R(10-14)	1.435	A(1-2-5)	119.3	A(13-18-25)	119.9
R(11-13)	1.4	A(1-2-7)	117.6	A(17-14-20)	122.2
R(11-15)	1.515	A(3-1-4)	122.2	A(14-17-23)	120.3
R(13-18)	1.439	A(1-3-6)	120.3	A(14-17-26)	120.5
R(14-17)	1.346	A(1-3-8)	120.5	A(19-15-21)	110.5
R(14-20)	1.073	A(5-2-7)	123.1	A(19-15-22)	108.4
R(15-19)	1.458	A(2-5-9)	117.7	A(15-19-24)	124.9
R(15-21)	1.081	A(2-5-11)	118	A(15-19-27)	117
R(15-22)	1.077	A(2-7-10)	119	A(21-15-22)	106.3
R(17-23)	1.432	A(6-3-8)	119.2	A(23-17-26)	119.2
R(17-26)	1.074	A(3-6-9)	120.8	A(17-23-18)	120.8
R(18-23)	1.348	A(3-6-12)	119.2	A(17-23-30)	119.2
R(18-25)	1.072	A(9-5-11)	124.3	A(23-18-25)	119.2
R(19-24)	1.335	A(5-9-6)	121.2	A(18-23-30)	120
R(19-27)	0.996	A(5-9-16)	119.9	A(24-19-27)	117.4
R(23-30)	1.075	A(5-11-13)	118.7	A(19-24-28)	126.6
R(24-28)	1.755	A(5-11-15)	121	A(19-24-29)	127.4
R(24-29)	1.29	A(9-6-12)	120	A(28-24-29)	106



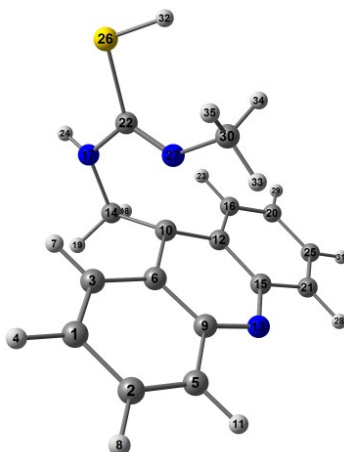
Ts VIIa

R(1-2)	1.44	R(26-30)	1.447	A(10-14-11)	123
R(1-3)	1.35	R(30-33)	1.085	A(10-14-21)	119.3
R(1-4)	1.073	R(30-34)	1.084	A(10-15-20)	121
R(2-5)	1.426	R(30-35)	1.084	A(10-15-23)	120.1
R(2-7)	1.399	A(2-1-3)	121	A(11-14-21)	117.6
R(3-6)	1.432	A(2-1-4)	120	A(16-12-18)	109.2
R(3-8)	1.075	A(1-2-5)	117.9	A(16-12-19)	107.2
R(5-9)	1.437	A(1-2-7)	124.2	A(12-16-22)	114.9
R(5-11)	1.322	A(3-1-4)	118.9	A(12-16-24)	111
R(6-9)	1.348	A(1-3-6)	120.8	A(18-12-19)	106.8
R(6-13)	1.075	A(1-3-8)	119.9	A(14-21-25)	120.7
R(7-10)	1.401	A(5-2-7)	118	A(14-21-29)	117.2
R(7-12)	1.514	A(2-5-9)	119.3	A(20-15-23)	118.9
R(9-17)	1.074	A(2-5-11)	123.1	A(15-20-25)	120.8
R(10-14)	1.426	A(2-7-10)	118.8	A(15-20-28)	119.9
R(10-15)	1.441	A(2-7-12)	121	A(22-16-24)	110
R(11-14)	1.321	A(6-3-8)	119.3	A(16-22-26)	120.8
R(12-16)	1.474	A(3-6-9)	120.3	A(16-22-27)	100.6
R(12-18)	1.079	A(3-6-13)	119.3	A(25-20-28)	119.3
R(12-19)	1.08	A(9-5-11)	117.6	A(20-25-21)	120.3
R(14-21)	1.437	A(5-9-6)	120.7	A(20-25-31)	119.3
R(15-20)	1.35	A(5-9-17)	117.2	A(25-21-29)	122.1
R(15-23)	1.073	A(5-11-14)	119.1	A(21-25-31)	120.4
R(16-22)	1.475	A(9-6-13)	120.4	A(26-22-27)	138.7
R(16-24)	1.006	A(6-9-17)	122.1	A(22-26-30)	120.2
R(20-25)	1.432	A(10-7-12)	120.3	A(26-30-33)	113.3
R(20-28)	1.075	A(7-10-14)	118	A(26-30-34)	108.8
R(21-25)	1.348	A(7-10-15)	124.2	A(26-30-35)	108.8
R(21-29)	1.074	A(7-12-16)	110.9	A(33-30-34)	109
R(22-26)	1.239	A(7-12-18)	111.3	A(33-30-35)	109.2
R(22-27)	1.762	A(7-12-19)	111.3	A(34-30-35)	107.6
R(25-31)	1.075	A(14-10-15)	117.8		

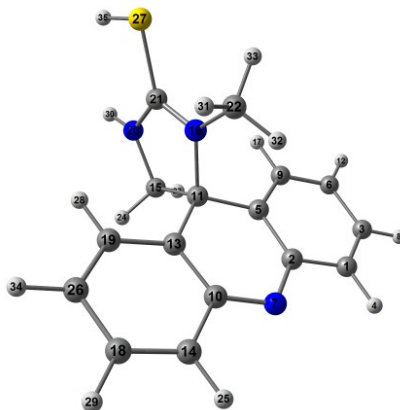


VIIa

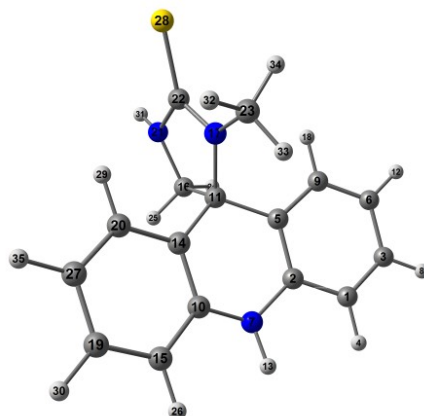
R(1-2)	1.438	R(20-33)	1.087	A(8-12-27)	119.9
R(1-3)	1.35	R(20-34)	1.088	A(9-11-15)	117.5
R(1-21)	1.072	R(20-35)	1.082	A(13-10-25)	111.3
R(2-4)	1.423	A(2-1-3)	121	A(13-10-26)	108.3
R(2-6)	1.401	A(2-1-21)	119.6	A(10-13-16)	118.2
R(3-5)	1.431	A(1-2-4)	118.1	A(10-13-28)	114.3
R(3-22)	1.076	A(1-2-6)	123.5	A(25-10-26)	105.8
R(4-7)	1.436	A(3-1-21)	119.5	A(11-15-17)	120.8
R(4-9)	1.324	A(1-3-5)	120.7	A(11-15-30)	117.3
R(5-7)	1.349	A(1-3-22)	120.1	A(14-12-27)	118.9
R(5-23)	1.075	A(4-2-6)	118.4	A(12-14-17)	120.7
R(6-8)	1.4	A(2-4-7)	119.3	A(12-14-29)	120
R(6-10)	1.516	A(2-4-9)	123	A(16-13-28)	115.2
R(7-24)	1.074	A(2-6-8)	118.4	A(13-16-18)	122.2
R(8-11)	1.428	A(2-6-10)	120.1	A(13-16-19)	114.8
R(8-12)	1.44	A(5-3-22)	119.3	A(17-14-29)	119.3
R(9-11)	1.322	A(3-5-7)	120.4	A(14-17-15)	120.3
R(10-13)	1.457	A(3-5-23)	119.3	A(14-17-31)	119.3
R(10-25)	1.081	A(7-4-9)	117.7	A(17-15-30)	121.9
R(10-26)	1.079	A(4-7-5)	120.6	A(15-17-31)	120.4
R(11-15)	1.437	A(4-7-24)	117.5	A(18-16-19)	123
R(12-14)	1.35	A(4-9-11)	118.9	A(16-18-20)	121.1
R(12-27)	1.072	A(7-5-23)	120.3	A(16-19-32)	97.3
R(13-16)	1.376	A(5-7-24)	121.9	A(18-20-33)	112.3
R(13-28)	1	A(8-6-10)	121.5	A(18-20-34)	111.8
R(14-17)	1.432	A(6-8-11)	118.1	A(18-20-35)	108.7
R(14-29)	1.075	A(6-8-12)	124.2	A(33-20-34)	108.2
R(15-17)	1.349	A(6-10-13)	109.6	A(33-20-35)	108.1
R(15-30)	1.074	A(6-10-25)	111.4	A(34-20-35)	107.6
R(16-18)	1.251	A(6-10-26)	110.3		
R(16-19)	1.796	A(11-8-12)	117.7		
R(17-31)	1.075	A(8-11-9)	123.2		
R(18-20)	1.446	A(8-11-15)	119.3		
R(19-32)	1.325	A(8-12-14)	121.2		

**Ts VIIIa**

R(1-2)	1.418	R(26-32)	1.323	A(15-12-16)	119.4
R(1-3)	1.363	R(27-30)	1.445	A(12-15-13)	125.3
R(1-4)	1.075	R(30-33)	1.08	A(12-15-21)	117.3
R(2-5)	1.358	R(30-34)	1.084	A(12-16-20)	122.2
R(2-8)	1.077	R(30-35)	1.084	A(12-16-23)	119.5
R(3-6)	1.417	A(2-1-3)	118.7	A(13-15-21)	117.4
R(3-7)	1.077	A(2-1-4)	120.5	A(17-14-18)	110
R(5-9)	1.432	A(1-2-5)	120.7	A(17-14-19)	110
R(5-11)	1.075	A(1-2-8)	119.5	A(14-17-22)	112.2
R(6-9)	1.412	A(3-1-4)	120.8	A(14-17-24)	120.1
R(6-10)	1.47	A(1-3-6)	122	A(18-14-19)	108.3
R(9-13)	1.337	A(1-3-7)	118.6	A(15-21-25)	121.8
R(10-12)	1.47	A(5-2-8)	119.8	A(15-21-28)	116.8
R(10-14)	1.552	A(2-5-9)	121.7	A(20-16-23)	118.3
R(12-15)	1.414	A(2-5-11)	121.4	A(16-20-25)	118.7
R(12-16)	1.417	A(6-3-7)	119.4	A(16-20-29)	120.8
R(13-15)	1.335	A(3-6-9)	119.6	A(22-17-24)	119.8
R(14-17)	1.462	A(3-6-10)	120.9	A(17-22-26)	116.8
R(14-18)	1.079	A(9-5-11)	116.8	A(17-22-27)	114.6
R(14-19)	1.079	A(5-9-6)	117.2	A(25-20-29)	120.5
R(15-21)	1.433	A(5-9-13)	117.5	A(20-25-21)	120.7
R(16-20)	1.362	A(9-6-10)	119.4	A(20-25-31)	119.5
R(16-23)	1.077	A(6-9-13)	125.2	A(25-21-28)	121.4
R(17-22)	1.345	A(6-10-12)	113.5	A(21-25-31)	119.8
R(17-24)	0.996	A(6-10-14)	116	A(26-22-27)	128.6
R(20-25)	1.418	A(9-13-15)	116.8	A(22-26-32)	96.7
R(20-29)	1.075	A(12-10-14)	116.7	A(22-27-30)	128.4
R(21-25)	1.357	A(10-12-15)	119.3	A(27-30-33)	107.6
R(21-28)	1.074	A(10-12-16)	121.2	A(27-30-34)	111.1
R(22-26)	1.765	A(10-14-17)	108.3	A(27-30-35)	111.3
R(22-27)	1.265	A(10-14-18)	110.5	A(33-30-34)	108.2
R(25-31)	1.077	A(10-14-19)	109.7	A(33-30-35)	108.5

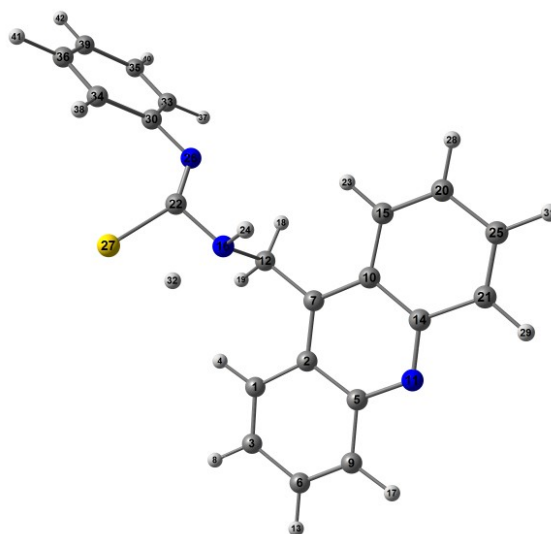
**IXa**

R(1-2)	1.427	R(22-33)	1.082	A(15-11-16)	99.5
R(1-3)	1.367	R(26-34)	1.077	A(11-15-20)	104.1
R(1-4)	1.077	R(27-35)	1.337	A(11-15-23)	111.7
R(2-5)	1.41	A(2-1-3)	122.1	A(11-15-24)	111.5
R(2-7)	1.349	A(2-1-4)	117.2	A(11-16-21)	111.7
R(3-6)	1.408	A(1-2-5)	116.8	A(11-16-22)	122
R(3-8)	1.078	A(1-2-7)	117.7	A(13-19-26)	122.4
R(5-9)	1.404	A(3-1-4)	120.7	A(13-19-28)	119.3
R(5-11)	1.511	A(1-3-6)	120.7	A(18-14-25)	120.7
R(6-9)	1.374	A(1-3-8)	119.6	A(14-18-26)	120.6
R(6-12)	1.077	A(5-2-7)	125.5	A(14-18-29)	119.6
R(7-10)	1.35	A(2-5-9)	119.9	A(20-15-23)	110.1
R(9-17)	1.079	A(2-5-11)	120.4	A(20-15-24)	110.3
R(10-13)	1.409	A(2-7-10)	116.9	A(15-20-21)	111.3
R(10-14)	1.426	A(6-3-8)	119.8	A(15-20-30)	124.1
R(11-13)	1.512	A(3-6-9)	118.2	A(23-15-24)	109
R(11-15)	1.566	A(3-6-12)	120.9	A(21-16-22)	126.1
R(11-16)	1.53	A(9-5-11)	119.7	A(16-21-20)	113.1
R(13-19)	1.403	A(5-9-6)	122.4	A(16-21-27)	122.4
R(14-18)	1.367	A(5-9-17)	119.3	A(16-22-31)	110.9
R(14-25)	1.077	A(5-11-13)	111.3	A(16-22-32)	107.8
R(15-20)	1.461	A(5-11-15)	113.3	A(16-22-33)	110.3
R(15-23)	1.08	A(5-11-16)	109.6	A(26-18-29)	119.8
R(15-24)	1.079	A(9-6-12)	120.9	A(18-26-19)	118.2
R(16-21)	1.297	A(6-9-17)	118.4	A(18-26-34)	120.9
R(16-22)	1.455	A(7-10-13)	125.5	A(26-19-28)	118.3
R(18-26)	1.407	A(7-10-14)	117.7	A(19-26-34)	120.9
R(18-29)	1.078	A(13-10-14)	116.8	A(21-20-30)	123.9
R(19-26)	1.374	A(10-13-11)	120.4	A(20-21-27)	124.5
R(19-28)	1.079	A(10-13-19)	119.9	A(21-27-35)	96.5
R(20-21)	1.316	A(10-14-18)	122.1	A(31-22-32)	109.3
R(20-30)	1.005	A(10-14-25)	117.2	A(31-22-33)	110
R(21-27)	1.748	A(13-11-15)	113.1	A(32-22-33)	108.5
R(22-31)	1.082	A(13-11-16)	109.4		
R(22-32)	1.078	A(11-13-19)	119.7		



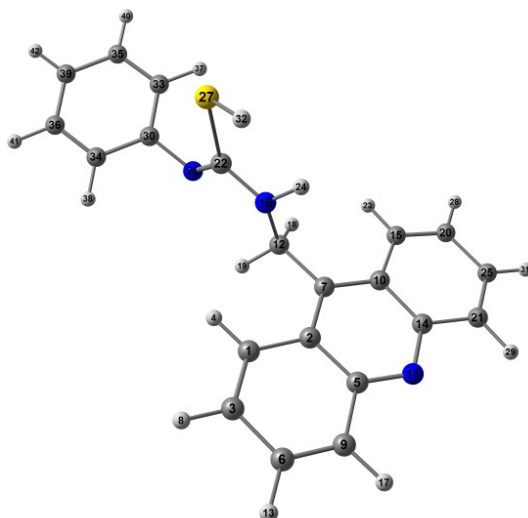
Xa

R(1-2)	1.4	R(23-33)	1.079	A(10-14-20)	118.4
R(1-3)	1.378	R(23-34)	1.08	A(10-15-19)	120.3
R(1-4)	1.078	R(27-35)	1.076	A(10-15-26)	119.3
R(2-5)	1.391	A(2-1-3)	120.3	A(14-11-16)	111.7
R(2-7)	1.385	A(2-1-4)	119.3	A(14-11-17)	110.7
R(3-6)	1.394	A(1-2-5)	120	A(11-14-20)	121.2
R(3-8)	1.077	A(1-2-7)	119.6	A(16-11-17)	100.6
R(5-9)	1.396	A(3-1-4)	120.4	A(11-16-21)	102.3
R(5-11)	1.525	A(1-3-6)	120.2	A(11-16-24)	111.2
R(6-9)	1.381	A(1-3-8)	119.6	A(11-16-25)	111.9
R(6-12)	1.076	A(5-2-7)	120.4	A(11-17-22)	112.5
R(7-10)	1.386	A(2-5-9)	118.6	A(11-17-23)	122.4
R(7-13)	1.002	A(2-5-11)	120.5	A(14-20-27)	121.7
R(9-18)	1.076	A(2-7-10)	121.1	A(14-20-29)	119.6
R(10-14)	1.392	A(2-7-13)	116.5	A(19-15-26)	120.4
R(10-15)	1.399	A(6-3-8)	120.2	A(15-19-27)	120.2
R(11-14)	1.529	A(3-6-9)	119.1	A(15-19-30)	119.6
R(11-16)	1.561	A(3-6-12)	120.6	A(21-16-24)	110.8
R(11-17)	1.477	A(9-5-11)	120.8	A(21-16-25)	111.5
R(14-20)	1.396	A(5-9-6)	121.6	A(10-14-20)	118.4
R(15-19)	1.378	A(5-9-18)	119.2	A(10-15-19)	120.3
R(15-26)	1.078	A(5-11-14)	111.1	A(10-15-26)	119.3
R(16-21)	1.449	A(5-11-16)	111.2	A(14-11-16)	111.7
R(16-24)	1.083	A(5-11-17)	111.1	A(14-11-17)	110.7
R(16-25)	1.081	A(9-6-12)	120.3	A(11-14-20)	121.2
R(17-22)	1.331	A(6-9-18)	119.1	A(16-11-17)	100.6
R(17-23)	1.453	A(10-7-13)	116.5	A(11-16-21)	102.3
R(19-27)	1.393	A(7-10-14)	120.4	A(11-16-24)	111.2
R(19-30)	1.077	A(7-10-15)	119.4	A(11-16-25)	111.9
R(20-27)	1.382	A(14-10-15)	120.2	A(11-17-22)	112.5
R(20-29)	1.075	A(10-14-11)	120.3	A(11-17-23)	122.4
R(21-22)	1.332	A(10-14-20)	118.4	A(14-20-27)	121.7
R(21-31)	1.003	A(7-10-15)	119.4	A(14-20-29)	119.6
R(22-28)	1.702	A(14-10-15)	120.2	A(19-15-26)	120.4
R(23-32)	1.083	A(10-14-11)	120.3	A(15-19-27)	120.2

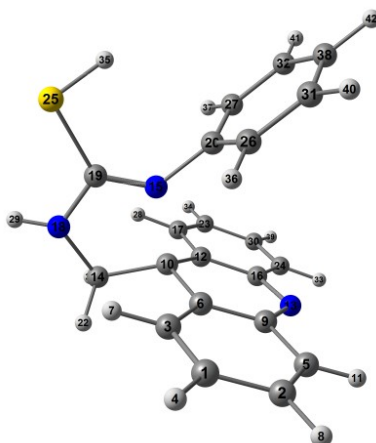


Ts VIIb

R(1-2)	1.44	R(26-30)	1.41	A(6-9-17)	122.1
R(1-3)	1.35	R(30-33)	1.392	A(10-7-12)	120.3
R(1-4)	1.073	R(30-34)	1.391	A(7-10-14)	118
R(2-5)	1.426	R(33-35)	1.384	A(7-10-15)	124.2
R(2-7)	1.399	R(33-37)	1.075	A(7-12-16)	110.7
R(3-6)	1.432	R(34-36)	1.387	A(7-12-18)	111.4
R(3-8)	1.075	R(34-38)	1.073	A(7-12-19)	111.3
R(5-9)	1.437	R(35-39)	1.388	A(14-10-15)	117.8
R(5-11)	1.322	R(35-40)	1.076	A(10-14-11)	123
R(6-9)	1.348	R(36-39)	1.386	A(10-14-21)	119.3
R(6-13)	1.075	R(36-41)	1.076	A(10-15-20)	121
R(7-10)	1.4	R(39-42)	1.075	A(10-15-23)	120.1
R(7-12)	1.514	A(2-1-3)	121	A(11-14-21)	117.6
R(9-17)	1.074	A(2-1-4)	120.1	A(16-12-18)	109.2
R(10-14)	1.426	A(1-2-5)	117.8	A(16-12-19)	107.2
R(10-15)	1.441	A(1-2-7)	124.2	A(12-16-22)	115.2
R(11-14)	1.321	A(3-1-4)	118.9	A(12-16-24)	111
R(12-16)	1.475	A(1-3-6)	120.8	A(18-12-19)	106.8
R(12-18)	1.078	A(1-3-8)	119.9	A(14-21-25)	120.7
R(12-19)	1.08	A(5-2-7)	118	A(14-21-29)	117.2
R(14-21)	1.437	A(2-5-9)	119.3	A(20-15-23)	118.9
R(15-20)	1.35	A(2-5-11)	123.1	A(15-20-25)	120.8
R(15-23)	1.073	A(2-7-10)	118.8	A(15-20-28)	119.9
R(16-22)	1.475	A(2-7-12)	121	A(22-16-24)	109.9
R(16-24)	1.006	A(6-3-8)	119.3	A(16-22-26)	119.7
R(20-25)	1.432	A(3-6-9)	120.3	A(16-22-27)	100.5
R(20-28)	1.075	A(3-6-13)	119.3	A(25-20-28)	119.3
R(21-25)	1.348	A(9-5-11)	117.6	A(20-25-21)	120.3
R(21-29)	1.074	A(5-9-6)	120.7	A(20-25-31)	119.3
R(22-26)	1.244	A(5-9-17)	117.2	A(25-21-29)	122.1
R(22-27)	1.754	A(5-11-14)	119.2	A(21-25-31)	120.4
R(25-31)	1.075	A(9-6-13)	120.4	A(26-22-27)	139.8

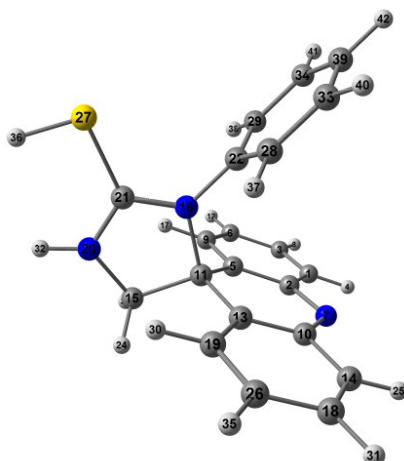
**VIIb**

R(1-2)	1.438	R(26-30)	1.406	R(35-39)	1.386
R(1-3)	1.35	R(27-32)	1.326	R(35-40)	1.076
R(1-4)	1.072	R(30-33)	1.392	R(36-39)	1.389
R(2-5)	1.423	R(30-34)	1.393	R(36-41)	1.076
R(2-7)	1.402	R(33-35)	1.388	R(39-42)	1.075
R(3-6)	1.431	R(33-37)	1.075	A(2-1-3)	121
R(3-8)	1.075	R(34-36)	1.385	A(2-1-4)	119.6
R(5-9)	1.435	R(34-38)	1.075	A(1-2-5)	118
R(5-11)	1.324	R(35-39)	1.386	A(1-2-7)	123.6
R(6-9)	1.349	R(35-40)	1.076	A(3-1-4)	119.4
R(6-13)	1.076	R(36-39)	1.389	A(1-3-6)	120.6
R(7-10)	1.399	R(36-41)	1.076	A(1-3-8)	120.1
R(7-12)	1.517	R(39-42)	1.075	A(5-2-7)	118.4
R(9-17)	1.074	A(2-1-3)	121	A(2-5-9)	119.3
R(10-14)	1.429	A(2-1-4)	119.6	A(2-5-11)	123
R(10-15)	1.441	A(1-2-5)	118	A(2-7-10)	118.4
R(11-14)	1.321	A(1-2-7)	123.6	A(2-7-12)	120
R(12-16)	1.457	A(3-1-4)	119.4	A(6-3-8)	119.3
R(12-18)	1.081	A(1-3-6)	120.6	A(3-6-9)	120.4
R(12-19)	1.079	A(1-3-8)	120.1	A(3-6-13)	119.3
R(14-21)	1.437	A(5-2-7)	118.4	A(9-5-11)	117.8
R(15-20)	1.349	A(2-5-9)	119.3	A(5-9-6)	120.7
R(15-23)	1.073	A(2-5-11)	123	A(5-9-17)	117.5
R(16-22)	1.365	A(2-7-10)	118.4	A(5-11-14)	119
R(16-24)	0.998	R(26-30)	1.406	A(9-6-13)	120.4
R(20-25)	1.432	R(27-32)	1.326	A(6-9-17)	121.9
R(20-28)	1.075	R(30-33)	1.392	A(10-7-12)	121.6
R(21-25)	1.348	R(30-34)	1.393	A(7-10-14)	118.1
R(21-29)	1.074	R(33-35)	1.388	A(7-10-15)	124.2
R(22-26)	1.257	R(33-37)	1.075	A(7-12-16)	110
R(22-27)	1.794	R(34-36)	1.385	A(7-12-18)	111.5
R(25-31)	1.076	R(34-38)	1.075	A(7-12-19)	110.1



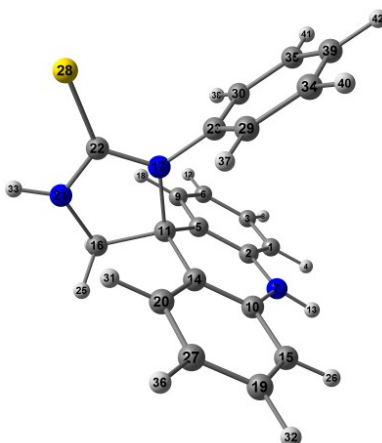
Ts VIIIb

R(1-2)	1.418	R(25-35)	1.324	A(10-12-17)	121.2
R(1-3)	1.363	R(26-31)	1.404	A(10-14-18)	108.3
R(1-4)	1.075	R(26-36)	1.103	A(10-14-21)	110.5
R(2-5)	1.358	R(27-32)	1.405	A(10-14-22)	109.8
R(2-8)	1.076	R(27-37)	1.103	A(16-12-17)	119.3
R(3-6)	1.417	R(30-39)	1.076	A(12-16-13)	125.3
R(3-7)	1.077	R(31-38)	1.404	A(12-16-24)	117.3
R(5-9)	1.432	R(31-40)	1.104	A(12-17-23)	122.2
R(5-11)	1.075	R(32-38)	1.405	A(12-17-28)	119.5
R(6-9)	1.413	R(32-41)	1.103	A(13-16-24)	117.4
R(6-10)	1.471	R(38-42)	1.103	A(18-14-21)	110
R(9-13)	1.336	A(2-1-3)	118.7	A(18-14-22)	109.9
R(10-12)	1.469	A(2-1-4)	120.4	A(14-18-19)	112.3
R(10-14)	1.552	A(1-2-5)	120.7	A(14-18-29)	120.1
R(12-16)	1.415	A(1-2-8)	119.5	A(21-14-22)	108.4
R(12-17)	1.417	A(3-1-4)	120.8	A(19-15-20)	128.3
R(13-16)	1.335	A(1-3-6)	121.9	A(15-19-18)	114.5
R(14-18)	1.463	A(1-3-7)	118.7	A(15-19-25)	128.7
R(14-21)	1.078	A(5-2-8)	119.8	A(15-20-26)	120
R(14-22)	1.078	A(2-5-9)	121.8	A(15-20-27)	120
R(15-19)	1.265	A(2-5-11)	121.4	A(16-24-30)	121.8
R(15-20)	1.5	A(6-3-7)	119.4	A(16-24-33)	116.8
R(16-24)	1.433	A(3-6-9)	119.6	A(23-17-28)	118.3
R(17-23)	1.363	A(3-6-10)	120.9	A(17-23-30)	118.7
R(17-28)	1.077	A(9-5-11)	116.8	A(17-23-34)	120.9
R(18-19)	1.345	A(5-9-6)	117.2	A(19-18-29)	119.8
R(18-29)	0.996	A(5-9-13)	117.6	A(18-19-25)	116.7
R(19-25)	1.765	A(9-6-10)	119.4	A(19-25-35)	96.7
R(20-26)	1.405	A(6-9-13)	125.2	A(26-20-27)	120
R(20-27)	1.405	A(6-10-12)	113.4	A(20-26-31)	120
R(23-30)	1.418	A(6-10-14)	116	A(20-26-36)	120
R(23-34)	1.075	A(9-13-16)	116.8	A(20-27-32)	120
R(24-30)	1.358	A(12-10-14)	116.7	A(20-27-37)	120.1
R(24-33)	1.074	A(10-12-16)	119.3	A(30-23-34)	120.4



IXb

R(1-2)	1.427	R(22-29)	1.388	A(7-10-13)	125.4
R(1-3)	1.366	R(26-35)	1.077	A(7-10-14)	117.7
R(1-4)	1.077	R(27-36)	1.338	A(13-10-14)	116.9
R(2-5)	1.41	R(28-33)	1.387	A(10-13-11)	120.1
R(2-7)	1.348	R(28-37)	1.074	A(10-13-19)	119.8
R(3-6)	1.408	R(29-34)	1.387	A(10-14-18)	122.1
R(3-8)	1.078	R(29-38)	1.074	A(10-14-25)	117.2
R(5-9)	1.405	R(33-39)	1.388	A(13-11-15)	113.2
R(5-11)	1.507	R(33-40)	1.077	A(13-11-16)	109.5
R(6-9)	1.373	R(34-39)	1.388	A(11-13-19)	120
R(6-12)	1.077	R(34-41)	1.077	A(15-11-16)	98.9
R(7-10)	1.348	R(39-42)	1.077	A(11-15-20)	104.7
R(9-17)	1.079	A(2-1-3)	122.1	A(11-15-23)	111.8
R(10-13)	1.41	A(2-1-4)	117.2	A(11-15-24)	111.4
R(10-14)	1.427	A(1-2-5)	116.9	A(11-16-21)	111.2
R(11-13)	1.508	A(1-2-7)	117.6	A(11-16-22)	124.2
R(11-15)	1.564	A(3-1-4)	120.7	A(13-19-26)	122.4
R(11-16)	1.561	A(1-3-6)	120.6	A(13-19-30)	119.4
R(13-19)	1.404	A(1-3-8)	119.6	A(18-14-25)	120.7
R(14-18)	1.366	A(5-2-7)	125.5	A(14-18-26)	120.6
R(14-25)	1.077	A(2-5-9)	119.8	A(14-18-31)	119.6
R(15-20)	1.46	A(2-5-11)	120.1	A(20-15-23)	110
R(15-23)	1.079	A(2-7-10)	116.9	A(20-15-24)	110.3
R(15-24)	1.079	A(6-3-8)	119.8	A(15-20-21)	111.8
R(16-21)	1.3	A(3-6-9)	118.2	A(15-20-32)	123.5
R(16-22)	1.433	A(3-6-12)	120.9	A(23-15-24)	108.6
R(18-26)	1.408	A(9-5-11)	120.1	A(21-16-22)	124.6
R(18-31)	1.078	A(5-9-6)	122.4	A(16-21-20)	113.2
R(19-26)	1.373	A(5-9-17)	119.4	A(16-21-27)	122.5
R(19-30)	1.079	A(5-11-13)	111.4	A(16-22-28)	119.8
R(20-21)	1.314	A(5-11-15)	113.4	A(16-22-29)	119.6
R(20-32)	1.005	A(5-11-16)	109.8	A(26-18-31)	119.8
R(21-27)	1.748	A(9-6-12)	120.9	A(18-26-19)	118.2
R(22-28)	1.388	A(6-9-17)	118.2	A(18-26-35)	120.9



Xb

R(1-2)	1.403	R(23-29)	1.388	A(6-9-18)	118.5
R(1-3)	1.375	R(23-30)	1.387	A(10-7-13)	118.1
R(1-4)	1.078	R(27-36)	1.076	A(7-10-14)	120.8
R(2-5)	1.391	R(29-34)	1.387	A(7-10-15)	119.1
R(2-7)	1.377	R(29-37)	1.074	A(14-10-15)	120.1
R(3-6)	1.396	R(30-35)	1.388	A(10-14-11)	121.6
R(3-8)	1.077	R(30-38)	1.074	A(10-14-20)	118.3
R(5-9)	1.399	R(34-39)	1.388	A(10-15-19)	120.4
R(5-11)	1.524	R(34-40)	1.077	A(10-15-26)	119.1
R(6-9)	1.378	R(35-39)	1.388	A(14-11-16)	111.4
R(6-12)	1.076	R(35-41)	1.077	A(14-11-17)	110.3
R(7-10)	1.377	R(39-42)	1.077	A(11-14-20)	120.1
R(7-13)	1.001	A(2-1-3)	120.4	A(16-11-17)	100.5
R(9-18)	1.077	A(2-1-4)	119.1	A(11-16-21)	103.1
R(10-14)	1.39	A(1-2-5)	120.1	A(11-16-24)	111.8
R(10-15)	1.403	A(1-2-7)	119.1	A(11-16-25)	111.5
R(11-14)	1.526	A(3-1-4)	120.4	A(11-17-22)	112.5
R(11-16)	1.561	A(1-3-6)	120.2	A(11-17-23)	122.7
R(11-17)	1.504	A(1-3-8)	119.6	A(14-20-27)	122
R(14-20)	1.399	A(5-2-7)	120.8	A(14-20-31)	119.4
R(15-19)	1.375	A(2-5-9)	118.2	A(19-15-26)	120.4
R(15-26)	1.078	A(2-5-11)	121.6	A(15-19-27)	120.2
R(16-21)	1.447	A(2-7-10)	122.6	A(15-19-32)	119.6
R(16-24)	1.081	A(2-7-13)	118.2	A(21-16-24)	110.9
R(16-25)	1.08	A(6-3-8)	120.2	A(21-16-25)	111.3
R(17-22)	1.336	A(3-6-9)	119	A(16-21-22)	113.7
R(17-23)	1.431	A(3-6-12)	120.6	A(16-21-33)	123.9
R(19-27)	1.396	A(9-5-11)	120.2	A(24-16-25)	108.2
R(19-32)	1.077	A(5-9-6)	122.1	A(22-17-23)	124.7
R(20-27)	1.378	A(5-9-18)	119.4	A(17-22-21)	109.4
R(20-31)	1.077	A(5-11-14)	111.8	A(17-22-28)	127.2
R(21-22)	1.328	A(5-11-16)	111.8	A(17-23-29)	120.1
R(21-33)	1.003	A(5-11-17)	110.4	A(17-23-30)	119.9
R(22-28)	1.703	A(9-6-12)	120.4	A(27-19-32)	120.2

Literature

1. Leach, A. R., *Molecular Modeling: Principles and Applications*. 2nd ed.; Prentice Hall, **2001**.
2. Gonzalez, C.; Schlegel, H. B. *J. Chem. Phys.* **1989**, *90*, 2154.
3. Gonzalez, C.; Schlegel, H. B. *J. Phys. Chem.* **1990**, *94*, 5523.
4. Tomasi, J.; Perisco, M. *Chem. Rev.* **1994**, *94*, 2027.
5. Demeunynck, M.; Charmantray, F.; Martelli, A. *Current pharmaceutical design* **2001**, *7*, (17), 1703-24.
6. Brana, M. F.; Cacho, M.; Gradillas, A.; De Pascual-Teresa, B.; Ramos, A. *Current Pharmaceutical Design* **2001**, *7*, (17), 1745-1780.
7. Bernat, J.; Chomca, I.; Kristian, P.; GundulaVoss. *Synthetic Communications* **1998**, *28*, (22), 4171-4178.
8. Bernat, J.; Chomca, I.; Kristian, P.; Pihlaja, K.; Klika, K. D.; Imrich, J. *Heterocycles* **1999**, *51*, (1), 137-140.
9. Bernat, J.; Kristian, P.; Mazagova, D.; Cernak, J.; Busova, T.; Lipkowski, J. *Synthetic Communications* **1995**, *25*, (24), 3973-9.
10. Kristian, P.; Bernat, J.; Imrich, J.; Danihel, I.; Suchar, G.; Chomca, I.; Hocova, S.; Busova, T.; Guspanova, J.; Linden, A. *Molecules [Electronic Publication]* **1996**, *1*, 181-189.
11. Kristian, P.; Chomca, I.; Bernat, J.; Imrich, J. *Chemical Papers* **1999**, *53*, (1), 49-52.
12. Raspoet, G.; Nguyen, M. T.; McGarraghy, M.; Hegarty, A. F. *Journal of Organic Chemistry* **1998**, *63*, (20), 6878-6885.
13. *Gaussian 98* (Revision A.7), M. J. Frisch, G. W. T., H. B. Schlegel, G. E. Scuseria, M. A. Robb, J. R. Cheeseman, V. G. Zakrzewski, J. A. Montgomery, Jr., R. E. Stratmann, J. C. Burant, S. Dapprich, J. M. Millam, A. D. Daniels, K. N. Kudin, M. C. Strain, O. Farkas, J. Tomasi, V. Barone, M. Cossi, R. Cammi, B. Mennucci, C. Pomelli, C. Adamo, S. Clifford, J. Ochterski, G. A. Petersson, P. Y. Ayala, Q. Cui, K. Morokuma, D. K. Malick, A. D. Rabuck, K. Raghavachari, J. B. Foresman, J. Cioslowski, J. V. Ortiz, A. G. Baboul, B. B. Stefanov, G. Liu, A.

- Liashenko, P. Piskorz, I. Komaromi, R. Gomperts, R. L. Martin, D. J. Fox, T. Keith, M. A. Al-Laham, C. Y. Peng, A. Nanayakkara, C. Gonzalez, M. Challacombe, P. M. W. Gill, B. G. Johnson, W. Chen, M. W. Wong, J. L. Andres, M. Head-Gordon, E. S. Replogle and J. A. Pople, Gaussian, Inc., Pittsburgh PA, 1998.
14. *Gaussian 03* (Revision C.02), Frisch, M. J. T., G. W.; Schlegel, H. B.; Scuseria, G. E.; Robb, M. A.; Cheeseman, J. R.; Montgomery, Jr., J. A.; Vreven, T.; Kudin, K. N.; Burant, J. C.; Millam, J. M.; Iyengar, S. S.; Tomasi, J.; Barone, V.; Mennucci, B.; Cossi, M.; Scalmani, G.; Rega, N.; Petersson, G. A.; Nakatsuji, H.; Hada, M.; Ehara, M.; Toyota, K.; Fukuda, R.; Hasegawa, J.; Ishida, M.; Nakajima, T.; Honda, Y.; Kitao, O.; Nakai, H.; Klene, M.; Li, X.; Knox, J. E.; Hratchian, H. P.; Cross, J. B.; Bakken, V.; Adamo, C.; Jaramillo, J.; Gomperts, R.; Stratmann, R. E.; Yazyev, O.; Austin, A. J.; Cammi, R.; Pomelli, C.; Ochterski, J. W.; Ayala, P. Y.; Morokuma, K.; Voth, G. A.; Salvador, P.; Dannenberg, J. J.; Zakrzewski, V. G.; Dapprich, S.; Daniels, A. D.; Strain, M. C.; Farkas, O.; Malick, D. K.; Rabuck, A. D.; Raghavachari, K.; Foresman, J. B.; Ortiz, J. V.; Cui, Q.; Baboul, A. G.; Clifford, S.; Cioslowski, J.; Stefanov, B. B.; Liu, G.; Liashenko, A.; Piskorz, P.; Komaromi, I.; Martin, R. L.; Fox, D. J.; Keith, T.; Al-Laham, M. A.; Peng, C. Y.; Nanayakkara, A.; Challacombe, M.; Gill, P. M. W.; Johnson, B.; Chen, W.; Wong, M. W.; Gonzalez, C.; and Pople, J. A., Gaussian, Inc., Wallingford CT, 2004.
 15. Peng, C.; Schlegel, H. B. *Isr. J. Chem.* **1993**, 33, 449.
 16. Peng, C.; Ayala, P. Y.; Schlegel, H. B.; Frisch, M. J. *J. Comput. Chem.* **1996**, 16, 49-56.
 17. Hariharen, P. C.; Pople, J. A. *Chem. Phys. Lett.* **1972**, 66, 217.
 18. Hehre, W. J.; Radom, L.; Schleyer, P. v. R.; Pople, J. A., *Ab initio Molecular Orbital Theory*. Wiley, New York, **1986**.
 19. McQuarrie, D. A.; Simon, J. D., *Molecular Thermodynamics*. University Science Books, Sausalito, **1999**; 656.
 20. Atkins, P., *Physical Chemistry*. 6th; W. H. Freeman and Co., New York, **1998**.

21. Patai, S. Ed., Wiley J.; *The Chemistry of Cyanates and Their Thio Derivates*. **1977**, 2, 1003-1221.
22. Butler, R. N.; Grogan, D. C.; McDonald, P. D.; Burke, L. A. *J.Chem.Soc., Perkin Trans.1* **1997**, 24, 3587-3599.
23. Foresman, J. B.; Frisch, A., *Exploring Chemistry with Electronic Structure Methods*. 2nd ed.; Gaussian, Pittsburgh, **1996**.
24. Zhang, K.; Chung-Phillips, A. *J. Chem. Inf. Comput. Sci.* **1999**, 39, 382-395.
25. Head-Gordon, M.; Pople, J. A.; Frisch, M. J. *Chem. Phys. Lett.* **1988**, 153, 503.
26. Frisch, M. J.; Head-Gordon, M.; Pople, J. A. *Chem. Phys. Lett.* **1990**, 166, (3), 275-280.
27. Wei, D.; Truchon, J.-F.; Sirois, S.; Salahub, D. *J. Chem. Phys.* **2002**, 116, (14), 6028-6038.
28. Herrera, B.; Toro-Labbe, A. *J. Phys. Chem. A* **2004**, 108, 1830.
29. Meuwly, M.; Bach, A.; Leutwyler, S. *J. Am. Chem. Soc.* **2001**, 123, 11446.
30. Drew, M. G. B.; Pal, P. K.; Chowdhury, S.; Datta, D. *New J. Chem.* **2003**, 27, 1026-1028.
31. Ito, M.; Re, S.; Tokiwa, H. *J. Phys. Chem. A* **2003**, 108, 5417.
32. Kim, H.; Green, R. J.; Qian, J.; Anderson, S. L. *J. Chem. Phys.* **2000**, 112, 5717-5721.
33. Podolyan, Y.; Gorb, L.; Leszczynski, J. *J. Phys. Chem.* **2002**, 106, 12103-12109.
34. Shi, T.; Wang, X.; Shi, X.; Tian, Z.; Zhu, Q. *Journal of Molecular Structure (Theochem)* **2002**, 578, 135-143.
35. Becke, A. D. *J. Chem. Phys.* **1993**, 98, 5648.
36. Cramer, C. J.; Truhlar, D. G. *Chem. Rev.* **1999**, 99, (2161).
37. Rablen, P. R.; Pearlman, S. A.; Miller, D. A. *J. Am. Chem. Soc.* **1999**, 121, 227.
38. Tomasi, J.; Cammi, R.; Mennucci, B.; Cappelli, C.; Corni, S. *Phys. Chem. Chem. Phys.* **2002**, 4, 5697.
39. Miertus, S.; Scrocco, E.; Tomasi, J. *J. Chem. Phys.* **1981**, 55.
40. Cammi, R.; Tomasi, J. *J. Chem. Phys.* **1994**, 100, 7495.
41. Mennucci, B.; Tomasi, J. *J. Chem. Phys.* **1997**, 106, 5151.
42. Mennucci, B.; Cancès, E.; Tomasi, J. *J. Phys. Chem. B* **1997**, 101, 10506.

43. Cammi, R.; Mennucci, B.; Tomasi, J. *J. Phys. Chem. A* **1999**, 103, 9100.
44. Cammi, R.; Mennucci, B.; Tomasi, J. *J. Phys. Chem. A* **2000**, 104, 5631.
45. Klika, K. D.; Janovec, L.; Imrich, J.; Suchar, G.; Kristian, P.; Sillanpaae, R.; Pihlaja, K. *Eur. J. Org. Chem.* **2002**, 7, 1248.
46. Klika, K. D.; Valtamo, P.; Janovec, L.; Suchar, G.; Kristian, P.; Imrich, J.; Kivela, A.; Pihlaja, K. *Rapid Commun. Mass Spectrom.* **2004**, 18, 87.
47. Ilieva, S.; Galabov, B.; Musaev, D. G.; Morokuma, K.; Schaefer, H. F. *J. Org. Chem.* **2003**, 68, 1496.
48. Gorb, L.; Podolyan, Y.; Leszczynski, J. *Journal of Molecular Structure (Theochem)* **1999**, 487, 47.
49. Jencks, W. P.; Carriuolo, J. *J. Am. Chem. Soc.* **1960**, 82, 675.
50. Kuc, T.; Pawelka, Z.; Sobczyk, L. *Phys. Chem. Chem. Phys.* **2001**, 3, 5201.
51. Kryachko, E. S.; Zeegers-Huyskens, T. *Journal of Molecular Structure (Theochem)* **2002**, 615, 251.
52. Scheiner, S., *Hydrogen Bonding*. Oxford University Press, New York, **1997**.
53. Jeffrey, G. A., *An Introduction to Hydrogen Bonding*. Oxford University Press, New York, **1997**.
54. Desiraju, G. R.; Steiner, T., *The Weak Hydrogen Bond in Structural Chemistry and Biology*. New York, **1997**.
55. Steiner, T.; Lutz, B.; van der Maas, J.; Veldman, N.; Schreurs, M. M.; Kroon, J.; Kanters, J. A. *Chem. Commun.* **1997**, 191.
56. Remko, M.; Van Duijnen, P. T.; Swart, M. *Structural Chemistry* **2003**, 14, 271.
57. Saenger, W., *Principles of Nucleic Acid Structure*. Springer-Verlag, New York, **1984**.
58. Friedberg, E. C. *Mol. Microbiol.* **1991**, 5, 2303.
59. Dickerson, R. E.; Drew, H. R.; Conner, B. N.; Wing, R. M.; Fratini, A. V.; Kopka, M. L. *Science* **1982**, 216, 475.
60. Lavery, R.; Sklenar, H. *J. Biomol. Struct. Dyn.* **1988**, 63.
61. Lu, X.-J.; Olson, W. K. *Nucleic Acids Res.* **2003**, 31, 5108.
62. Behrens, C.; Burgdorf, L. T.; SchwDgler, A.; Carell, T. *Angew. Chem. Int. Ed.* **2002**, 41, 1763.

63. Carell, T.; Behrens, C.; Gierlich, J. *Org. Biomol. Chem.* **2003**, 1, 2221.
64. Giese, B.; Barbara, C.; Thomas, C.; Carell, T.; Behrens, C.; Hennecke, U.; Schiemann, O.; Feresin, E. *Angew. Chem. Int. Ed.* **2004**, 43, 1848.
65. Pearlman, D. A.; Case, D. A.; Caldwell, J. W.; Ross, W. R.; Cheatham, T. E.; DeBolt, S.; Ferguson, D.; Seibel, G.; Kollman, P. *Comp. Phys. Commun.* **1995**, 91, 1.
66. Weiner, S. J.; Kollman, P. A.; Case, D. A.; Singh, U. C.; Ghio, C.; Alagona, G.; Profeta, S. J.; Weiner, P. *J. Am. Chem. Soc.* **1984**, 106, 765.
67. Weiner, S. J.; Kollman, P. A.; Nguyen, D. T.; Case, D. A. *J. Comp. Chem.* **1986**, 7, 230.
68. Cornell, W. D.; Cieplak, P.; Bayly, C. I.; Gould, I. R.; Merz, K. M. J.; Ferguson, D. M.; Spellmeyer, D. C.; Fox, T.; Caldwell, J. W.; Kollman, P. A. *J. Am. Chem. Soc.* **1995**, 117, 5179.
69. Cheatham, T. E.; Miller, J. L.; Spector, T. I.; Cieplak, P.; Kollman, P. A. *ACS Symp. Ser.* **1998**, 682, 285.
70. Sprous, D.; Young, M. A.; Beveridge, D. L. *J. Phys. Chem. B* **1998**, 102, 4658.
71. Reddy, S. Y.; Leclerc, F.; Karplus, M. *Biophys. J.* **2003**, 84, 1421.
72. Spector, T. I.; Cheatham, T. E.; Kollman, P. A. *J. Am. Chem. Soc.* **1997**, 119, 7095.
73. Breneman, C. M.; Wiberg, K. B. *J. Comp. Chem.* **1990**, (11), 361.
74. Essmann, U.; Perera, L.; Berkowitz, M. L.; Darden, T.; Lee, H.; Pedersen, L. G. *J. Chem. Phys.* **1995**, 103, 8577.
75. Park, H.; Zhang, K.; Ren, Y.; Nadji, S.; Sinha, N.; Taylor, J.-S.; Kang, C. *Proceedings of the National Academy of Sciences of the United States of America* **2002**, 99, 15965.
76. McAteer, K.; Jing, Y.; Kao, J.; Taylor, J.-S.; Kennedy, M. A. *J. Mol. Biol.* **1998**, 282, 1013.
77. Pearlman, D. A.; Holbrook, S. R.; Pirkle, D. H.; Kim, S.-H. *Science* **1985**, 227, 1304.

List of Symbols and Abbreviations

Abbreviations:

A	adenine
Acr	acridine
C	cytosine
CPD	cyclobutane pyrimidine dimer
DFT	density functional theory
DNA	deoxyribonucleic acid
Ee	internal energy due to electronic motion
Er	internal energy due to rotational motion
Etot	total internal energy ($E_t + E_r + E_v + E_e$)
Et	internal energy due to translation
Ev	internal energy due to vibrational motion
G	guanine
Gcorr	correction to the Gibbs free energy due to internal energy
Hcorr	correction to the enthalpy due to internal energy
HF	Hartree-Fock theory
I	moment of inertia
IRC	intrinsic reaction coordinate
K	index of vibrational modes
k	rate constant
Me	methyl
MD	molecular dynamics
MP	Møller-Plesset theory
N	number of moles
P	pressure (default is 1 atmosphere)
PCM	polarized continuum model
PES	potential energy surface
Ph	phenyl
PME	particle mesh ewald

PT	proton transfer
RMSD	root mean square deviation
RNA	ribonucleic acid
Se	entropy due to electronic motion
Sr	entropy due to rotational motion
Stot	total entropy (St + Sr + Sv + Se)
St	entropy due to translation
Sv	entropy due to vibrational motion
T	thymine
T	temperature (default is 298.15)
TS	transition state
V	volume

Units and Constants:

Å	Ångstrom, $1 \text{ Å} = 10^{-10} \text{ m}$
e	elementary charge, $e = 1.602 \cdot 10^{-19} \text{ C}$
h	Planck's constant = $6.626176 \cdot 10^{-34} \text{ J.s}$
R	gas constant, $8.413 \text{ J.K}^{-1} \cdot \text{mol}^{-1}$
k_B	Boltzmann constant = $1.3807 \cdot 10^{-23} \text{ J.K}^{-1}$

Curriculum Vitae

Name: Stanislav
Family Name: Ivan
Date of Birth: February 22, 1978
Place of Birth: Humenne, Slovakia
Nationality: Slovak

Work address

Department of Chemistry
University of Basel
St. Johannis-Ring 19
CH-4056 Basel
Switzerland
Phone: Int. +41 61 267 11 44
Fax: Int. +41 61 267 11 05
Email: stanislav.ivan@unibas.ch

Academic Education:

July 2001 – June 2005 Doctoral Thesis (Computational Chemistry)
Subject: Elucidation of Chemical Phenomena by
Means of Computational Chemistry
University of Basel, Switzerland
Director: Professor Dr. Bernd Giese

Optional lectures attended:
Computer Chemistry
Advanced Molecular Modeling
Computational Chemistry: MD Simulations and Applications
The Art of Developing Scientific JAVA Applets

Sep 99 – May 2001 Diploma Work (Computational Chemistry)
Subject: Theoretical Study of Nucleophilic
Additions of Isothiocyanates Using Semiempirical
and Ab initio Methods
University of Natural Sciences of Pavol Jozef
Safarik, Slovakia
Research Director: Dr. Marcel Török

Sep 96 – May 2001

Studies of Chemistry

University of Natural Sciences of Pavol Jozef
Safarik, Slovakia
MS in Organic Chemistry

Professional Experience:

July 2001 – July 2005

Scientific staff member at the Department of
Chemistry, University of Basel
Network administrator, IT support

September 2004

Summer School in Computational Chemistry,
Lugano, Switzerland

May 2004 – July 2004

Molecular Dynamics training (AMBER package)
University of Notre Dame, Indiana, USA

Key qualifications:

- Organic Chemistry
- Physical Chemistry
- Computational Chemistry
- Molecular mechanics
- Monte Carlo simulations
- Molecular Dynamics
- Semiempirical and ab initio quantum chemical calculations
- Structure-activity relationship
- Chemoinformatics
- Nanoscale science
- Data mining
- Software packages: MacroModel (Maestro GUI), Amber, Charmm, Spartan, Moloc, Mopac, Gaussian, Gamess
- Object oriented programming: JAVA
- IT support
- Network administration
- LAN, TCP/IP, DNS
- NFS, Samba server
- Beowulf cluster
- Parallel computing
- Word, Excel, PowerPoint, EndNote, FileMaker
- RedHat Linux, UNIX, AIX

- Win98, WinNT, Win2000, WinXP

Hobbies and Interests: Computers, programming, history of flying, sports: judo, football and ice hockey

Languages: English - fluent
German – fluent

References: Professor Dr. Bernd Giese
Department of Chemistry
St.Johanns-Ring 19
CH-4056 Basel
Tel: +41 61 267 11 06
FAX: +41 61 267 11 05
Bernd.Giese@unibas.ch

Prof. Dr. Helma Wennemers
Department of Chemistry
St.Johanns-Ring 19
CH-4056 Basel
Tel: 061 267 1146
FAX: 061 267 11 05
Helma.Wennemers@unibas.ch

Marcel Török, PhD
Department of Organic Chemistry
University of Pavol Jozef Safarik
Moyzesova 14
04001 Kosice
Slovakia
Tel.: +421 6222610/192
mtorok@upjs.sk